ポリフィリン分子繊維の形成と光子注入によるその電子過程制御

（課題番号：１１６５０９３５）

平成１１年度～１２年度　科学研究費補助金（基盤研究(C)）

研究成果報告書

平成１３年３月

研究代表者：小　松　晃　之
（早稲田大学・理工学総合研究センター・講師）

目　次

研究組織

研究代表者：小松　晃之　（早稲田大学・理工学総合研究センター・講師）

研究協力者：土田　英俊　（早稲田大学・理工学部・教授）

柳本　徹也　（早稲田大学・理工学部・助手）

研究経費

平成１１年度	１，３００　千円
平成１２年度	９００　千円
計	２，２００　千円

１）はじめに

本報告書は、文部省科学研究費補助金（基盤研究（C)、課題番号：11650935、平成11年度～12年度（2年間））の助成のもとに実施された研究課題「ポリフィリン分子繊維の形成と光子注入によるその電子過程制御」に関する成果のまとめである。研究代表者は、得られた新知見が単なる学術的な貢献に留まることなく、近い将来何らかの形で社会に還元できる革新技術へと繋がることを強く願っている。

本研究の発端は、ポルフィリン鉄錯体に両親媒性構造を付与すると、それがリン脂質小胞体の二分子層膜中へ均一に包埋され、錯体部の内圏型電子移動が抑止できるので、従来不可能とされていた生理条件下(水中、pH 7.4、37°C)における可逆的な酸素配位錯体系が実現できたことに遡る（1983年)。この発見を契機として、一群の両親媒性ポルフィリン誘導体（リピドポルフィリン類）を設計・合成し、それらが単独でも水中で自己集合して様々な形態の組織体（小胞体、紐状繊維、平板など）を形成することを見出した（1993年)。さらに、自己組織化したリピドポルフィリン鉄組織体がヘモグロビンと同様に酸素を吸脱着できることを明らかにし、その高濃度水溶液が生体内で酸素輸送のできる全合成系酸素運搬体として機能することを実証してきた。水相系における可逆的な酸素配位錯体系が達成された後に残る未解決課題は、酸素分子の脱着により自動酸化された高酸化状態中心鉄(III)の再還元過程の実現ある。

本研究では、この点に焦点を絞り、分子内軸塩基導入による酸素配位錯体の安定度向上と、光電子変換を利用した高酸化状態ポルフィリン鉄の還元活性化を計画した。具体的には、リピドポルフィリン鉄が水相系で自己集合して形成する組織体を対象に、自動酸化した中心鉄(III)の酸素配位活性能を復元するため、光を照射するだけで錯体部を非酵素的に還元する方法の確立を目的とした。(1) 微量の亜鉛ポルフィリンを共存させた共集合体中で、その光励起種から鉄ポルフィリンへの電子移動経路を構築する系、(2) Fe(III)-Cl^-のLigand-Metal Charge Transfer （LMCT）吸収帯の励起により生起する分子内電子移動を利用する系、の２つを構築、光電子移動過程を組織の三次元構造と相関させて解明した。二年間の期限内に予想を上回る進展が見られ、本研究で確立した中心鉄(III)の光還元方法が、ヘム蛋白質にも応用可能であることが実験的に示された。

成果の多くは既に報文として印刷済みであるが、未発表知見もいくつか残されおり、今後も継続展開の成果を合わせながら、続報としてまとめていきたい。文部省科学研究費補助金の支援のもとに、本研究が支障なく推進できたことはもちろん、当初の予測を遥かに超える成果が得られたことを大変光栄に思う。ここに厚く御礼申し上げるとともに、研究推進に当たりお世話になった関係各位に謝意を評する。

2）研 究 発 表

2-1）研究報文

1. "Self-Assembled Fibers Made of Lipidporphyrinnato-zinc(II) and -iron(II) Complexes with an Intramolecular Coordinated Axial Imidazole", T. Komatsu, T. Yanagimoto, Y. Furubayashi, J. Wu, E. Tsuchida, *Langmuir*, **15**, 4427-4433 (1999).

2. "Molecular Environment Effect on O_2-Binding to Lipidporphyrinatoiron(II) Complexes in Aqueous Media", E. Tsuchida, T. Komatsu, T. Yanagimoto, *J. Porphyrins and Phthalocyanines*, **4**, 81-87 (2000).

3. "Photoreduction of Self-assembled Lipidporphyrinato-iron(III) Chloride with Hyaluronic Acid under Semi-physiological Conditions", T. Komatsu, T. Yanagimoto, A. Nakagawa, E. Tsuchida, *Chem. Lett.*, **2000**, 84-85 (2000).

4. "Photoinduced Electron Transfer between Lipidporphyrinato-zinc(II) and -iron(III) Complexes in Phospholipid Vesicular Membrane", T. Yanagimoto, T. Komatsu, E. Tsuchida, *Inorg. Chim. Acta.*, **305**, 26-31 (2000).

5. "Photoreduction of Autooxidized Albumin-heme Hybrid in Saline Solution: Revival of Its O_2-Binding Ability", A. Nakagawa, T. Komatsu, E. Tsuchida, *Bioconjugate Chem.*, **12**, 648-652 (2001).

6. "Photoreduction of a Self-assembled (Lipidporphyrinato)iron(III) Complex in Saline by LMCT Excitation: Co-aggregated Hyaluronic Acid Allows an Irreversible Electron Transfer", T. Yanagimoto, A. Nakagawa, T. Komatsu, E. Tsuchida, *Bull. Chem. Soc., Jpn.*, **74**, 2123-2128 (2001).

2-2）口頭発表

（国内学会）

1. 柳本徹也、中川晶人、小松晃之、土田英俊／LMCT 遷移の光励起を利用したリピドポルフィリン鉄(III)集合体の還元反応／第 48 回高分子学会年次大会、京都、1999 年 5 月

2. 小松晃之／ポルフィリン組織体とその酸素輸液への応用 (招待講演) ／第 23 回高分子錯体若手懇談会、湯河原、1999 年 7 月

3. 中川晶人、小松晃之、土田英俊／光照射を利用したアルブミン-ヘムの還元反応／第 78 日本化学会春季年会、船橋、2000 年 3 月

4. 早川祥一、小早川牧子、柳本徹也、小松晃之、土田英俊／イミダゾリル基を共有結合したオクトパスポルフィリン鉄の合成／第78日本化学会春季年会、船橋、2000年3月

5. 柳本徹也、小松晃之、土田英俊／自己組織化したリピドポルフィリン集合体の構造と酸素配位／第78日本化学会春季年会、船橋、2000年3月

6. 小松晃之／ポルフィリン組織体の構築とその酸素輸液への応用（若手招待講演）／第49回高分子学会年次大会、名古屋、2000年5月

7. 中川晶人、小松晃之、土田英俊／光照射によるアルブミン-ヘムの還元反応／第49回高分子討論会、仙台、2000年9月

8. 柳本徹也、早川祥一、小松晃之、土田英俊／オクトパスポルフィリン組織体の構造と酸素配位／第49回高分子討論会、仙台、2000年9月

（国際会議）

1. E. Tsuchida, "The Latest Progress on Electron Transfer in Macromolecule-Metal Complexes and Future Scope of MMC", IUPAC 8th International Symposium on Macromolecule-Metal Complexes, Tokyo, 5–8 Sept. 1999. (Plenary Lecture)

2. T. Yanagimoto, T. Komatsu, E. Tsuchida, "Self-Assembled Fibers Made of Lipidporphyrinato-zinc(II) and -iron(III) Complexes with an Intramolecular Coordinated Axial Imidazole", IUPAC 8th International Symposium on Macromolecule-Metal Complexes, Tokyo, 5–8 Sept. 1999.

3. T. Komatsu, T. Yanagimoto, E. Tsuchida, "Self-Assembled Fibers Made of Lipidporphyrinato-zinc(II) and -iron(II) Complexes with an Intramolecular Coordinated Axial Imidazole", 1st International Conference on Porphyrins and Phthalocyanines, Dijion (France), 25–30 June 2000.

4. T. Komatsu, T. Yanagimoto, S. Hayakawa, E. Tsuchida, "Nano-structure and Dioxygenation of Self-assembled Lipidporphyrins in Aqueous Media", The 2000 International Chemical Congress of Pacific Basin Societies, Honolulu (USA), 14–19 Dec. 2000.

5. A. Nakagawa, T. Komatsu, E. Tsuchida, "Photoreduction of Tetraphenylporphinato-iron(III) Derivative Incorporated into Recombinant Human Serum Albumin by LMCT Irradiation", The 2000 International Chemical Congress of Pacific Basin Societies, Honolulu (USA), 14–19 Dec. 2000.

6. A. Nakagawa, T. Komatsu, E. Tsuchida, "Photoreduction of Self-assembled Lipidporphyrinato-iron(III) Complex in Saline by LMCT Excitation", IUPAC 9th International Symposium on Macromolecule-Metal Complexes, New York (USA), 19–23 Aug. 2001.

3）研究目的

ポルフィリン鉄錯体が構成する組織体を利用して、水中における可逆的な酸素配位錯体系を実現した後に残る最重要課題は、酸素分子の脱着により自動酸化した高酸化状態中心鉄(III)の再還元過程の具体化にある。いわゆるメトヘムの化学還元は従来報告例も多いが、本研究では化学試剤を全く使用しない光電子によるポルフィリン鉄(III)錯体の酸素配位能復活法の確立を目指した。特に両親媒性置換基を導入したポルフィリン鉄誘導体（リピドポルフィリン）が水相系で自己集合して形成する組織体を対象に、自動酸化した中心鉄(III)の酸素配位活性能を復元するため、光照射による錯体部の非酵素的還元系の確立と、その機構解明を研究目的とした。

4）研究成果

4-1）近位塩基を有するリピドポルフィリンの自己組織体とその酸素配位

酸素錯体寿命の延長を志向する場合、軸配位子の電子供与度調節が電子過程制御の鍵となるので、軸塩基を分子内に導入した新しいポルフィリン誘導体を設計、ポルフィリン面上に4つのアルキルホスホコリン基と、ポルフィリン環2位置にイミダゾリルアルキル基を共有結合したリピドポルフィリン金属（Zn, Fe）錯体（**1**）を合成した。**1**は水中で容易に分散して、赤色均一の水溶液を与える。得られた水溶液は安定で、調製1年後でも沈殿凝集などは全く認められなかった。TEM観察から、**1**が自己集合して繊維状組織を形成することを解明（図1a）。cryo-TEMから見積もった繊維の幅（10 nm）は分子長（4.6 nm）の二倍に相当した（図1b）。

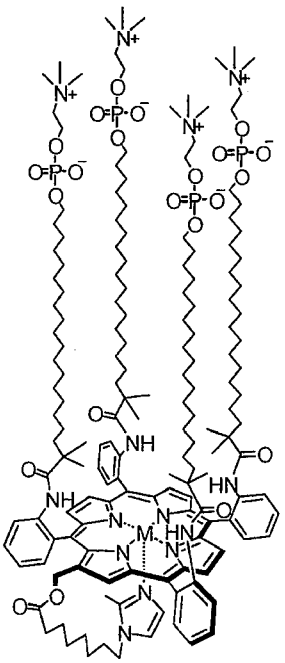

リピドポルフィリン（**1**）

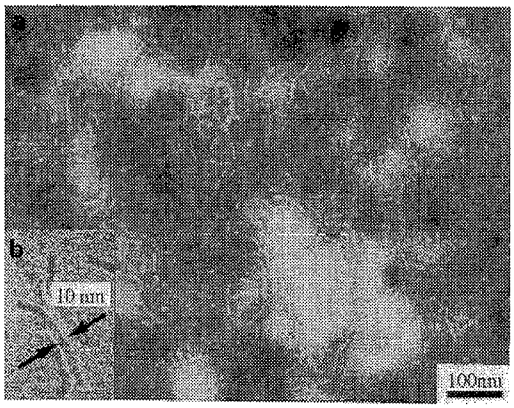

図1 リピドポルフィリン（**1**）繊維の（a）TEMと（b）cryo-TEM.

このリピドポルフィリン（**1**）繊維のAFM観察では、高さ2.8 nmの配向繊維像が得られ、ポルフィリン環 4 分子から成る管状構造の形成が示唆された。さらに、液中AFM観測によりリピドポルフィリン繊維の径（5.6 nm）を初めて実測（図 2a)、その三次元構造をsub-nm単位で明らかにすることができた。中心部はポルフィリン4量体が環構造を構成しており、それが 一次元に連続配列して繊維形成すると考えられる（図 2b)。このリピドポルフィリン繊維はきわめて安定で、pH 1 でも形態変化はない。酸性下（pH 3 以下）でも軸配位子にプロトン付加は起きず、これはイミダゾール部位が繊維の疎水中心に位置すると考えている。

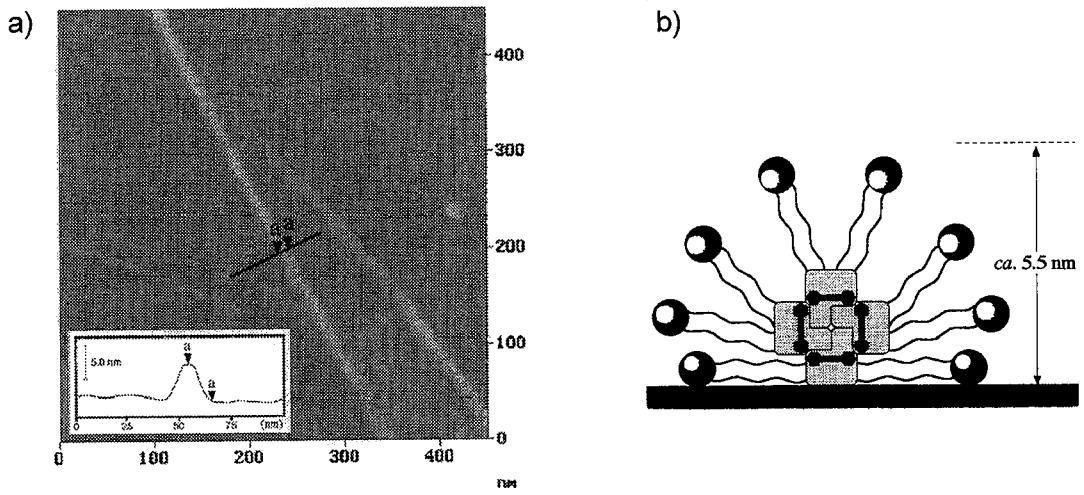

図 2 リピドポルフィリン（**1**）繊維の（a）水溶液中における AFM 像、（b）断面予想図.

リピドポルフィリン鉄(II)（**1**）繊維のUV-Vis.スペクトルは、窒素雰囲気下でλ_{max}: 444, 542, 567 nmを示した（図3a)。これは、中心鉄にイミダゾリル基が配位した5配位鉄(II)高スピン錯体の形成を示す。そこへ酸素を通気すると速やかに酸素錯体を形成（λ_{max}: 424, 549 nm）し、その酸素結合解離は酸素／窒素の吹き込みに伴い可逆的に変化した。また、一酸化炭素を通気すると、安定なカルボニル錯体（λ_{max}: 425, 540 nm）が得られた。ポルフィリン鉄錯体のみから構成される繊維状組織で安定な酸素錯体が観測された初めての例となった。

さらに、共鳴ラマンスペクトルから繊維を構成している鉄(II)ポルフィリン錯体の軸配位構造を解析した。中心鉄(II)は窒素雰囲気下で5配位高スピン状態をとるが、酸素の通気により6配位低スピン状態へ移行し、end-on型の酸素配位錯体の形成が明らかとなった（図3b)。

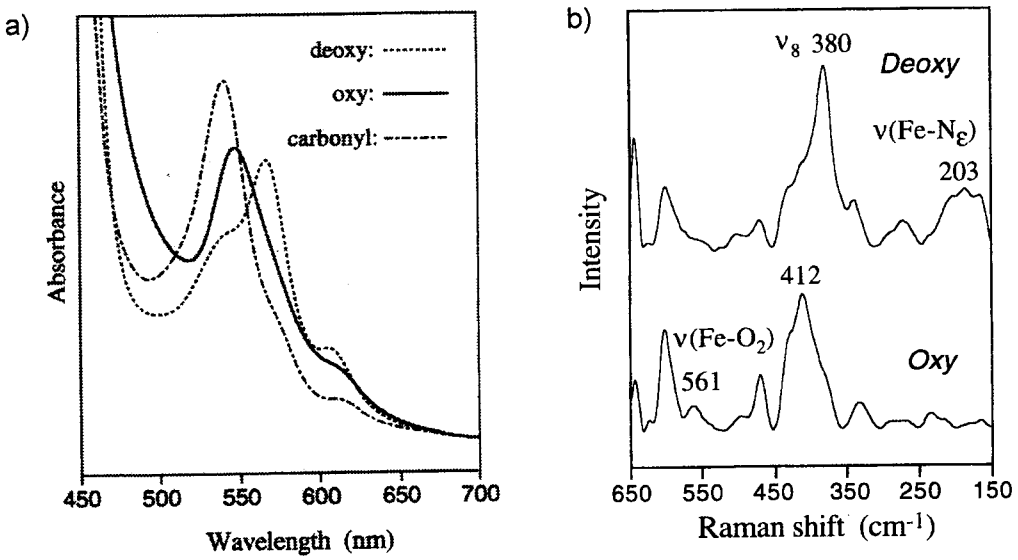

図 3 リピドポルフィリン（**1**）繊維の（a）酸素結合解離に伴う可視吸収スペクトル変化、（b）共鳴ラマンスペクトル変化.

酸素親和度（$P_{1/2}^{O2}$）は 25 Torr（25 °C）、酸素錯体半減期（$\tau_{1/2}$）は 約 4 hrs（25 °C）であった。レーザーフラッシュホトリシス法により、酸素結合解離速度定数（k_{on}, k_{off}）を決定、それらの値が単量体のものと変わらないことを明らかにした。

他方、メタノール添加により繊維構造は崩壊し、20%メタノール水溶液中では球状ミセル、80%を超えると単量体に解離した。球状ミセルを形成している時の酸素錯体寿命は、繊維構造の場合に比べて 10%に減少し、繊維構造が安定酸素錯体形成の必要条件と成ることが明確となった。

4-2) リピドポルフィリン鉄(III)－亜鉛(II)共組織体の光電子移動反応

リピドポルフィリン鉄(III)錯体（**1**）と微量のリピドポルフィリン亜鉛(II)錯体を混合し、過剰のリン脂質と共に水中で超音波攪拌すると、赤色の均一分散液が得られた。TEM 観察から、それら 3 種の成分が共集合して、粒径 30～40 nm の一枚膜小胞体を形成していることが明らかとなった。その水分散液を可視光照射すると、励起された亜鉛(II)錯体から鉄(III)錯体へ電子移動が生起した。蛍光寿命、励起三重項寿命の消光解析より求めた速度定数は、各々1.2×10^{11}、6.2×10^{4} $M^{-1}s^{-1}$で、トンネル機構と動的過程により鉄(III)錯体へ電子移動が起きている。この小胞体の外水相へトリエタノールアミン（犠牲試薬）を添加し光照射すると、**1** の鉄(II) 5 配位錯体が蓄積され、酸素の通気に伴い、速やかに酸素錯体を形成した。

4-3) リピドポルフィリン鉄繊維の光照射による中心鉄の還元と酸素配位能の復元

リピドポルフィリン鉄錯体（**1**）は、中心鉄が 2 価の場合、水中で自己組織化して繊維状組織を形成したが、3 価の場合は生理塩水溶液中（pH 7.3, [NaCl]=0.15 M）で粒径約 10 nm の球状ミセルを形成した。得られた水溶液は Fe(III)-Cl^-間の電荷移動吸収帯（LMCT）に基づく吸収をλ_{max}: 362 nm に示した。中心鉄の対ハロゲンイオンの電気陰性度の増大に伴いλ_{max}が低波長移動したことから、これが LMCT 吸収帯であることを確認。この吸収帯を窒素雰囲気下で光照射（λ: 365 nm, 250 W）しても、中心鉄の還元は起こらないが、グルコースなどの糖類を共存させて光照射すると、徐々に中心鉄の還元が生起し、最終的には 100% 還元された鉄(II) 5 配位高スピン錯体が得られた（図 4)。共存させる糖質は、グルコースのほか、ムコ多糖類（特にヒアルロン酸類）が有効であった（図 5)。

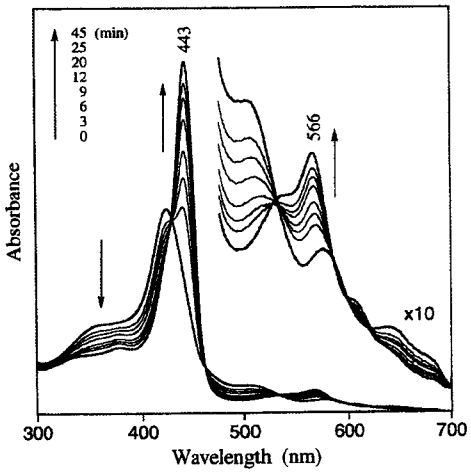

図 4 リピドポルフィリン鉄(III)水溶液へ光照射した時の可視吸収スペクトル変化（グルコース存在下、窒素雰囲気、λ: 365 nm）.

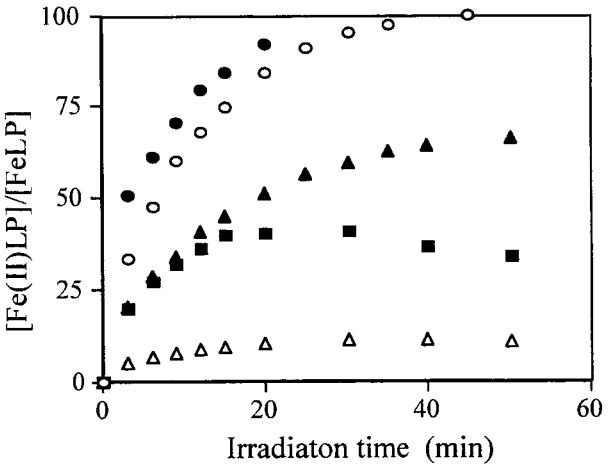

図 5 リピドポルフィリン鉄(III)水溶液の光還元（○: グルコース 150 mM、●: ヒアルロン酸 21mg/L、▲: アミロース 25 mg/L、■: コンドロイチン-6-硫酸 23mg/L、△: グルクロン酸、窒素雰囲気、λ: 365 nm）.

この光照射による中心鉄の還元反応は、LMCT 吸収帯を励起した時のみに進行することから、Cl^-と Fe(III)間の分子内電子移動により生成した Cl ラジカルが糖質に捕捉され、その結果、逆電子移動反応が阻止されたものと考察した。興味あることに、ヒアルロン酸の添加により、リピドポルフィリン鉄(III)錯体の集合形態は球状ミセルから繊維状組織に変化した。この共組織構造が効率の高い光還元反応に寄与しているもの推測される。溶液粘度は光還元の進行と共に減少。これはラジカル捕捉によりヒアルロン酸の解重合が進行したためと考えられる。

さらに、過渡吸収スペクトルの測定結果は、レーザー照射後 50 ns 以内に中心鉄

(III)の還元とイミダゾールの分子内配位が完了し、鉄(II)5 配位錯体が形成されることを示した。量子収率は0.007と高くはない。高い励起状態LMCT*から、分子内電子移動が起こり、電荷分離状態が生成、その過程で多くの励起種はS_2へ失活する（図6)。また、電荷分離した分子の多くも逆電子移動反応により基底状態へ戻る。生成した$Cl^{\cdot}$が糖に捕捉された場合にのみ還元が不可逆になるのであるから、妥当な量子収率と考えられる。得られた還元体（鉄(II)錯体）は、酸素の通気で速やかに酸素錯体を形成できた。

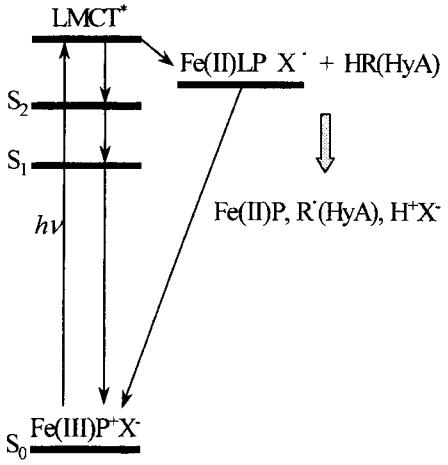

図 6　リピドポルフィリン鉄(III)－ヒアルロン酸からなる繊維組織体における光還元反応のメカニズム

4-4）アルブミン-ヘムの光照射による中心鉄の還元と酸素配位能の復元

ヒト血清アルブミンに疎水性のリピドポルフィリン鉄(II)錯体（**2**）を包接させて得たアルブミン-ヘム複合体（rHSA-FeP、図7）は、生理条件下（pH 7.3、37°C）で酸素を可逆的に結合解離できる合成ヘム蛋白質である。上記リピドポルフィリン鉄(III)繊維系で確立した中心鉄(III)の還元方法をアルブミン－ヘム複合体に適用したところ、添加物なしでも光還元が進行することが明らかとなった。

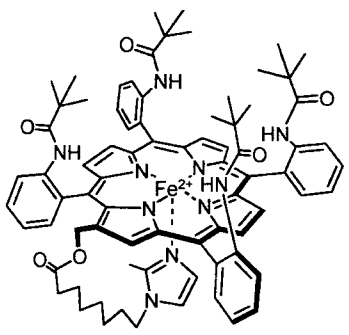

リピドポルフィリン（**2**）

図7　アルブミン－ヘムの構造

自動酸化して酸素配位活性を失った rHSA-Fe(III)P の UV-Vis. スペクトルは、330, 422, 565 nm にλ_{max}を有し、分子内イミダゾールと塩素イオンが両軸配位座に結合した 6 配位錯体の形成を示した。テトラフェニルポルフィリン鉄(III)-Cl^-への 1,2-ジメチルイミダゾールの配位定数は 4 M^{-1}と低いが、FeP が rHSA 内に固定されているために、6 配位錯体を形成すると考えられる。λ_{max}: 330 nm を Fe(III)-Cl^-間の LMCT 吸収帯と帰属した。CO 雰囲気下で rHSA-Fe(III)P 溶液を光照射 (λ: 365 nm, 250 W) すると、25 分後には Fe(II)-CO 錯体 (λ_{max}: 428, 540, 608 nm) が得られた (Φ: 0.01) (図 8a)。生成した鉄(II)錯体が CO と結合して安定な Fe(II)-CO 錯体を形成するため、逆電子移動反応が抑止されたものと推測される。CO 雰囲気でも NaCl が存在しないと還元率は著しく低い。

一方、Ar 雰囲気下で rHSA-Fe(III)P 溶液を光照射すると、15 分で 83%まで還元が進行し、鉄(II)5 配位錯体 (λ_{max}: 443, 541, 566 nm) が得られた (Φ: 0.008) (図 8b)。アルブミン内部では生成した $Cl^{\cdot}$がアミノ酸残基により捕捉されるため、糖質が共存しなくとも、Ar 雰囲気下で光還元が進むと考えられる。完全に還元が進行しないのは、自動酸化した Fe(III)P の一部でイミダゾールが脱離し、還元後に再配位できないためであろう。

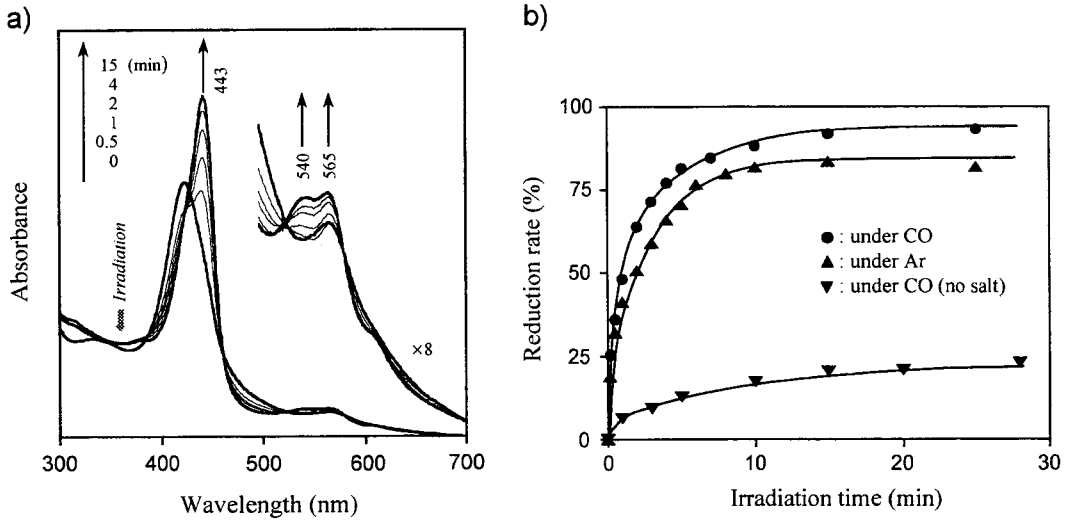

図 8 (a) rHSA-Fe(III)P 水溶液へ光照射した時の可視吸収スペクトル変化 (Ar 雰囲気、λ: 365 nm)、(b) LMCT 光照射による rHSA-Fe(III)P の光還元反応効率.

また、レーザーフラッシュ照射 100 ns 後の過渡吸収スペクトルが、鉄(II)5 配位錯体と鉄(III)-Cl^-錯体の差スペクトルに一致したことから、光照射による中心鉄の還元は 100 ns 以内に終了し、イミダゾールが分子内配位した 5 配位錯体を形成することが明らかとなった。LMCT 励起状態の多くは S_2 状態へ失活する。一部生成した電荷分

離状態（Fe(II)P…Cl˙）も、再結合前に rHSA が Cl˙を捕捉した場合に限り鉄(II)体の生成が不可逆となるため、本反応の量子収率は低い。得られた還元体に酸素を吹き込むと速やかに酸素錯体を形成し、その結合解離は可逆的であった。

以上の結果は、ヘム蛋白質の酸素配位能復活に限らず、この種の Redox 系に光電子利用が有効であることを明確にしたもので、具体的な応用展開にも繋がる成果と考えている。

5）まとめ

リピドポルフィリン鉄が水相系で自己組織化して形成する集合体を対象に、自動酸化した中心鉄(III)の酸素配位能を復元するため、(1) 微量の亜鉛ポルフィリンを共存させた共集合体中で、その光励起種から鉄ポルフィリンへの電子移動経路を構築する系、(2) Fe(III)-Cl^-の Ligand-Metal Charge Transfer (LMCT) 吸収帯の励起により生起する分子内電子移動を利用する系、の２つの非酵素的還元系を確立、その反応機構を解明した。

まず、分子内に軸塩基配位子としてイミダゾリルアルキル基を共有結合した新規なリピドポルフィリンを合成、これが水中で自己組織化して繊維状集合体（幅 10 nm、繊維長 2～3 μm）を形成することを明らかにした。さらに、液中 AFM 観測からポルフィリン４量体が一次元に連続配列した構造であることを実証。鉄(II)錯体は酸素を可逆的に結合解離できた。配位酸素の分極構造を共鳴ラマンスペクトルから解明、酸素親和度、酸素結合解離速度をレーザーフラッシュホトリシス法を用いて決定した。

リピドポルフィリン鉄(III)錯体と微量のリピドポルフィリン亜鉛(II)錯体を包埋したリン脂質二分子膜小胞体（粒径 30～40 nm）を可視光照射すると、励起された亜鉛(II)錯体から鉄(III)錯体へ電子移動が生起した。蛍光寿命、励起三重項寿命の消光解析より速度定数を算出。この分散液へトリエタノールアミンを添加し光照射すると、鉄(II)5配位錯体が蓄積され、酸素の通気に伴い、速やかに酸素錯体が形成された。

一方、リピドポルフィリン鉄(III)錯体の生理塩水溶液は、Fe(III)-Cl^-間の電荷移動（LMCT）に基づく吸収帯をλ_{max}:362nm に示した。対ハロゲンイオンの電気陰性度増大に伴いλ_{max}の低波長移行が認められたことから、これがLMCT帯であることを確認。少量の糖質（ヒアルロン酸、グルコースなど）を添加し、窒素雰囲気下で LMCT 吸収帯を光照射（365 nm）すると、中心鉄の還元が起こり5配位鉄(II)高スピン錯体が得られた。光還元反応の初期過程は分子内電子移動であるが、共存する糖質はこの電子移動の欠損を補充して酸化され、逆電子移動を抑止する。過渡吸収分光測定から 100 ns 以内に 5 配位鉄(II)高スピン錯体が形成されることを明らかにした。LMCT 励起状態からS_2への失活と、解離した FeP と $Cl^{\cdot}$の再結合により、量子収率は約 0.01 に留まる。得られた還元体（鉄(II)錯体）は、酸素の通気により速やかに酸素錯体を形成した。この機作に関しては、リピドポルフィリン鉄(III)錯体とヒアルロン酸が繊維状共集合体を形成することに意味があると考えている。

さらに、本還元系がアルブミン-ポルフィリン鉄(III)複合体に適応できることも実証。この場合アルブミン自身が電子供与体としての役割を果たし、光還元が進行する。

Self-Assembled Fibers Made of Lipidporphyrinato−Zinc(II) and −Iron(II) Complexes with an Intramolecular Coordinated Axial Imidazole

Teruyuki Komatsu, Tetsuya Yanagimoto, Yuka Furubayashi, Jian Wu, and Eishun Tsuchida*,†

Department of Polymer Chemistry, Advanced Research Institute for Science & Engineering, Waseda University, Tokyo 169-8555, Japan

Received November 5, 1998. In Final Form: March 23, 1999

Amphiphilic tetraphenylporphyrinato−metal (Zn(II), Fe(II)) derivatives with four alkylphosphocholine chains and an intramolecular coordinated axial imidazole (*lipidporphyrins*) produced stable colloidal solutions in water. Electron microscopy showed rodlike fibers with a uniform thickness of 10 nm, which corresponds to a double length of lipidporphyrin. The obtained fibers had some micellar characteristics and were sensitive to neither addition of electrolyte (for example, NaCl) nor change in pH. Scanning force microscopy (SFM) revealed evaporated fibers with a height of 2.8 nm on graphite. In the center of the fiber, there is probably a tetragonal tube constructed by densely packed porphyrin planes. The red shift in the broadened Soret band absorption by exciton interaction and the photophysical properties of the Zn(II) complex fibers suggested the formation of porphyrin *J-aggregates*. Furthermore, the first SFM images of the porphyrin fibers under liquid conditions are given. A Benesi−Hildebrand analysis revealed that the unit aggregate number for the Zn(II) complex was four, supporting a tetramer repeating structure. Fe(II) complex fibers, on the other hand, produced a kinetically stable O_2 adduct reversibly at 25 °C. The coordination structures of the axial imidazole and O_2 molecule in the Fe(II) complex have been clarified by resonance Raman spectroscopy. The O_2-binding equilibrium and kinetic parameters were also evaluated.

Introduction

It has been of great interest to construct a three-dimensional molecular structure using noncovalent bond formation which involves self-assembling of amphiphilic molecules in water.[1−4] A topic of current concern is now being shifted from their topologies to specific functions associated with their structures. Porphyrin amphiphiles are one of the attractive building blocks for creating functional molecular architecture in aqueous media. Systematically aligned multiporphyrins will act as novel hemoprotein analogues and/or photochemical devices which should have different characteristics from those in natural systems. The most prominent porphyrin in nature, namely protoporphyrin IX, is an amphiphile with two propionic acid side chains. It actually forms micelles in water with a split Soret band absorption.[5,6] The nanostructure of this aggregate has, however, not been clarified so far, because of its low stability. More recently, several synthetic porphyrin amphiphiles have been self-organized in bulk aqueous solution, producing well-defined structures (monomolecular fibers, platelets, and bimolecular vesicles), in which the highly ordered porphyrin arrays can, for example, act as light harvesting centers for photoinduced charge separation.[7−9]

If one designs the hemoprotein functions, one should attach an axial base, for example, imidazole, covalently to the parent porphyrinato−iron(II), because it plays a crucial role in displaying the biological activity of hemoproteins. Indeed, an imidazole directly attached onto the porphyrin periphery has enhanced the stability of the O_2 adduct and also avoided oxidation of the central Fe(II) ion.[10] A great deal of labor has been, however, required to introduce an imidazolyl group into the porphyrin structure during construction of a bulky cavity around the O_2-binding site to prevent undesirable μ-oxo dimer formation.[11−13] There has been no example of molecular assembly consisting of amphiphilic porphyrins wherein

* To whom correspondence should be addressed. Phone: +81 3-5286-3120. Fax: +81 3-3205-4740. E-mail: eishun@mn.waseda.ac.jp.

† CREST investigator, Japan Science and Technology Corporation.

(1) Fendler, J. H. *Membrane Mimetic Chemistry*; John Wiley and Sons: New York, 1982.

(2) Vögtle, F. *Supramolecular Chemistry*; Wiley: Chichester, U.K., 1991.

(3) (a) Fuhrhop, J.-H.; Helfrich, W. *Chem. Rev.* **1993**, *93*, 1565. (b) Fuhrhop, J.-H.; Köning, J. *Membranes and Molecular Assemblies: The Synkinetic Approach*; The Royal Society of Chemistry: Cambridge, U.K., 1994.

(4) *Comprehensive Supramolecular Chemistry, Vol. 9; Templating, Self-assembly, and Self-organization*; Sauvage, J.-P., Hosseini, M. W., Eds.; Pergamon: Oxford, U.K., 1996; Chapters 9−11.

(5) Fuhrhop, J.-H.; Demoulin, C.; Böttcher, C.; Köning, J.; Siggel, U. *J. Am. Chem. Soc.* **1992**, *114*, 4159.

(6) Inamura, I.; Uchida, K. *Bull. Chem. Soc. Jpn.* **1991**, *64*, 2005.

(7) (a) Fuhrhop, J.-H.; Bindig, U.; Siggel, U. *J. Am. Chem. Soc.* **1993**, *115*, 11036. (b) Endisch, C.; Böttcher, C.; Fuhrhop, J.-H. *J. Am. Chem. Soc.* **1995**, *117*, 8273.

(8) (a) Tsuchida, E.; Komatsu, T.; Arai, K.; Yamada, K.; Nishide, H.; Böttcher, C.; Fuhrhop, J.-H. *Langmuir* **1995**, *11*, 1877. (b) Tsuchida, E.; Komatsu, T.; Arai, K.; Yamada, K.; Nishide, H.; Böttcher, C.; Fuhrhop, J.-H. *Chem. Commun.* **1995**, 1877. (c) Komatsu, T.; Yamada, K.; Tsuchida, E.; Siggel, U.; Böttcher, C.; Fuhrhop, J.-H. *Langmuir* **1996**, *12*, 6242. (d) Komatsu, T.; Tsuchida, E.; Böttcher, C.; Donner, D.; Messerschmidt, C.; Siggel, U.; Stocker, W.; Rabe, J. P.; Fuhrhop, J.-H. *J. Am. Chem. Soc.* **1997**, *119*, 11660. (e) Komatsu, T.; Yanagimoto, T.; Tsuchida, E.; Siggel, U.; Fuhrhop, J.-H. *J. Phys. Chem. B* **1998**, *102*, 6759.

(9) Guilard, R.; Senglet, N.; Liu, Y. H.; Sazou, D.; Findsen, E.; Fanre, D.; Courieres, T. D.; Kadish, K. M. *Inorg. Chem.* **1991**, *30*, 1898.

(10) Chang, C. K.; Traylor, T. G. *J. Am. Chem. Soc.* **1973**, *95*, 5810, 8477.

(11) Baldwin, J. E.; Cameron, J. H.; Crossely, M. J.; Dagley, I. J.; Hall, S. R.; Klose, T. *J. Chem. Soc., Dalton Trans.* **1984**, 1739.

(12) Collman, J. P.; Brauman, J. I.; Doxsee, K. M.; Halbert, T. R.; Bunnenberg, E.; Linder, R. E.; LaMar, G. N.; Gaudio, J. D.; Lang, G.; Spartalian, K. *J. Am. Chem. Soc.* **1980**, *102*, 4182.

(13) Momenteau, M.; Mispelter, J.; Loock, B.; Lhoste, J.-M. *J. Chem. Soc., Perkin Trans. 1* **1985**, *1995*, 221.

10.1021/la981566s CCC: $18.00
Published on Web 05/22/1999

the imidazole is actually attached to their structures. We report herein for the first time long-lived fibers made of tetraphenylporphyrinato–metal (Zn(II), Fe(II)) derivatives with four alkylphosphocholine groups on one side of the ring plane and an imidazolylalkyl arm at the periphery (*lipidporphyrins*). The images of scanning force microscopy (SFM) under ambient conditions showed a uniform height of the fiber on graphite, suggesting regular alignment of the rigid porphyrin planes in the center. The Zn(II) complex fibers fluoresce strongly, and the Fe(II) fibers produce a reversible O_2 adduct in aqueous solution as do hemoglobin and myoglobin. The coordination structure of the axial imidazole and O_2 molecule in lipidporphyrinato–iron(II) has been clarified by resonance Raman spectroscopy. The O_2-binding equilibrium and kinetic properties were also evaluated.

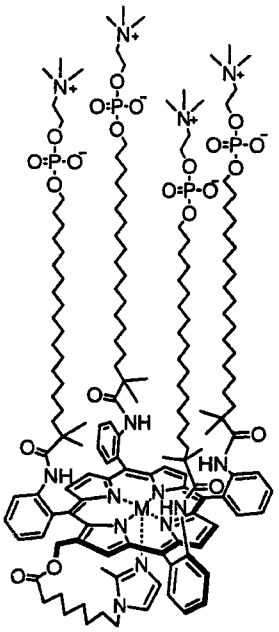

6

M: Zn(II) **c**
Fe(III)Br **d**
Fe(II) **e**

Experimental Section

Methods and Materials. Infrared spectra were recorded with a JASCO FT/IR-410 spectrometer. ^{1}H NMR spectra were measured with samples dissolved in $CDCl_3$ or CD_3OD using a JEOL Lambda 500 spectrometer. Chemical shifts were expressed in parts per million downfield from Me_4Si as an internal standard. FAB-MS spectra were obtained from a JEOL JMS-SX102A spectrometer. UV–vis absorption spectra were recorded on a JASCO V-570 spectrophotometer. Thin-layer chromatography (TLC) was carried out on 0.2 mm precoated plates of silica gel 60 F_{254} (Merck). Purification was performed by silica gel 60 (Merck) or Sephadex LH-60 gel (Pharmacia) column chromatography. Fluorescence emission spectra were measured with a Hitachi F-4500. Circular dichroism (CD) spectra were obtained with a JASCO J-720WI spectropolarimeter.

5,10,15,20-Tetrakis{α,α,α,α-*o*-(2,2-dimethyl-20-hydroxyicosanamide)phenyl}porphin, 8-(2-methylimidazolyl-1-yl)octanoic acid, and 2-chloro-2-oxo-1,3,2-dioxophospholane were prepared according to the previously reported procedures.[14,15] All solvents were purified by distillation before use. Other chemicals were commercial high-purity grades and not further purified. The water used was deionized using a ADVANTEC GS-200 system.

We applied Vilsmeir formylation to join an ω-imidazolylalkyl arm to the β-pyrrolic position of 5,10,15,20-tetrakis{α,α,α,α-*o*-(2,2-dimethyl-20-hydroxyicosanamido)phenyl}porphin (Scheme 1).[15] The four hydroxyl terminals of the C_{20} chains were first protected by chloroacetyl groups, giving **1a**. The Vilsmeier reaction with its copper complex (**1b**) in refluxing $CHCl_3$ led to creation of a formyl group at the 2-position of the porphyrin (**2b**: 34%). After demetalation in H_2SO_4/CH_2Cl_2 (70%), the formyl appendix was reduced to a hydroxymethylene group with $NaBH_4$ (**3a**: 83%), which was coupled with 8-(2-methylimidazolyl-1-yl)-octanoic acid by a mixed anhydride method with pivaloyl chloride, affording **4a** (57%). The chloroacetyl protections were selectively removed with hydrazinedithiocarbonate at 0 °C (**5a**: 45%).[16] The four phosphocholine moieties were then introduced as hydrophilic head groups to produce lipidporphyrin (**6a**). A zinc ion was finally inserted to yield the lipidporphyrinato–zinc(II) complex (**6c**), while the iron insertion was carried out before the phosphorylation. Experimental details of the syntheses, ^{1}H NMR spectra, and IR, UV–vis, and MS spectra are supplied as Supporting Information.

Preparation of Aqueous Lipidporphyrin Solutions. *(a) Lipidporphyrinato–Zinc(II) or –Iron(III) Solution.* A methanol solution of **6c** (or **6d**) (50 μL, 1.2 mM) was, for example, rapidly injected into deionized water (3 mL) heated to 70 °C ([CH_3OH] < 2 vol %), and the obtained homogeneous solution (20 μM) was incubated for 4 h at room temperature.

(b) Lipidporphyrinato–Iron(II) Solution. A 4-fold molar excess of aqueous ascorbic acid was first added to a **6d** methanol solution (50 μL, 1.2 mM) under a CO atmosphere. The color of the solution immediately changed from brown to bright red, giving the carbonyl iron(II) complex. The injection of this methanolic **6e** into water (3 mL, 70 °C) under CO and incubation for 4 h at room temperature provided an aqueous dispersion of CO-coordinated **6e** (20 μM). Excess ascorbic acid was then removed by dialysis with a cellulose tube in deionized water for 4 h at 4 °C to less than 4 mol % of the **6e** concentration. Light irradiation (incandescent lamp, 500 W) of this dispersion under argon allowed CO dissociation, providing a red homogeneous aqueous solution of the five-N-coordinated lipidporphyrinato–iron(II).

Transmission Electron Microscopy (TEM). The negatively stained specimens for TEM and the vitrified specimens for cryo-TEM were prepared as previously reported.[8] The obtained grids were observed in a JEOL JEM-100CX electron microscope or a Phillips CM12 using a Gatan cold stage model 626 at an acceleration of 100 kV.

Scanning Force Microscopy (SFM). *(a) Ambient Conditions.* A droplet of **6c** fiber solution (1–5 μM) was pipetted onto freshly cleaved highly oriented pyrolytic graphite (HOPG STM-1, Advanced Ceramics Co.) or mica. After 1 min, excess fluid was carefully blotted off with filtration paper and the HOPG was air-dried for another 1 h. SFM measurements were carried out using a Nanoscope III system (Digital Instruments Inc.) in the tapping mode under ambient laboratory conditions. Silicon cantilevers (length 125 μm) with a spring constant between 21 and 78 N/m and a resonance frequency in the range 260–410 kHz were used. The scanning rate was usually 1.0 Hz. Imaging was performed displaying the amplitude signal and the height signal, simultaneously.

(b) Liquid Conditions. For in situ SFM measurements under liquid conditions, the specimens were prepared as follows. A droplet of the **6c** fiber solution (1–5 μM) was first put onto freshly cleaved HOPG. After excess fluid was blotted off, the HOPG was immediately placed into the SFM unit equipped with a MTFML liquid cell holder (Digital Instruments Inc.). During SFM imaging in the tapping mode, the specimen was immersed in deionized water in the liquid cell. Si_3N_4 cantilevers (length 200 μm) with a spring constant between 0.01 and 0.2 N/m and a resonance frequency in the range 5–50 kHz were used.

Excited-State Lifetime Measurements. Singlet lifetimes of **6c** were measured using a Horiba NAES-500 single-photon counter with a hydrogen lamp (excited at 300–400 nm, emission

(14) Matsushita, Y.; Hasegawa, E.; Eshima, K.; Tsuchida, E. *Chem. Lett.* **1983**, 1387.
(15) Tsuchida, E.; Komatsu, T.; Kumamoto, S.; Ando, K.; Nishide, H. *J. Chem. Soc., Perkin Trans. 2* **1995**, 747.
(16) van Boeckel, C. A. A.; Beetz, T. *Tetrahedron Lett.* **1983**, *24*, 3775.

Scheme 1. Synthetic Scheme of Lipidporphyrinato–Zinc(II) (6c) and –Iron(III) Bromide (6d) Complexes[a]

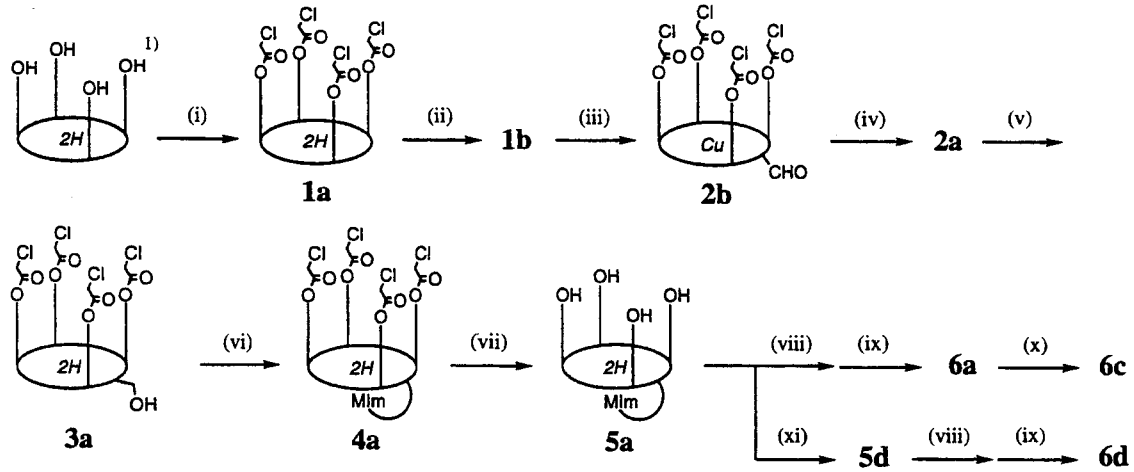

[a] 1) *meso*-tetrakis{α,α,α,α-*o*-(2,2-dimethyl-20-hydroxyicosanamide)phenyl}porphin; (i) chloroacetyl chloride/CH_2Cl_2, TEA; (ii) $CuCl_2$/$CHCl_3$, CH_3OH, TEA; (iii) $POCl_3$, DMF/$CHCl_3$; (iv) conc H_2SO_4/CH_2Cl_2; (v) $NaBH_4$/CH_2Cl_2, CH_3OH; (vi) 8-(2-methylimidazolyl-1-yl)octanoic acid pivalic acid anhydride/THF, DMAP; (vii) hydradinedithiocarbonate/AcOH, 2,6-lutidine; (viii) 2-chloro-2-oxo-1,3,2-dioxophospholane/CH_2Cl_2, TEA; (ix) trimethylamine/DMF; (x) $Zn(AcO)_2$/CH_3OH; (xi) $FeBr_2$/THF, 2,6-lutidine.

monitored at <400 nm). The samples were held in a cuvette (optical path length 1 cm) and purged of dioxygen by argon bubbling for 30 min. All experiments were carried out at 25 °C.

Triplet lifetime measurements were performed using a Unisoku TSP-600 time-resolved spectrophotometer system with a Continuum Surelite I-10 Q-switched Nd:YAG laser, which generated a second-harmonic (532 nm) pulse of 6 ns duration with an energy of 200 mJ per pulse (10 Hz). A 150 W xenon arc-lamp was used as the monitor light source. The triplet decay of **6c** was monitored by transient absorption at 455 nm. The concentration of **6c** was normally 5 μM, and experiments were carried out at 25 °C.

Estimation of Aggregate Size. When the aqueous solution of the **6c** fibers (10–25 μM) and the 1,2-bis(myristoyl-*sn*-glycero)-3-phosphocholine (DMPC) vesicular solution (200 μM) were mixed, the absorption spectrum of **6c** changed slowly from the aggregate type to the monomer one: the broadened Soret band became sharp within 30 h at 35 °C. This observation indicates the gradual incorporation of the **6c** molecules into the DMPC bilayer membrane. The isosbestic points observed show that only two dominant species, an aggregate and a monomer, are involved in the process. On the basis of a modified Benesi–Hildebrand plot of the absorbance of the aggregate and monomer equilibrium with the moderate ratio, the aggregate size was estimated.[19,20]

Resonance Raman Spectroscopy. The obtained **6e** (0.5 mL, 1.5 mM) solution in a quartz cuvette (optical path length 2 mm) was used for resonance Raman spectroscopic measurements. Dioxygenation was achieved by O_2 bubbling into the solution for 1 min. Resonance Raman spectra were obtained with excitation of the 457.9 nm line of an NEC GLG2162 Ar^+ ion laser in a backscattering geometry at 25 °C. All the spectra were recorded using a JASCO NRS-2000 laser Raman spectrometer equipped with a CCD multichannel detector. Calibration of the spectrometer was performed with indene.

O_2 and CO Binding Equilibrium and Kinetics. O_2 and CO binding to the lipidporphyrinato–iron(II) was expressed by

$$\mathrm{FeP} + \mathrm{L} \underset{k_{off}^{L}}{\overset{k_{on}^{L}}{\rightleftharpoons}} \mathrm{FeP{\cdot}L} \qquad (1)$$

$$(K^{L} = k_{on}{}^{L}/k_{off}{}^{L})$$

where FeP is lipidporphyrinato–iron(II) (**6e**) and L is the gaseous ligand, O_2 or CO. The O_2 and CO binding affinities (gaseous pressure at half O_2 or CO binding for **6e**, $P_{1/2}{}^{L} = 1/[K^{L}]$) were determined by spectral changes at various partial pressures of O_2 and CO, as in previous reports.[8a,15–18] For UV–vis absorption spectroscopy, **6e** concentrations of 20 μM were normally used. The spectra were recorded within the range 350–700 nm. O_2 binding kinetics were measured with a competitive rebinding technique provided by Gibson and Traylor using a laser flash photolysis apparatus (a Unisoku TSP-600 system described above).[8a,15–18] The O_2 and CO association and dissociation rate constants (k_{on}, k_{off}) were determined as described previously.

Results and Discussion

Lipidporphyrinato–Zinc(II) Assembly. The UV–vis absorption spectrum of the monomeric Zn(II) complex (**6c**) in methanol showed typical five-N-coordinated species (λ_{max}: 426, 520, 559, 598 nm) and followed Beer's law in the range 1 μM to 2 mM and 5–55 °C. In the ^1H NMR spectrum of **6c** in CD_3OD, all signals for the imidazole ring and the neighboring methylene groups were significantly upfield shifted (e.g., δ: 0.8 ppm, 2-CH_3 (Im)) by the porphyrin ring current. These results show that the covalent linkage between the axial base and the porphyrin periphery is long enough to allow Zn(II)–imidazole coordination.

Upon rapid injection of the methanolic **6c** into deionized water, a bright-red homogeneous solution was obtained ([CH_3OH] < 2 vol %). This solution did not change for more than 6 months at room temperature, and no precipitation was observed. Transmission electron microscopy of the negatively stained and evaporated colloid showed rodlike fibers with a uniform thickness of 10 nm, which corresponded to the double length of **6c** (Figure 1a). Cryomicroscopy of the vitreous ice layer of this solution also showed the same images (Figure 1b).

Most probably, **6c** forms a micellar fiber in which the hydrophobic tetraphenylporphyrin moieties with an intramolecular coordinated imidazole are all forced together into the center. If this is true, a low-density area of lipophilic chains would be present on the periphery, because only a few porphyrin boxes (1.3 × 1.3 × 1.4 nm^3) can occupy the middle of the thin fiber (Figure 1d, vide

(17) Traylor, T. G.; Tsuchiya, S.; Campbell, D.; Mitchell, M.; Stynes, D.; Koga, N. *J. Am. Chem. Soc.* **1985**, *107*, 604.

(18) Collman, J. P.; Brauman, J. I.; Iverson, B. L.; Sessler, J. L.; Morris, R. M.; Gibson, Q. H. *J. Am. Chem. Soc.* **1983**, *105*, 3052.

(19) Benesi, H. A.; Hildebrand, J. H. *J. Am. Chem. Soc.* **1949**, *71*, 2703.

(20) (a) Song, X.; Geiger, C.; Leinhos, U.; Perlstein, J.; Whitten, D. G. *J. Am. Chem. Soc.* **1994**, *116*, 4103. (b) Chen, H.; Farahat, M. S.; Law, K.-Y.; Whitten, D. G. *J. Am. Chem. Soc.* **1996**, *118*, 2584.

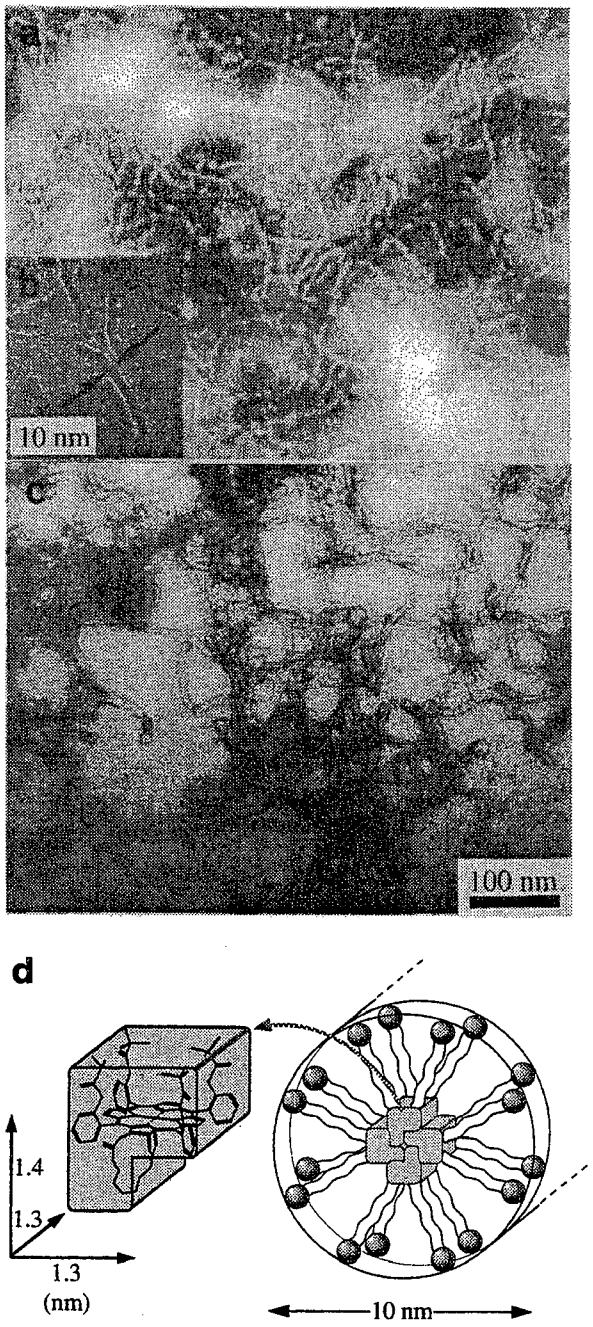

Figure 1. Transmission electron micrographs of the **6c** fibers: (a) negatively stained sample with phosphotangstate at pH 7; (b) cryopreparation in vitreous ice without staining; (c) negatively stained sample with uranyl acetate at pH 1; and (d) proposed structure of the **6c** (or **6e**) fibers.

infra). Indeed, the alkylphosphocholine groups of the **6c** fibers have some micellar characteristics: (1) the DSC thermogram did not show any definite peak at 10–70 °C, indicating no gel-to-liquid-crystal phase transition, and (2) the ^{1}H NMR spectra of the fibers with D_2O showed a symmetrically sharp signal of the choline methyl group at 3.4 ppm ($\Delta\delta_{1/2}$: 100–60 Hz) independent of the temperature range (30–70 °C). In contrast, the resonances of the porphyrin planes and imidazole protons are rather broadened even at 70 °C, representing a densely packed porphyrin arrangement.

In the UV–vis absorption spectrum of the **6c** fibers, the most remarkable observation is the red-shifted Soret band (λ_{max}: 426 → 432 nm) with a shoulder (443 nm) relative to that of the monomeric methanol solution (Figure 2).

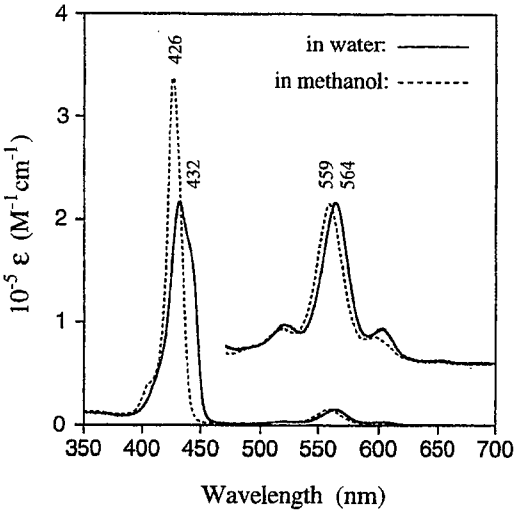

Figure 2. UV–vis absorption spectra of **6c** at 25 °C.

The bandwidth at half-height ($\Delta\lambda_{1/2}$: 24 nm) was significantly larger than that of the monomer ($\Delta\lambda_{1/2}$: 13.5 nm). This broadened Soret band was constant with relative intensities independent of concentration (1 μM to 2 mM) and did not exhibit a shift with changing temperature (5–70 °C), indicating the restrained mobility of the porphyrin planes. The red shift of the Soret band should be, therefore, due to exciton interactions, which are attributed to a lateral arrangement (*J-aggregate*) of the transition moments of the porphyrin chromophores.[21]

The **6c** fibers were not sensitive to the presence of electrolytes. Sodium chloride (0.15 M), for example, caused no precipitation. To our surprise, addition of hydrochloric acid down to pH 1 also did not change their morphology (Figure 1c) and the UV–vis absorption spectrum as well. This implies that HCl cannot react with the coordinated imidazole (no dissociation) and the central Zn(II) ion (no demetalation). The fiber's center, constructed of tetraphenylporphyrin moieties with eight methyl groups on each ring plane, is sufficiently shielded from the bulk aqueous solution. The imidazole rings coordinated to the porphyrin plane should be located in the hydrophobic core of the fibers. Actually, monomeric **6c** in CH_3OH/H_2O (10/1: v/v) dissociates the imidazole easily below pH 4, owing to the protonation of the imidazole ring, producing four-coordinated species (λ_{max}: 425, 557 nm). Addition of excess methanol could only destroy the fibers. Its absorption spectrum (λ_{max}: 432 nm) was shifted relative to that of the monomer (λ_{max}: 426 nm) by increasing the methanol concentration. Up to 30 vol % of methanol, which is a critical concentration for the fiber formation, the structure was gradually dissociated, and it completely disappeared above 75 vol % of methanol.

SFM Measurements and Porphyrin Arrangement in the Fiber. The aqueous **6c** fiber solution was then transferred to highly oriented pyrolytic graphite (HOPG) and subjected to scanning force microscopy (SFM) under ambient conditions. The parallel stripes with a width of 15–20 nm became detectable (Figure 3a). They are obviously images of dried and flattened **6c** fibers on the graphite surface. In contrast, the fibers were collapsed on mica. We assumed that hydration is responsible for the strong absorption of the fibers on the hydrophilic mica. Zooming in to a smaller scan area (320 × 320 nm^2) on HOPG reveals more detailed information (Figure 3b). The

(21) Hochstrasser, R. M.; Kasha, M. *Photochem. Photobiol.* **1964**, *3*, 317.

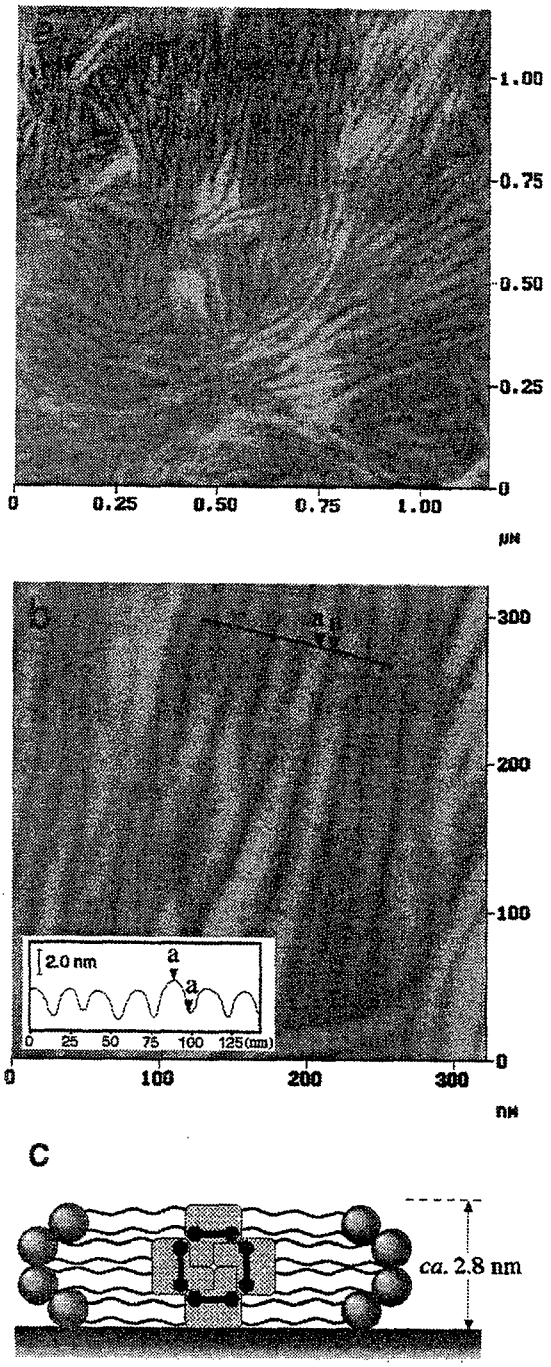

Figure 3. SFM images (tapping mode) and proposed model of the evaporated sample of the **6c** fibers on HOPG. (a) Image size is 1.17 × 1.17 μm^2 (z-range: 20 nm). (b) Image size is 320 × 320 nm^2 (z-range: 20 nm) (vertical a–a distance: 2.8 nm). (c) Schematic illustration of the perpendicular cross section of the dried fiber on the graphite surface. The black areas indicate the tetraphenylporphyrin planes, where all Zn(II)-coordinated imidazolylalkyl arms are forced together into the center, producing a hydrophobic tetragonal porphyrin unit. They are then laterally ordered to form a fiber.

measured heights of the evaporated fibers were regularly 2.8 nm (vertical distance between a and a in Figure 3b), which should correspond to the diameter of the rigid fiber's center. For evaluation of the lateral size, one should consider the horizontal broadening effect of the tip's shape, but it is not necessary for the vertical distance.[22,23] We

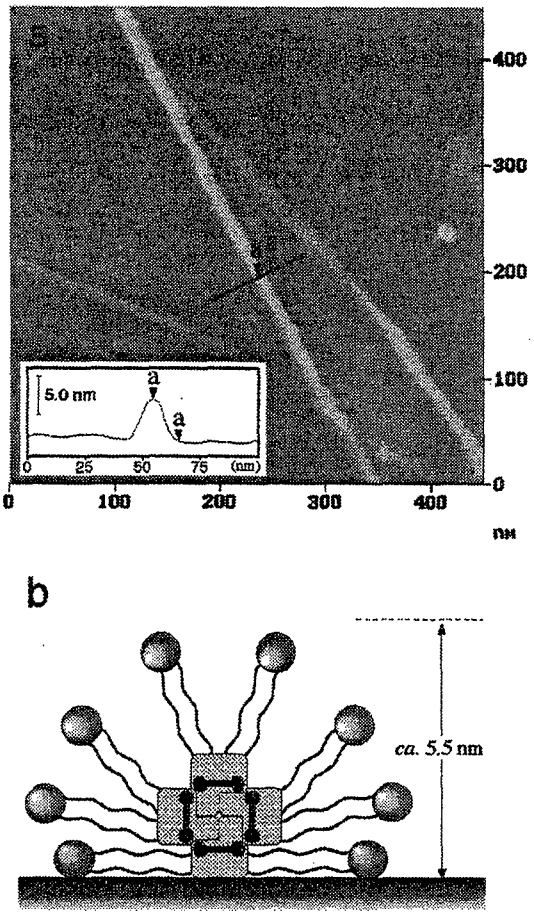

Figure 4. SFM image (tapping mode) and proposed model of the water-immersed sample of the **6c** fibers on HOPG. (a) Image size is 450 × 450 nm^2 (z-range: 10 nm) (vertical a–a distance: 5.6 nm). (b) Schematic illustration of the perpendicular cross section of the fiber. The black areas indicate the tetraphenylporphyrin planes, where axially coordinated imidazolylalkyl arms are forced together into the center, producing a hydrophobic tetragonal porphyrin unit. The bottom part of the fiber is bound to the hydrophobic HOPG surface, and the rest of the fiber has a more dynamic micellar structure.

therefore proposed a tetragonal tube model constructed by the porphyrin macrocycles (Figure 1d). In the middle of the fiber's section, four porphyrin planes are oriented perpendicularly to each other, forming a tetragonal unit, and the interior is occupied by Zn(II)-coordinated imidazolylalkyl arms. The porphyrin planes are then aligned laterally, producing long fibers. The heights of evaporated fiber (2.8 nm) coincided to the sum of one side, and a double thickness of the tetraphenylporphyrin moiety involved four amide substituents on the ortho position of the phenyl rings (2.9 nm) (Figure 3c).

SFM force curves generally show a much smaller adhesion between the sample and the tip under liquid conditions rather than under air.[24] As expected, imaging of the **6c** fibers immersed in water gave better resolution. This is the first SFM picture of the fibrous porphyrin assembly in aqueous media. The morphology was observed to be rather straight, which may indicate that these fibers recognize the lattice axes of the graphite.[25] The height of

(22) Butt, H.-J.; Gerharz, B. *Langmuir* **1995**, *11*, 4735.
(23) Odin, C.; Aime, J. P.; Kaakour, Z. El.; Bouhacina, T. *Surf. Sci.* **1994**, *317*, 321.
(24) (a) Hansma, H. G.; Vesenka, J.; Siegerist, C.; Kelderman, G.; Morrett, H.; Sinsheimer, R. L.; Elings, V.; Bustamante, C. *Science* **1992**, *256*, 1180. (b) Guthold, M.; Bezanilla, M.; Erie, D. A.; Jenkins, B.; Hansma, H. G.; Bustamante, C. *Proc. Natl. Acad. Sci. USA* **1994**, *91*, 12927.
(25) Manne, A.; Cleveland, J. P.; Gaub, H. E.; Stucky, G. D.; Hansma, P. K. *Langmuir* **1994**, *10*, 4409.

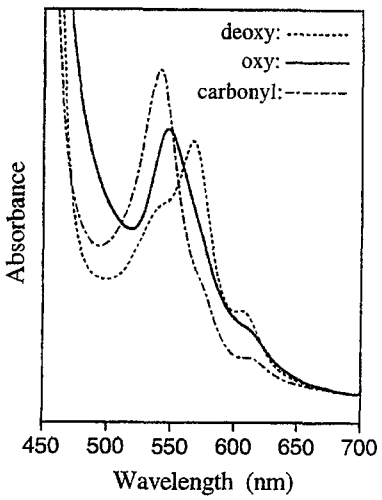

Figure 5. Visible absorption spectral changes of **6e** fibers in water at 25 °C.

the fiber now becomes 5.5 nm (vertical distance between a and a in Figure 4a). The bottom molecules are probably bound to the graphite, while the rest of the fibrous micelle is more dynamic (Figure 4b). The measured distance is exactly the same as the calculated value of the hemimicellar rod adhered onto the surface (5.6 nm).

Excitation State Properties of the Lipidporphyrinato–Zinc(II) Fibers. The aqueous solution of the **6c** fibers fluoresces, but the fluorescence emission intensity was approximately 38% of the methanolic monomer solution. The excitation spectrum of the fibers corresponded to its absorption pattern, clearly indicating that the fluorescence emission originates from the aggregates. Concomitantly, the excited singlet state lifetime of the fibers was determined to be 3.6 ± 0.9 ns, which was also identical to that of the monomers ($\tau_F = 5.3 \pm 0.9$ ns). The decrease in fluorescence intensity suggests an acceleration of the nonradiative decay from the first excited singlet state presumably due to vibrational interaction in the assembly.

Laser flash photolysis was also carried out by nanosecond laser excitation. The transient absorption spectra of the methanolic **6c** monomer solution essentially displayed the triplet–triplet (T–T) absorption in which the dark decay obeyed first-order kinetics ($\tau_T = 350$ μs) and was strongly accelerated by the presence of O_2. Excitation of the **6c** fibers, on the other hand, gave only 5% of the monomer signals with a short lifetime ($\tau_T \approx 30$ μs). These observations in the excited singlet and triplet states are quite similar to those of the porphyrin bilayered vesicles[8a] and monolayered sheets,[8e] which are made of lateral porphyrin aggregates. Whitten has also reported a large decrease in the τ_T for 5,10,15,20-tetrakis(α^4-hexanamidophenyl)porphin *J-aggregates* with a small amount of surfactant in aqueous media.[26] By contrast, fluorescent octopus-porphyrin fibers wherein the porphyrin rings stacked with a relatively large distance of 1.1 nm showed a long-lived T–T absorption.[8c] Thus the **6c** fibers are obviously classified as the former "*J-aggregate*" type. The large quenching in the triplet state compared to their fluorescence is presumably due to the increase in the rate constant of triplet deactivation by the edge-to-edge arrangement of the porphyrin planes in the fiber.[8e]

Mixing of DMPC vesicular solution with the **6c** fibers leads to clean spectral changes from the aggregate to the monomer. The isosbestic points observed in the dilution process allow determination of the aggregate number by a modified Benesi–Hildebrand analysis.[19,20] This was found to be 4.1, representing four **6c** molecules per unit aggregate. From these results and SFM measurements, the tetramer repeating structure in the fiber is conceivable. On the other hand, no induced circular dichroism (ICD) signal was observed for the aqueous solution of the **6c** fibers, suggesting the tetramer units do not have any chirality.

(26) Barber, D. C.; Freitag-Beestron, R. A.; Whitten, D. G. *J. Phys. Chem.* **1991**, *95*, 4074.

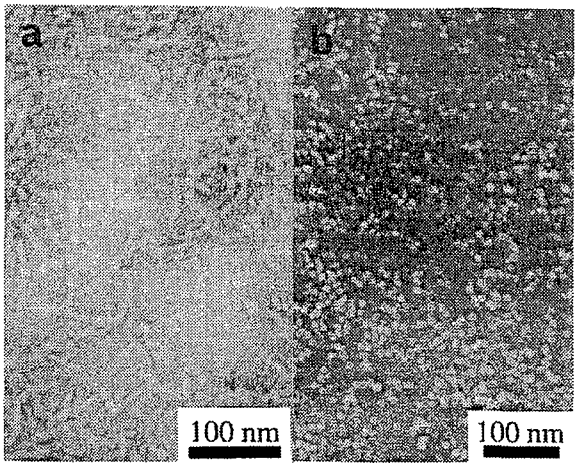

Figure 6. Transmission electron micrographs of (a) negatively stained samples of dioxygenated **6e** fibers and (b) ferric state **6d** micelles.

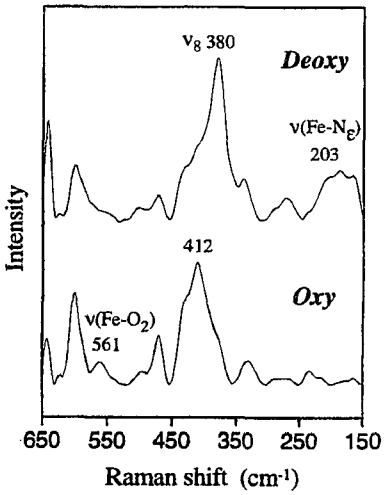

Figure 7. Resonance Raman spectra of the **6e** fibers in aqueous solution with 457.9 nm excitation.

O_2-Coordination Properties and Structures of the Lipidporphyrinato–Iron(II) Fibers. The UV–vis absorption spectrum of the aqueous carbonyl–Fe(II) complex **6e** solution displayed a typical CO-coordinated low-spin Fe(II) species (λ_{max}: 425, 540 nm) (Figure 5). Transmission electron microscopy of the solution, which was negatively stained by uranyl acetate, again showed long fibers with a width of a double-layer thickness (10 nm) (Figure 6a). The obtained fibers are stable similarly to the Zn(II) complex fibers. In contrast, the ferric **6d** in which the axial imidazole coordination is dissociated from the central Fe(III) formed only tiny round micelles with a diameter of 10 nm (Figure 6b) which never changed to fibers. This significantly indicates that the intramolecular imidazole coordination to the central metal plays an essential role in fiber formation.

Table 1. O_2 and CO Binding Parameters of Lipidporphyrinato–Iron(II) 6e at 25 °C

		O_2			CO	
system	solvent	$P_{1/2}$/Torr	$10^{-7}k_{on}$/M^{-1} s^{-1}	$10^{-3}k_{off}$/s^{-1}	$10^{3}P_{1/2}$/Torr	$10^{-6}k_{on}$/M^{-1} s^{-1}
6e fiber	water	25	4.7	2.5	4.8	4.0
6e	methanol	6.7	17	6.2	1.2	15

Light irradiation of this colloid under nitrogen allowed CO dissociation, affording the five-N-coordinated species, which exhibit constant absorption spectra in the range 1 μM to 2 mM (λ_{max}: 444, 542, 567 nm). Upon exposure of these fibers to O_2, the UV–vis absorption spectrum immediately changed to that of a dioxygenated species (λ_{max}: 424, 549 nm). The dioxygenation was kinetically stable and reversible at 25 °C, depending on the partial O_2 pressure. We then employed resonance Raman spectroscopy to characterize the coordination structure of the **6e** complex assembled in fibrous form (Figure 7). Under argon, there is a medium band at 203 cm^{-1}, which is assigned to the Fe(II)–N(imidazole) stretching mode, ν(Fe–N_ϵ), on the basis of the similar assignment for other porphyrinato–iron(II) systems.[27] This result reflects the intramolecular coordination of axial imidazole. After O_2 bubbling, the deformation modes of the porphyrin ring (ν_8 and ν_4) were upshifted immediately from 380 and 1356 cm^{-1} to 412 and 1376 cm^{-1}, respectively, indicating the conversion of the five-coordinated high-spin state to the six-coordinated low-spin state of the **6e** complex.[27,28] A ν(Fe–O_2) vibration of dioxygenated **6e** was also observed at 561 cm^{-1}. This frequency corresponds to an end-on type O_2 coordination to the porphyrinato–iron(II), which is similar to those of other synthetic tetraphenylporphyrinato–iron(II) derivatives in organic solvents and of oxyhemoglobin in aqueous media.[29,30] All these shifts have been observed reversibly dependent on the O_2 concentration. We thus conclude that the **6e** fibers definitely bind and release O_2 molecules in aqueous solution. The fibrous morphology has remained during these dioxygenation cycles. This is the first porphyrin fiber which can coordinate O_2 reversibly in an aqueous system. The oxidation to an Fe(III) complex, however, took place (half-lifetime: ca. 4 h). The oxidized fibers became shorter, revealing again that the intramolecular imidazole coordination largely governs the fiber's structure.

The O_2 and CO binding affinities ($P_{1/2}^{O_2}$, $P_{1/2}^{CO}$: gaseous pressure at half O_2 or CO binding for the porphyrinato–iron(II)) of the **6e** fibers were determined on the basis of the UV–vis spectral changes by O_2 or CO titration. The isosbestic points were maintained in all cases. Furthermore, the O_2 and CO association and dissociation rate constants (k_{on}, k_{off}) were explored by laser flash photolysis (Table 1).[8a,11–13] The $P_{1/2}^{O_2}$ value of the fibers (25 Torr) was 4-fold lower than that of the monomer in methanol solution (6.7 Torr). Kinetically, this arises mainly from the low $k_{on}^{O_2}$ value of the fibers in comparison to that of the monomer. This might be caused by steric hindrance of the flexible long alkyl chains on the porphyrin planes. The O_2 binding profile did not show any cooperativity like that of hemoglobin; the Hill coefficient was 1.0. It is, however, rather remarkable that one fiber with a length of 1 μm (Mw: 8.5×10^6 Da), for instance, does bind an equivalent amount of O_2 to the porphyrin components, that is approximately 2.6×10^3 molecules under O_2 atmosphere ([O_2] = 760 Torr) at 25 °C, while one hemoglobin (Mw: 6.45×10^4 Da) coordinates only four O_2 molecules under the same conditions. This self-assembled fiber is definitely a new type of three-dimensional porphyrin structure with a capability of O_2 transport in an aqueous system.

Conclusions

The synthesized lipidporphyrin complexes are new amphiphilic building blocks involving a porphyrinato–metal with an intramolecular coordinated axial base in aqueous media. The self-assembled fibers of **6c** show fluorescence but extraordinarily short triplet lifetimes that are normally due to the edge-to-edge alignment of the porphyrin macrocycles. The hydrophobic tetraphenylporphyrin moieties of **6c** (or **6e**) with an axially coordinated imidazolylalkyl arm probably produce a unique tetragonal tube which performs a key role in the fiber formation. Furthermore, the N-coordinated high-spin Fe(II) complex **6e** fiber can bind an equivalent amount of O_2 molecules depending on the number of porphyrin components. This lipidporphyrinato–iron(II) fiber is a new type of synthetic O_2 carrier and will also be able to perform some of the catalytic activities of other hemoproteins. To develop a light-initiated function of the porphyrin assembly, a study of the photoinduced electron-transfer reactions of the hybrid lipidporphyrinato–zinc(II) and –iron(III) fibers is now under way.

Acknowledgment. We thank Dr. Christoph Böttcher and Prof. Dr. Jürgen-Hinrich Fuhrhop, Freie Univesrität Berlin, for cryo-TEM of the porphyrin fibers. This work was partially supported by the Core Research for Evolutional Science and Technology, JST. The work at the Free University Berlin was carried out under the German–Japanese Cooperative Research Project of DFG-JSPS and the International Scientific Research Program of the Ministry of Education, Science, and Culture, Japan.

Supporting Information Available: A description of the synthesis procedures is available free of charge via the Internet at http://pubs.acs.org.

LA981566S

(27) Hori, H.; Kitagawa, T. *J. Am. Chem. Soc.* **1980**, *102*, 3608.
(28) Desobois, A.; Momenteau, M.; Lutz, M. *Inorg. Chem.* **1989**, *28*, 825.
(29) Wu, J.; Komatsu, T.; Tsuchida, E. *J. Chem. Soc., Dalton Trans.* **1998**, 2503.
(30) Hirota, S.; Li, T.; Philips, G. N., Jr.; Olson, J. S.; Mukai, M.; Kitagawa, T. *J. Am. Chem. Soc.* **1996**, *118*, 7845.

Journal of Porphyrins and Phthalocyanines
J. Porphyrins Phthalocyanines **4**, 81–87 (2000)

Molecular environment effect on O_2 binding to lipidporphyrinatoiron(II) complexes in aqueous media

EISHUN TSUCHIDA*,†, TERUYUKI KOMATSU and TETSUYA YANAGIMOTO

Department of Polymer Chemistry, Advanced Research Institute for Science and Engineering, Waseda University, Tokyo 169-8555, Japan

Received 16 June 1999
Accepted 13 July 1999

ABSTRACT: Lipidporphyrinatoiron(II) complexes are tetrakis(*o*-substituted)phenylporphinatoiron(II) derivatives which can be easily dispersed in water by molecular assembling. The most remarkable aspect of lipidporphyrinatoiron(II) assemblies is their reversible binding of dioxygen under physiological conditions (in aqueous media, pH 7.3, 37 °C) like hemoglobin and myoglobin. In these structures the O_2-binding properties are largely influenced by the molecular environment around the coordination site. Tetrakis(*o*-pivalamido)-phenylporphinatoiron(II) with a covalently linked axial imidazole (lipidporphyrinatoiron(II), **1**) is incorporated into recombinant human serum albumin (rHSA), providing a totally synthetic O_2-carrying hemoprotein (rHSA–**1**). Electrospray ionization mass spectrometry revealed the molecular mass of this non-covalent albumin–porphyrin hybrid. The O_2 rebinding after laser flash photolysis represented a three-phase decay, suggesting that each porphyrin is embedded into different cavities in the albumin structure. On the other hand, amphiphilic lipidporphyrinatoiron(II) with four alkylphosphocholine chains (**2**) is self-organized in aqueous solution to produce bimolecular fibers with a uniform thickness of 10 nm. This fiber also gave a stable O_2 adduct, and the O_2 rebinding after laser flash irradiation showed monophasic kinetics. Up to 20 vol% of methanol, which is a critical concentration for fiber formation, the morphology was gradually dissociated into spherical micelles, and the stability of the dioxygenated species suddenly decreased to 10% of that of the fibers.

KEYWORDS: lipidporphyrinatoiron(II); molecular environment; molecular assembly; human serum albumin; dioxygen binding; electronspray ionization mass spectroscopy; laser flash photolysis

INTRODUCTION

The unique binding aspects of dioxygen to protoheme in hemoglobin are governed by the specific microenvironment around the coordination site, i.e. heme-pocket, and dynamic structural changes of the tetrameric proteins, i.e. globin chains. Although the O_2-binding mechanism of hemoglobin has been clarified in detail, it is still difficult to achieve the cooperative O_2-binding profile using synthetic polymers. However, the hydrophobic atmosphere constructed by a synthetic molecular assembly, e.g. a phospholipid bilayer membrane, can prevent unfavorable electron transfer of the porphyrinatoiron(II), affording a stable O_2 adduct in aqueous solution [1–3]. In this paper we report the molecular environment effect on O_2 binding to tetrakis(*o*-substituted)phenylporphinatoiron(II) derivatives with a covalently linked axial imidazole (*lipidporphyrinatoiron(II)*) in two types of molecular assembling systems.

Human serum albumin (HSA) is the most abundant plasma protein and plays two major roles in the bloodstream, namely (i) maintaining the colloidal osmotic pressure and (ii) transporting numerous endogenous and exogenous compounds. Indeed, serum albumin can bind a great variety of metabolites and organic molecules [4–7]. Hemin released from hemoglobin is also transported to the liver by albumin for metabolic processing. Interest in this molecular binding led to association studies of serum albumin with several porphyrin derivatives [8–11]; however, little

*Correspondence to: E. Tsuchida, Department of Polymer Chemistry, Advanced Research Institute for Science and Engineering, Waseda University, Tokyo 169-8555, Japan.
†CREST investigator.

CCC 1088–4246/2000/010081–07 $17.50

attention has been paid to the physiological applications of these albumin–porphyrin hybrids [12, 13].

Unexpectedly, the three-dimensional structure of this very usual protein has been recently clarified. In 1989, Carter *et al.* first reported a structure of HSA to 6.0 Å derived from tetragonal crystals obtained from defatted commercial albumin [14]. Three years later, monoclinic crystals of recombinant HSA (rHSA) were also prepared and the structure was solved to 2.8 Å [15, 16]. The 585 amino acids consist of a unique heart-shaped structure which can be approximated as an equilateral triangle (8 nm × 3 nm). HSA has homologous repeating domains (I, II and III) with nine loops formed by 17 disulfide linkages, and each domain is constructed of two subdomains (IA, IB, etc.). The majority of the compounds are bound at one or both sites within specialized cavities of subdomains IIA and IIIA with typical equilibrium constants (K) ranging from 10^6 to 10^4 M^{-1} [4–6]. We have recently found that water-insoluble lipidporphyrinatoiron(II) with a covalently linked imidazole (**1**) is incorporated into HSA or recombinant HSA (rHSA) [17–20]. The obtained albumin–**1** hybrid can coordinate dioxygen reversibly under physiological conditions (in aqueous media, pH 7.3, 37 °C) in a similar fashion to myoglobin.

On the other hand, it is of current interest to construct a three-dimensional molecular structure using self-assembling of amphiphilic porphyrins in water [21–25]. Systematically aligned multiporphyrins will act as novel hemoprotein analogues and photochemical devices. More recently, several synthetic porphyrin amphiphiles have been self-organized in bulk aqueous solution, producing well-defined structures (monomolecular fibers, platelets and bimolecular vesicles) in which the highly ordered porphyrin arrays can act as light-harvesting centers for photoinduced charge separation and as active sites for hemoproteins [26–30]. We have reported long-lived fibers made of lipidporphyrinato-metals (Zn(II), Fe(II)) with four alkylphosphocholine groups on one side of the ring plane and an imidazolylalkyl arm at the periphery (**2**) [31]. The **2** fibers also produce a reversible O_2 adduct in aqueous media. In the above two systems the molecular environment effect on O_2 binding to the lipidporphyrinatoiron(II) complexes is described.

EXPERIMENTAL

Materials and Spectroscopy Apparatus

The lipidporphyrinatoiron(II) derivatives (**1** and **2**; Fig. 1) were synthesized by the previously reported procedures [31, 32]. rHSA (25 wt%) was provided by Yoshitomi Pharmaceutical Industries Ltd. The water used was deionized using an Advantec GS-200 system. The rHSA-incorporated **1** and self-assembled fibers of **2** were prepared according to the previously reported procedures [20, 31]. HSA–**1**(n) denotes HSA incorporated with n (1–8) molecules of **1**. UV-vis absorption spectra were recorded on a Jasco V-570 spectrophotometer. Electrospray ionization time-of-flight mass spectrometry (ESI-TOFMS) measurements were carried out using a Perceptive Biosystems Mariner.

Transmission Electron Microscopy (TEM)

The negatively stained specimens for TEM and the vitrified specimens for cryo-TEM were prepared as previously reported [28]. The obtained grids were observed in a Jeol JEM-100CX electron microscope or a Phillips CM12 using a Gatan cold-stage model 626 at an acceleration voltage of 100 kV.

O_2-binding Equilibrium and Kinetics

O_2 binding to lipidporphyrinatoiron(II) was expressed by

$$\mathrm{FeP} + \mathrm{O_2} \underset{k_{off}}{\overset{k_{on}}{\rightleftharpoons}} \mathrm{FeP(O_2)} \qquad (1)$$

$$(K = k_{on}/k_{off})$$

The O_2-binding affinity (gaseous pressure at half O_2 binding for lipidporphyrinatoiron(II), $P_{1/2} = 1/K$) was determined by the spectral changes at various partial pressures of O_2 [2, 33]. Porphyrin concentrations of 20 μM were normally used for UV-vis absorption spectroscopy. The spectra were recorded within the range 350–700 nm. The O_2-association and -dissociation rate constants (k_{on} and k_{off}) were measured by a competitive rebinding technique using a Unisoku TSP-600 laser flash photolysis apparatus [2, 33, 34].

RESULTS AND DISCUSSION

Incorporation of Lipidporphyrinatoiron(II) into rHSA

Incorporation of hydrophobic lipidporphyrinatoiron(II) with a covalently linked imidazole (**1**) into HSA or rHSA provides a new type of albumin–porphyrin hybrid which can reversibly bind dioxygen

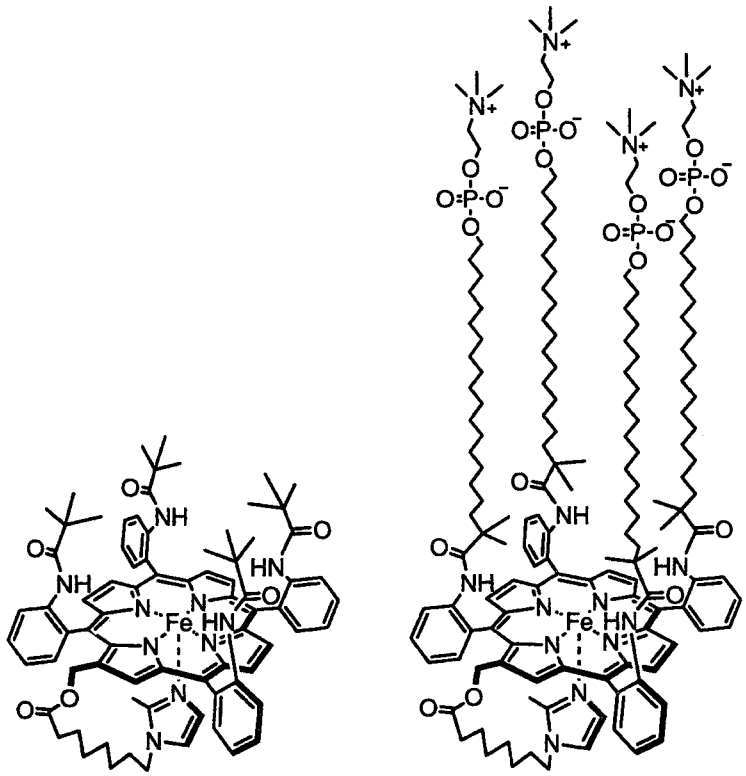

1 2

Fig. 1. Structure of lipidporphyrinatoiron(II) complex with covalently linked axial imidazole.

under physiological conditions [17–20]. From a quantitative analysis of the free porphyrin in the rHSA–**1** solution, the maximum binding number of compound **1** to an albumin was determined to be eight [19]. Furthermore, the binding sites were estimated to be subdomains IB–IIA, IIA and IIIB of HSA with binding constants (K) from 10^6 to 10^4 M^{-1} [19].

The isoelectric points (pI) of rHSA–**1** (**1**/ rHSA = 1–8 (mol/mol)) were all 4.8, i.e. exactly the same as that of rHSA [19, 20]. This observation indicates that lipidporphyrinatoiron(II) (**1**) without any ionic residue interacts non-specifically with a hydrophobic cavity of rHSA, so that its surface charge distributions are not changed. Based on circular dichroism (CD) spectroscopy [19, 20], the association of **1** did not cause any secondary or tertiary structural change of rHSA. Thus we can conclude that hydrophobic interaction is the major molecular force of the binding of **1** to rHSA.

Electrospray ionization mass spectrometry (ESI-MS) is a gentle method for transferring protein ions from solution into the gas phase and accurately determining their molecular masses [35, 36]. A feature of ESI-MS is its ability to detect non-covalent interactions between proteins and molecular partners [37]. A typical ESI time-of-flight mass spectrum (ESI-TOFMS) of multiply charged ions of rHSA is shown in Fig. 2(a). Deconvolution of these data yields a molecular weight of 66 505 Da, which corresponds to the theoretical molecular mass of 66 451. On the other hand, the ESI-TOFMS of the rHSA–**1**(4) hybrid showed additional broadened signals in the range of high molecular mass (Fig. 2(b)). Although some of the incorporated **1** is dissociated from the albumin host during ionization, these high-molecular-weight fragments demonstrate the formation of the rHSA–**1** complex. The calculated mass of rHSA–**1**(4) is 71 806, therefore the intense peak maxima at 4261, 3989 and 3750 coincided with the rHSA–**1** charge states +17, +18 and +19 respectively. Unfortunately, the

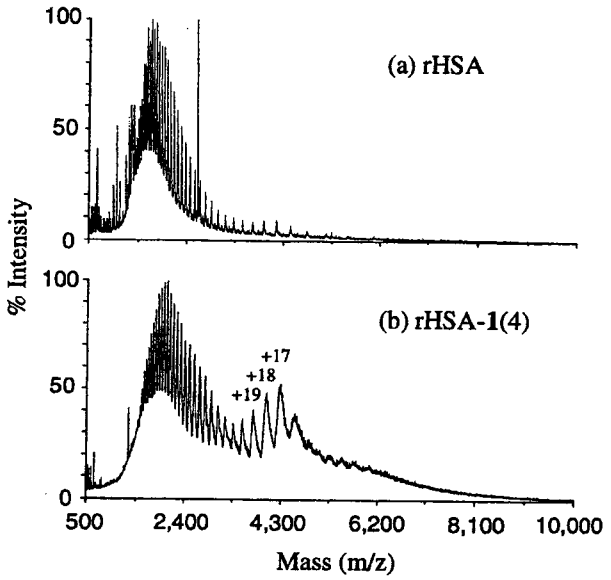

Fig. 2. ESI-TOF mass spectra of multiply charged ions of (a) rHSA and (b) rHSA–1(4).

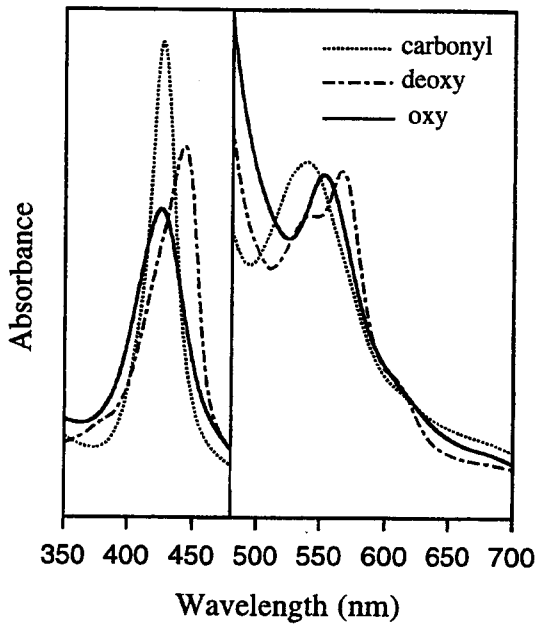

Fig. 3. UV-vis absorption spectral changes of rHSA–**1** in phosphate-buffered saline solution (pH 7.3) at 25 °C.

deconvolution of these data proved unsuccessful because of the broadness of the peaks.

O_2-binding Properties of rHSA–Lipidporphyrinatoiron(II)

The UV-vis absorption spectral changes of the rHSA–**1** solution upon exposure to dioxygen and argon were reversible in phosphate-buffered saline solution (pH 7.3) (Fig. 3).

The O_2-association and -dissociation rate constants (k_{on} and k_{off}) were then explored by laser flash photolysis. The absorption decays accompanying O_2 recombination were composed of three phases of first-order kinetics, and the curves of the absorption decays ($\Delta A(t)$) were fitted by a triple-exponential equation [20]

$$\Delta A(t) = C_1 \exp(-k_1 t) + C_2 \exp(-k_2 t) + C_3 \exp(-k_3 t) \quad (2)$$

where k_1, k_2 and k_3 are the apparent rate constants for each reaction. The minor (less than 10%) component k_1, which is the fastest rate constant, was always independent of the O_2 concentration. It is presumably correlated with a base elimination reaction [38]. From the slopes of linear plots of k_2 and k_3 versus O_2 concentration, two association rate constants for fast O_2 rebinding (k_{on}) and slow O_2 rebinding (k'_{on})were obtained (Table 1). The k_{on} values are three times larger than those of k'_{on}. The ratio of the fast reaction and the slow reaction was approximately two for rHSA–**1**(4) and three for rHSA–**1**(8). In the case of rHSA–**1**(1), k_{on} (3.2×10^7 M^{-1} s^{-1}) was the only major component. Thus we concluded that the O_2 association to **1** embedded into certain domains of serum albumin is significantly affected by the molecular environment around each porphyrin complex, e.g. steric hindrance by the protein residues and polarity.

The O_2-binding affinities ($P_{1/2}$, gaseous pressure at half O_2 binding for porphyrinatoiron(II)) of rHSA–**1** were determined on the basis of the UV-vis spectral changes by O_2 titration. According to the results of the kinetics experiments, the $P_{1/2}$ values were divided into two components: $K = (P_{1/2})^{-1}$ and $K' = (P'_{1/2})^{-1}$. The obtained $P_{1/2}$ and $P'_{1/2}$ are almost identical for rHSA–**1**(4) and rHSA–**1**(8) (Table 1).

Stability of O_2 Adduct of Lipidporphyrinatoiron(II) Fibers

Amphiphilic lipidporphyrinatoiron(II) (**2**) is self-organized in aqueous media to form long-lived

Table 1. O_2-association rate constants and O_2-binding affinities of lipidporphyrinatoiron(II) at 25 °C (pH 7.3)

	$10^{-7}\,k_{on}$ ($M^{-1}\,s^{-1}$)	$10^{-6}\,k'_{on}$ ($M^{-1}\,s^{-1}$)	$P_{1/2}$ (Torr)	$P'_{1/2}$ (Torr)
rHSA–1(4)	3.2	10	14	13
rHSA–1(8)	3.4	9.5	14	13
2 fibers	4.7	–	25	–
2 in methanol	17	–	6.7	–
Hb(T-state)α[a]	0.29	–	40	–

[a] pH 7, 20 °C, from Ref. 39.

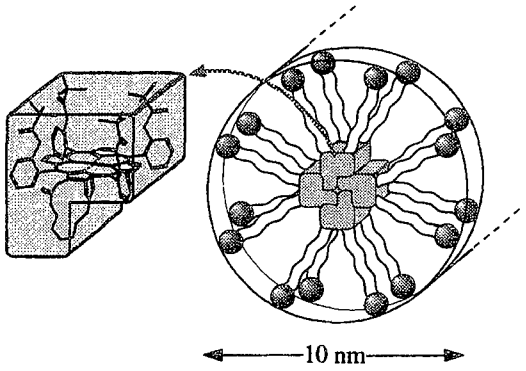

Fig. 5. Proposed structure of 2 fiber.

micellar fibers [31]. Transmission electron microscopy of the solution showed long fibers with the width of a double-layer thickness (10 nm) (Fig. 4(a)). Based on the results for the corresponding zinc(II) complex fibers, it is concluded that the iron(II) complex 2 also produces a similar fiber in which the hydrophobic tetraphenylporphyrin moieties with an intramolecular coordinated imidazole all produce J-aggregates at the center (Fig. 5) [31]. In the middle of the fiber section, four porphyrin planes are oriented perpendicularly to each other, forming a tetragonal unit, and the interior is occupied by iron(II)-coordinated imidazolylalkyl arms. The porphyrin planes are then aligned laterally, producing long fibers.

Upon exposure of these fibers to dioxygen, the UV-vis absorption spectrum immediately changed to that of an O_2-adduct species (λ_{max} 424, 549 nm). The dioxygenation was stable and reversible at 25 °C, depending on the partial O_2 pressure. The fibrous morphology remained during these dioxygenation cycles. Oxidation to the iron(III) complex, however, took place (half-lifetime *ca* 4 h).

The 2 fibers were not sensitive to the presence of electrolytes; sodium chloride (0.15 M) caused no precipitation. Addition of excess methanol could only destroy the fibers. The absorption spectrum (λ_{max} 424 nm) of the carbonylated 2 fibers was blue-shifted to that of the monomer (λ_{max} 420 nm) by increasing the methanol concentration (Fig. 6). Up to 20 vol% of methanol, which is a critical concentration for fiber formation, the structure was gradually dissociated into

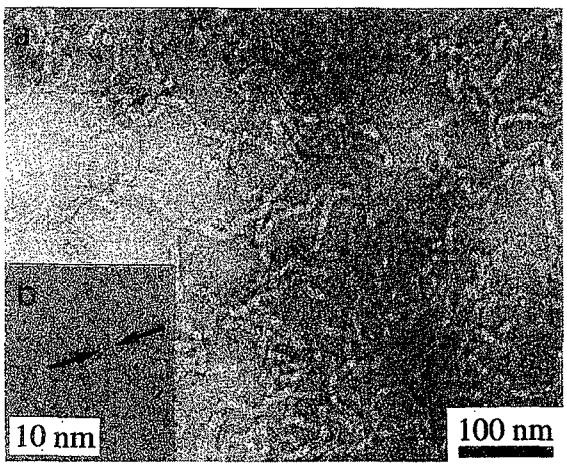

Fig. 4. Transmission electron micrographs of 2 fibers: (a) negatively stained sample with uranyl acetate; (b) cryo preparation in vitreous ice without staining.

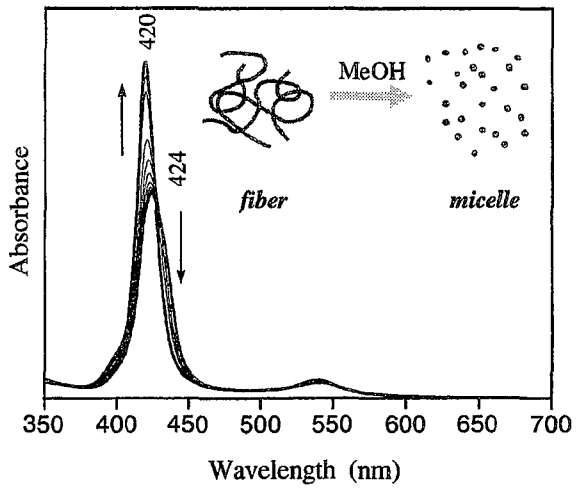

Fig. 6. UV-vis absorption spectral changes of carbonylated 2 fibers in aqueous media upon addition of methanol at 25 °C.

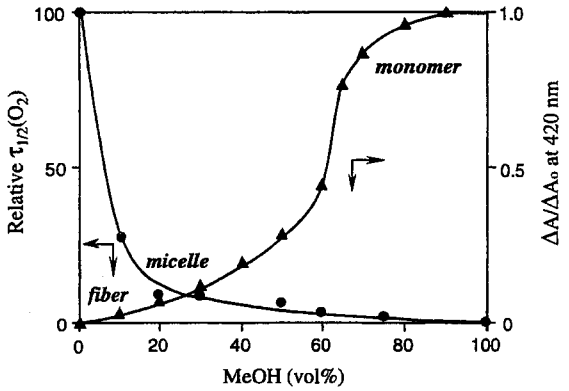

Fig. 7. Changes in half-lifetime of O_2 adduct and Soret band absorption maximum of **2** fibers on addition of methanol.

spherical micelles, and the stability of the dioxygenated species suddenly decreased to 10% of that of the fibers (Fig. 7). It can therefore be concluded that the fiber structure, which involves the hydrophobic porphyrin core at the center, is necessary for stable O_2 adduct formation.

In contrast with rHSA–**1**, the O_2 rebinding to the **2** fibers after laser flash photolysis was monophasic, indicating that all the porphyrin units are aligned in the same fashion and located in a uniform molecular environment. The $P_{1/2}$ value of the fibers (25 Torr) was four times lower than that of the monomer in methanol solution (6.7 Torr) (Table 1). Kinetically, this arises mainly from the low k_{on} value of the fibers in comparison with that of the monomer. This might be caused by steric hindrance of the flexible long alkyl chains on the porphyrin planes.

CONCLUSIONS

The microenvironment around the lipiporphyrinatoiron(II) (**1**) in the albumin obviously retarded the irreversible oxidation of the central iron(II) ion, because **1** homogenized with Triton X-100 in water was rapidly oxidized upon exposure to dioxygen. Furthermore, the O_2-binding affinity of **1** in rHSA is rather high relative to the value supposed. Since $P_{1/2}$ of **1** is 38 Torr in toluene solution at 25 °C, the value in water should become approximately 300 Torr as inferred from the O_2 solubility. This result clearly shows that the polar amide environment in the albumin peptide causes an increase in polarity around the coordination sphere of **1**. In addition, the two-phase kinetics of O_2 association to rHSA–**1** may indicate two types of orientation of the tetrapivalamide substituents on the porphyrin plane. If the O_2-binding side of the porphyrin plane, namely the pivalamide side, faced the center of the albumin molecule, the O_2-association rate should be decreased. On the other hand, the stability of the O_2-adduct species of lipidporphyrinatoiron(II) (**2**) fibers is largely affected by the aggregate morphology. The half-lifetime for the O_2 adduct of the **2** micelles is only one-tenth of that for the bimolecular long fibers. In the tubular structure of the tetragonal porphyrin units the mobility of the porphyrin plane is restrained and the obtained hydrophobic core plays a role in the prevention of oxidation of dioxygenated species.

Acknowledgements

We thank Dr Christoph Böttcher and Professor Dr Jürgen-Hinrich Fuhrhop of the Free University of Berlin for cryo-TEM of the porphyrin fibers. This work was partially supported by the Core Research for Evolutional Science and Technology, JST. The work at the Free University of Berlin was carried out under the International Scientific Research Program of the Ministry of Education, Science and Culture, Japan.

REFERENCES AND NOTES

1. Tsuchida E, Nishide H. *Top. Curr. Chem.* 1986; **132**: 64.
2. Tsuchida E, Komatsu T, Arai K, Nishide H. *J. Chem. Soc., Dalton Trans.* 1993; 2465.
3. Tsuchida E, Nishide H, Yuasa M, Hasegawa E, Ejima K, Matsushita Y. *Macromolecules* 1989; **22**: 2103.
4. Kragh-Hansen U. *Pharmacol. Rev.* 1981; **33**: 17 and references cited therein.
5. Peters Jr T. *Adv. Protein Chem.* 1985; **37**: 161.
6. Peters Jr T. *All about Albumin, Biochemistry, Genetics, and Medical Applications*. Academic Press: San Diego, CA, 1997.
7. Brown JR. In *Albumin Structure, Function and Uses*. Rosenoer VM, Oratz MM, Rothschild MA (eds). Pergamon Press: New York, 1976; 27–51.
8. Little HN, Nelands JB. *Nature* 1960; **170**: 913.
9. Beaven GH, Chen S-H, D'Albis A, Gratzer WB. *Eur. J. Biochem.* 1974; **41**: 539.
10. Muller-Eberhand U, Morgan WT. *Ann. NY Acad. Sci.* 1975; **244**: 625.
11. Adams PA, Berman MC. *Biochem. J.* 1980; **191**: 95.
12. Marden MC, Hazard ES, Leclerc L, Gibson GH. *Biochemistry* 1989; **28**: 4422.
13. Bonaventura J, Brouwer M, Brouwer T, Cashon B, Cameron S. Paper presented at the 11th Congr. ISABI, Boston, MA, July 1994.

14. Carter DC, He X-M, Munson SH, Twigg PD, Gernert KM, Broom MB, Miller TR. *Science* 1989; **244**: 1195.
15. He XM, Carter DC. *Nature* 1992; **356**: 209.
16. Carter DC, Ho JX. *Adv. Protein Chem.* 1994; **45**: 153.
17. Komatsu T, Kawai N, Ando K, Nishide H, Tsuchida E. *Chem. Lett.* 1995; 813.
18. Tsuchida E, Ando K, Maejima H, Kawai N, Komatsu T, Tekeoka S, Nishide H. *Bioconjugate Chem.* 1997; **8**: 534.
19. Komatsu T, Hamamatsu K, Wu J, Tsuchida E. *Bioconjugate Chem.* 1999; **10**: 82.
20. Komatsu T, Matsukawa Y, Hamamatsu K, Wu J, Tsuchida E. *Bioconjugate Chem.* 1999; **10**: in press.
21. Guilard R, Senglet N, Liu YH, Sazou D, Findsen E, Fanre D, Courieres TD, Kadish KM. *Inorg. Chem.* 1991; **30**: 1898.
22. Fuhrhop J-H, Demoulin C, Böttcher C, Köning J, Siggel U. *J. Am. Chem. Soc.* 1992; **114**: 4159.
23. Inamura I, Uchida K. *Bull. Chem. Soc. Jpn.* 1991; **64**: 2005.
24. Fuhrhop J-H, Bindig U, Siggel U. *J. Am. Chem. Soc.* 1993; **115**: 11036.
25. Endisch C, Böcher C, Fuhrhop J-H. *J. Am. Chem. Soc.* 1995; **117**: 8273.
26. Tsuchida E, Komatsu T, Arai K, Yamada K, Nishide H, Böttcher C, Fuhrhop J-H. *Langmuir* 1995; **11**: 1877.
27. Tsuchida E, Komatsu T, Arai K, Yamada K, Nishide H, Böttcher C, Fuhrhop J-H. *J. Chem. Soc., Chem. Commun.* 1995; 1877.
28. Komatsu T, Yamada K, Tsuchida E, Siggel U, Böttcher C, Fuhrhop J-H. *Langmuir* 1996; **12**: 6242.
29. Komatsu T, Tsuchida E, Böttcher C, Donner D, Messerschmidt C, Siggel U, Stocker W, Rabe JP, Fuhrhop J-H. *J. Am. Chem. Soc.* 1997; **119**: 11 660.
30. Komatsu T, Yanagimoto T, Tsuchida E, Siggel U, Fuhrhop J-H. *J. Phys. Chem. B* 1998; **102**: 6759.
31. Komatsu T, Yanagimoto T, Furubayashi Y, Wu J, Tsuchida E. *Langmuir* 1999; **15**: 4427.
32. Tsuchida E, Komatsu T, Kumamoto S, Ando K, Nishide H. *J. Chem. Soc., Perkin Trans.* 2 1995; 747.
33. Collman JP, Brauman JI, Iverson BL, Sessler JL, Morris RM, Gibson QH. *J. Am. Chem. Soc.* 1983; **105**: 3052.
34. Traylor TG, Tsuchiya S, Campbell D, Mitchell M, Stynes D, Koga N. *J. Am. Chem. Soc.* 1985; **107**: 604.
35. Fenn JM, Mann CK, Meng SF, Whitehouse CM. *Science* 1989; **246**: 64.
36. Upmacic RK, Hajjar DP, Chait BT, Mirza VA. *J. Am. Chem. Soc.* 1997; **119**: 10424.
37. Smith RD, Light-Wahl KJ. *Biol. Mass Spectrom.* 1993; **22**: 493–501 and references cited therein.
38. Geibel J, Cannon J, Campbell D, Traylor TG. *J. Am. Chem. Soc.* 1978; **100**: 3575.
39. Sawicki CA, Gibson QH. *J. Biol. Chem.* 1977; **252**: 7538.

Photoreduction of Self-Assembled Lipidporphyrinato-iron(III) Chloride with Hyaluronic Acid under Semi-Physiological Conditions

Teruyuki Komatsu, Tetsuya Yanagimoto, Akito Nakagawa, and Eishun Tsuchida*†
Department of Polymer Chemistry, Advanced Research Institute for Science and Engineering, Waseda University, Tokyo 169-8555

(Received October 18, 1999; CL-990884)

Photoirradiation into the LMCT band (λ_{max}: 362 nm) of self-assembled amphiphilic tetraphenylporphyrinato-iron(III) (lipidporphyrinato-iron(III)) chloride with hyaluronic acid leads to reduction of the central ferric ion in saline solution (pH 7.4, 25 °C); the obtained lipidporphyrinato-iron(II) can reversibly bind and release dioxygen.

If the redox behavior of the iron center of the heme complex, which plays crucial roles in biological systems, can be controlled by light-irradiation, this chemistry allows the photomanipulation and/or photo-resuscitation of the activities of natural hemoproteins. From this point of view, the photochemistry of ferric porphyrins, especially the photoreduction of the central Fe(III) ion in aqueous media is of current interest.[1,2] The Fe(III)porphyrins generally coordinate a counter anion and show a ligand-to-metal charge-transfer (LMCT) transition in the near UV region. It has been known that photoirradiation into this LMCT band leads to reduction of the metal center involving radical dissociation.[2-5] Hendrickson and co-workers revealed the photoreduction of the tetraphenylporphyrinato-iron(III) halide ([Fe(III)TPP]$^+$Cl$^-$) by LMCT irradiation and photocatalytic hydrocarbon oxidation.[6] The produced chloride radicals, however, recombine with Fe(II)porphyrin in water, and the ferrous complex cannot be accumulated. We have recently found that an amphiphilic Fe(III)TPP derivative with an intramolecularly coordinated axial imidazole (lipidporphyrinato-iron(III), **1b**)[7] forms a fibrous aggregate with hyaluronic acid, and its central Fe(III) ion coordinates Cl$^-$ in saline solution. This paper describes, for the first time, a clean photoreduction of self-assembled lipidporphyrinato-iron(III) fibers under semi-physiological conditions (pH 7.4, in saline, 25 °C). The obtained lipidporphyrinato-iron(II) (**1a**) aggregate is able to reversibly bind and release dioxygen like hemoglobin. The reduction mechanism was also evaluated using laser flash photolysis experiments.

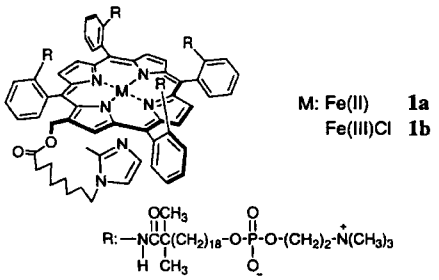

Upon the rapid injection of methanolic **1b** into phosphate buffered saline (pbs; 1 mM, pH 7.4, [NaCl]: 0.15 M), a homogeneous solution was produced ([**1b**]: 10 μM, [CH_3OH] < 0.3 vol%). The remaining methanol was completely removed by dialysis in pbs for 15 h at 4 °C. Transmission electron microscopy (TEM) of the evaporated **1b** solution showed spherical micelles with a diameter of 10 nm. The UV-vis. absorption spectrum showed that the dominant species of **1b** at pH 7.4 was the five-coordinated Fe(III) high-spin complex with axial chloride.[8,9] We assigned the distinct band at 362 nm (ε: 2.5 × 10^4 M^{-1}cm^{-1}) as a LMCT transition between the central Fe(III) and Cl$^-$, based on the following results. (i) This band significantly shifted to the lower energy with the decreasing electronegativity of the halides (I$^-$ < Br$^-$ < Cl$^-$), while the Soret or Q-bands, which are π-π^* transitions, were not affected.[6] (ii) The entire absorption spectrum changed with increasing pH and finally showed the five-coordinated Fe(III) complex with axial OH$^-$ at pH 10.[9] This spectral change was reversible and the pKa value was determined to be 7.7. From the absorption pattern, the formation of the six-coordinated Fe(III) low-spin complex with axially bound imidazole and Cl$^-$ was excluded.[10,11]

Upon photoirradiation of this **1b** micellar solution with a 250 W high-pressure Hg arc-lamp (365 nm) under an argon atmosphere, a negligible change in the absorption spectrum was observed. In contrast, the co-existence of a small amount of hyaluronic acid (21 mg L^{-1}, [unit]: 100 μM), which is a scavenger of free radicals in biological systems, led to complete photoreduction of the central ferric ion (Figure 1). After photoirradiation for 45 min, the UV-vis. spectrum of **1b** changed to that of a five-N-coordinated high-spin Fe(II) complex (**1a**) (λ_{max}: 443, 542, 566 nm). The well-defined isosbestic points (431, 462, 531, 584 nm) throughout the measurement revealed that no side reactions occurred; the quantum yield (Φ) was 7.0 × 10^{-3}.[12] The addition of hyaluronic acid to

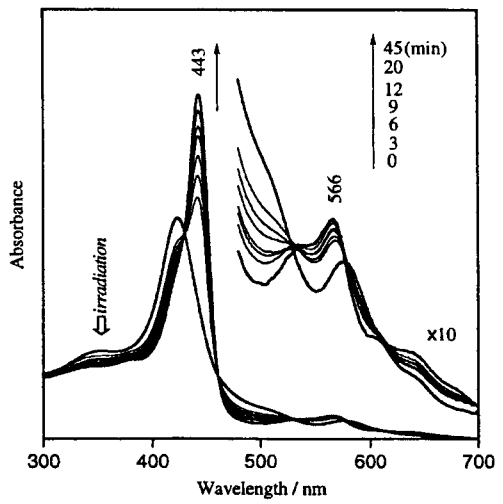

Figure 1. Visible absorption spectral changes in photoreduction of **1b** fibers in phosphate buffer saline (pH 7.4, [NaCl]: 0.15 M) at 25 °C.

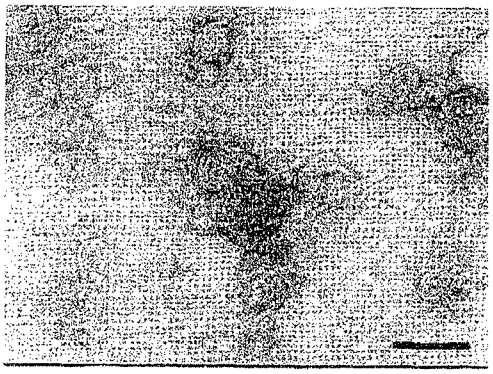

Figure 2. TEM of evaporated aqueous solution of the self-assembled **1b** with hyaluronic acid; short fibers before photoirradiation (bar: 100 nm).

the **1b** solution in the dark induced no absorption change, indicating the polysaccharide neither affects the coordination structure nor reduces the Fe(III) center. Irradiation into this CT band only causes the reduction of the ferric complex in the presence of hyaluronic acid. As expected, the complete reduction was not observed at pH 10. Glucose also showed efficacy for the photoreduction as well, but a large excess amount (0.15 M) was needed for achieving a 100% reduction. Other mucopolysaccharides (chondroitin sulfic acids, *etc.*) were also examined, but they were not as efficient compared to hyaluronic acid.

Interestingly, the addition of hyaluronic acid induced a remarkable morphology change in the **1b** aggregate from the spherical micelles into the unique short fibers (Figure 2). The width of the fiber is estimated to be 5 nm, corresponding to the molecular length of **1b** (4.6 nm). The fibers are presumably made of the polysaccharide chain combined with lipidporphyrins. These co-assembled structures of **1b** and hyaluronic acid may be responsible for the effective photoreduction process. On the other hand, addition of small amount of glucose did not induce any morphology change of the **1b** micelles.

Laser flash photolysis at 355 nm (THG of Nd:YAG) of the deaerated aqueous **1b** solution with hyaluronic acid showed that the photoreduction was finished within the duration of the laser pulse; the transient absorption spectral pattern measured at 50 ns after the pulse was in good agreement with the difference spectrum (five-N-coordinated Fe(II) complex minus Fe(III) complex with Cl^-) (Figure 3). These results suggest that the primary reaction step appears to be the homolytic cleavage of the ferric ion and the axial Cl^-, and that the imidazole arm immediately coordinates to the Fe(II) center within 50 ns. The produced chloride radical probably reacted with the active hydrogen in hyaluronic acid and the reduced ferrous complex was accumulated.[13]

Upon exposure of dioxygen to the aqueous solution of the photoreduced **1a**, the UV-vis. absorption spectrum changed to that of the dioxygenated species (λ_{max}: 425, 548 nm). The O_2 coordination was reversible at 25 °C depending on the O_2-partial pressure and the O_2-binding ability was almost identical to that of the **1a** fibers which were prepared by the previously reported procedure involving the chemical reduction of the Fe(III) center.[7]

In conclusion, photoirradiation into the LMCT band of the self-assembled **1b** fiber with hyaluronic acid leads to a clean

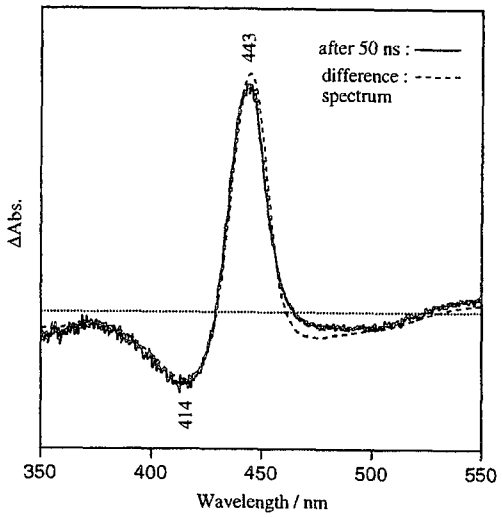

Figure 3. Transient absorption spectrum of aqueous **1b** solution with hyaluronic acid (21 mgL^{-1}) under argon (pH 7.4, [NaCl]: 0.15 M) at 50 ns after the laser pulse. The spectral pattern is in good agreement with the difference spectrum of five-N- coordinated Fe(II) complex minus Fe(III) complex.

reduction of the central ferric ion. Hyaluronic acid strings in the fibers are presumably very effective as a radical scavenger in this reaction.

This work was partially supported by the Core Research for Evolutional Science and Technology, JST, and a Grant-in-Aid for Scientific Research (No. 11650935) from the Ministry of Education, Science, Culture and Sports, Japan.

References and Notes

† CREST investigator, JST
1 I. Hamachi, S. Tanaka, and S. Shinkai, *J. Am. Chem. Soc.*, **115**, 10458 (1993); I. Hamachi, S. Tanaka, S. Tsukiji, S. Shinkai, and S. Oishi, *Inorg. Chem.*, **37**, 4380 (1998).
2 M. Hoshino, K. Ueda, M. Takahashi, M. Yamaji, and Y. Hama, *J. Chem. Soc., Faraday Trans.*, **88**, 405 (1992); H. Seki, M. Hoshino, and S. Kounose, *J. Chem. Soc., Faraday Trans.*, **92**, 2579 (1996); M. Hoshino and T. Baba, *J. Am. Chem. Soc.*, **120**, 6820 (1998).
3 C. Bartocci, F. Scandola, A. Ferri, and V. Carassiti, *J. Am. Chem. Soc.*, **102**, 7067 (1980); C. Bartocci, A. Maldotti, G. Varani, P. Battioni, and V. Carassiti, *Inorg. Chem.*, **30**, 1255 (1991).
4 D. Brault, C. Bizet, P. Morlière, M. Rougee, E. J. Land, R. Santus, and A. J. Swallow, *J. Am. Chem. Soc.*, **102**, 1015 (1980); C. Bizet, P. Morlière, D. Brault, O. Delgado, M. Bazin, and R. Santus, *Photochem. Photobiol.*, **34**, 315 (1981).
5 T. Imamura, T. Jin, T. Suzuki, and M. Fujimoto, *Chem. Lett.*, **1985**, 847.
6 D. N. Hendrickson, M. G. Kinnard, and K. S. Suslick, *J. Am. Chem. Soc.*, **109**, 1243 (1987).
7 T. Komatsu, T. Yanagimoto, Y. Furubayashi, J. Wu, and E. Tsuchida, *Langmuir*, **15**, 4427 (1999).
8 E. B. Fleischer, J. M. Palmer, T. S. Srivastava, and A. Chatterjee, *J. Am. Chem. Soc.*, **93**, 3162 (1971).
9 R.-J. Cheng, L. Latos-Grazynski, and A. L. Balch, *Inorg. Chem.*, **21**, 2412 (1983).
10 F. A. Walker, M.-W. Lo, and M. T. Ree, *J. Am. Chem. Soc.*, **98**, 5552 (1976).
11 C. L. Coyle, P. A. Rafson, and E. H. Abbott, *Inorg. Chem.*, **12**, 2007 (1973).
12 The light intensity was measured by the ferrioxalate acti-nometric procedure. C. G. Hatchard and C. A. Parker, *Proc. R. Soc. London, Ser. A*, **235**, 518 (1956).
13 B. C. Gilbert, D. M. King, and C. B. Thomas, *Carbohydr. Res.*, **125**, 217 (1984).

ELSEVIER

www.elsevier.nl/locate/ica

Inorganica Chimica Acta 305 (2000) 26–31

Inorganica Chimica Acta

Photoinduced electron transfer between lipidporphyrinato-zinc(II) and -iron(III) complexes in a phospholipid vesicular membrane

Tetsuya Yanagimoto, Teruyuki Komatsu, Eishun Tsuchida *,[1]

Department of Polymer Chemistry, Advanced Research Institute for Science & Engineering, Waseda University, Tokyo 169-8555, Japan

Received 19 November 1999; accepted 28 February 2000

Abstract

A tetraphenylporphyrin derivative having four alkylphosphocholine groups and a covalently-bound axial imidazole (lipidporphyrin) is easily self-organized in water to form spherical micelles or bilayer membranes with phospholipid molecules. The photoinduced electron transfer reactions between lipidporphyrinato-zinc(II) (**1**) and -iron(III) (**2**) complexes in these molecular assemblies were studied by fluorescence spectroscopy and laser flash photolysis. A mixture of **1** and **2** (molar ratio: 1/1) produced non-fluorescent micelles. The red-shifted Soret band absorption, relative to that of the methanolic monomer solution, suggests the formation of the photodeactive complex made of **1** and **2** in the ground state. On the other hand, both chromophores were homogeneously dispersed into the bilayer membrane of 1,2-dimyristoyl-*sn*-glycero-3-phosphatidylcholine (DMPC), and the reductive electron transfer from the excited singlet state of **1** to **2** was observed. While this resulted in a significant decrease in the yield of intersystem crossing, the gradual quenching of the excited triplet state of **1** by **2** was also measured. In both cases, the corresponding Stern–Volmer plots showed a linear relationship and yielded quenching rate constants of 1.2×10^{11} and 6.2×10^{4} M^{-1} s^{-1} via the excited singlet state and the triplet state, respectively. In the presence of excess triethanolamine as a sacrificial reagent, the intermolecular electron transfer became partly irreversible, giving an intramolecularly imidazole-coordinated Fe(II) complex which is capable of reversibly binding dioxygen like hemoglobin.

Keywords: Electron transfer; Zinc complexes; Iron complexes; Lipidporphyrin complexes; Phospholipid bilayer membrane

1. Introduction

Studies on electron and energy transfer reactions between different metalloporphyrins, e.g. iron and other metal complexes, have been a topic of great interest because of the importance of their performance in biological systems [1–4]. Covalently linked metalloporphyrin dimers with different metal centers, in which the orientation and distance between the two porphyrins are strictly fixed, have been synthesized, and their photochemical properties in organic solution were evaluated [5,6]. However, a few studies have reported the intermolecular electron transfer reactions between different metalloporphyrins in biological conditions, namely in molecular assembly systems in aqueous media [7].

On the other hand, we have found that self-assembled amphiphilic tetraphenylporphyrinato-iron(II) derivatives (Fe(II)-lipidporphyrin) and phospholipid vesicles embedding Fe(II)-lipidporphyrin can reversibly bind and release dioxygen under physiological conditions like a hemoglobin and myoglobin [8,9]. However, the irreversible auto-oxidation of the central Fe(II) ion slowly takes place in all of the dioxygenated complexes, which results in the deactivation of the O_2-binding ability. If the oxidized Fe(III)-porphyrin can be reduced by light irradiation, facile regeneration of the O_2-binding ability will be realized. In this paper, we describe the photoinduced electron transfer reactions between the Zn(II)- and Fe(III)-lipidporphyrins having a covalently bound axial imidazole embedded into the phospholipid bilayer membrane. In the presence of triethanolamine as a sacrificial agent, a part of the

* Corresponding author. Tel.: +81-3-5286 3120; fax: +81-3-3205 4740.

E-mail address: eishun@mn.waseda.ac.jp (E. Tsuchida)

[1] CREST investigator, JST.

0020-1693/00/$ - see front matter
PII: S0020-1693(00)00106-7

electron transfer from the excited state of the Zn(II) complex to the Fe(III) complex became irreversible and then accumulation of the Fe(II)-lipidporphyrin was observed.

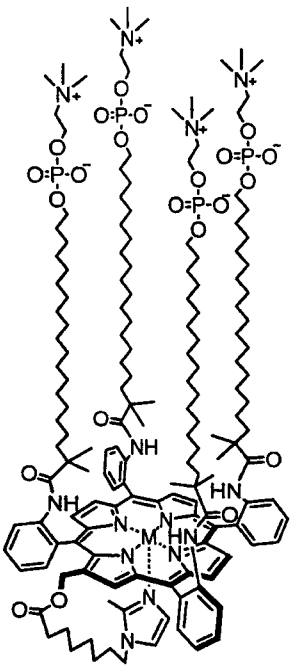

M: Zn(II) **1**
Fe(III) **2**

2. Experimental

2.1. Materials and general methods

2-[8-(2-Methylimidazole-1-yl)octanoyloxymethyl]-5,10,15,20-tetrakis{α,α,α,α-*o*-[2,2-dimethyl-20-({[2-trimethylammonio]ethoxy}phosphonatoxy)icosanamide]-phenyl}porphinato-zinc(II) (**1**) and -iron(III) (**2**) were prepared according to the previously reported procedures [9d]. 1,2-Dimyristoyl-*sn*-glycero-3-phosphatidylcholine (DMPC) was purchased from the Nihon Oil Fat Co. Other chemicals were purchased from the Kanto Chemical Co. All solvents were commercial high-purity grades used for spectroscopy. The water was deionized using an Advantec GS-200 system. Spectrophotometric measurements were performed with a Jasco UV-570 spectrophotometer. Dynamic light-scattering measurements were carried out using a submicron particle analyzer (Coulter Electronics N4-SD).

2.2. Preparation of aqueous lipidporphyrin solutions

2.2.1. Self-assembly dispersion

Methanol solutions of the lipidporphyrins (< 20 μl) with different **1**/**2** ratios were injected rapidly into a phosphate buffer (PB) solution (10 mM, pH 7.4, 3 ml) at 70°C and the obtained homogeneous solution was incubated for 4 h at room temperature (r.t.).

2.2.2. Phospholipid vesicle dispersion

A methanolic mixture of DMPC/**1**/**2** (molar ratio: 500/1/0–5; < 30 μl) was injected into the PB (3 ml) and the obtained solution was subsequently homogenized by a probe-type sonicator (Nihon Seiki UP-600) for 5 min under argon. The final concentrations of DMPC/**1**/**2** were 1000/2/0–10 μM. The homogeneous solution was then incubated for 4 h at r.t.

2.3. Transmission electron microscopy (TEM)

The negatively stained specimens for TEM were prepared according to previously reported procedures [9b,10]. The obtained grids were observed in a Jeol JEM-100CX electron microscope at an accelerating voltage of 100 kV.

2.4. Fluorescence lifetime measurement

The fluorescence emission spectra of **1** were measured with a Hitachi F-4500. Fluorescence lifetimes were measured using a Horiba NAES-500 single photon counter with a hydrogen lamp (excited at 300–400 nm, emission monitored at > 500 nm). The samples were held in a cuvette (optical path length 1 cm) and purged of dioxygen by argon bubbling for at least 30 min. All experiments were carried out at 20°C, which is below the gel-to-liquid crystal transition temperature of DMPC (23°C) [11].

2.5. Laser flash photolysis

Triplet lifetime measurements were performed using a Unisoku TSP-600 time-resolved spectrophotometer system with a Continuum Surelite I-10 Q-switched Nd-YAG laser, which generated a second-harmonic (532 nm) pulse of 6 ns duration with an energy of 200 mJ (10 Hz). A 150 W Xenon arc lamp was used as the monitor light source. The solutions were also bubbled with argon for 30 min before the laser flash photolysis. The triplet–triplet absorption decay of **1** was monitored by its transient absorption at 470 nm. The decay of the triplet state was almost constant when the molar ratio of **1** to DMPC was < 1/500. This ratio was therefore employed throughout our experiments.

3. Results and discussion

3.1. Self-assembled lipidporphyrin aggregate

The injection of the methanolic **1** and **2** (molar ratio: 1/1) into the PB provided a bright-red homogeneous solution. TEM of the negatively stained and evaporated colloid showed spherical micelles with a diameter of 10 nm (Fig. 1(a)), which corresponds to the double length of the lipidporphyrin (4.6 nm). The hydrophobic tetraphenylporphyrin moieties with an axial imidazole are presumably all forced together into the center of the micelle. In the UV–Vis absorption spectrum of this micellar solution, the remarkable observation is the red-shifted Soret band (λ_{max}: 431 → 435 nm) and Q bands (e.g. λ_{max}: 563 → 567 nm) relative to those of the

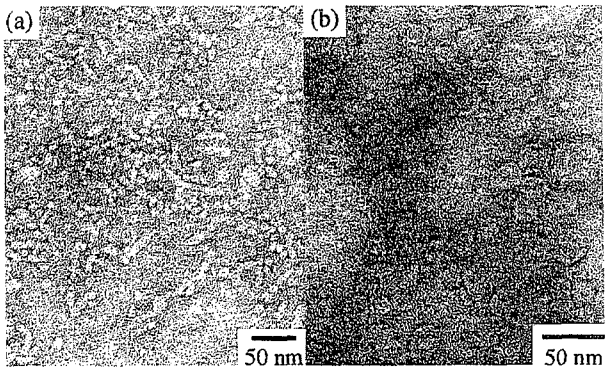

Fig. 1. Transmission electron micrographs of negatively stained samples of (a) **1**/**2** micelles (molar ratio: 1/1) and (b) DMPC vesicles embedding **1** and **2** (molar ratio: 500/1/1).

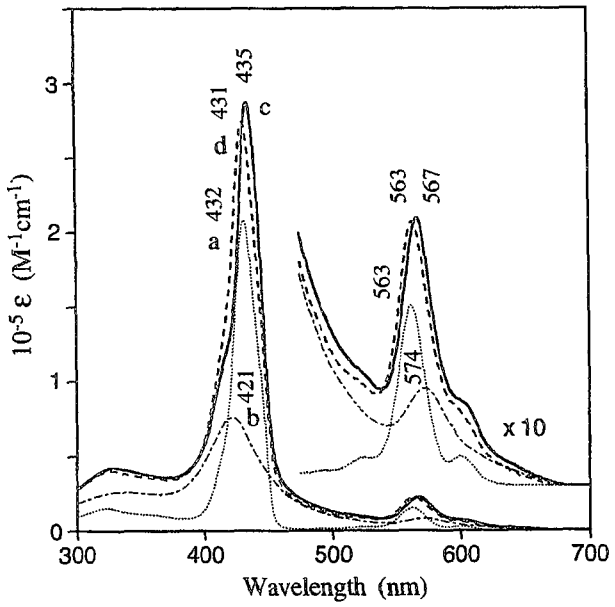

Fig. 2. UV–Vis absorption spectra of the aqueous solution of (a) **1** micelles, (b) **2** micelles, (c) **1**/**2** micelles (molar ratio: 1/1), and (d) the superposition of the spectra of (a) and (b).

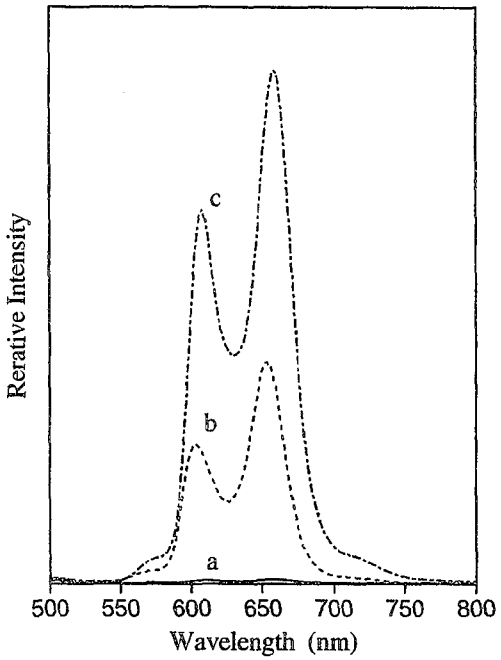

Fig. 3. Fluorescence emission spectra of (a) **1**/**2** micelles (molar ratio: 1/1), (b) monomeric **1** in methanol, and (c) DMPC vesicles embedding **1**. [**1**]: 1 μM.

superimposed spectrum for the individual monomer solutions (Fig. 2). Furthermore, this micelle showed almost no fluorescence as compared with the methanolic **1** monomer solution (Fig. 3). This quenching would be attributed to the formation of the photodeactive complex of the two chromophores in the ground state.

3.2. Phospholipid vesicle embedding lipidporphyrins

3.2.1. Morphology and structure

The lipidporphyrins were easily organized with an excess amount of 1,2-dimyristoyl-*sn*-glycero-3-phosphatidylcholine (DMPC) in the PB by ultrasonication to produce small unilamellar vesicles with diameters of 30–40 nm (Fig. 1(b)). The particle diameters agreed with the average size (35 ± 8 nm) determined by a light-scattering experiment. Incorporation of the lipidporphyrins into the bilayer membrane of the DMPC vesicles was confirmed by gel permeation chromatography (Sepharose CL-4B) monitored by the absorptions of **1** at 432 nm and the phospholipid having unsaturated fatty acid residues added as a probe[2] at 255 nm. The elution curves coincided with each other, which means that the porphyrins are incorporated into the bilayer membrane.

[2] A very small amount of the phospholipid, 1,2-di(octadeca-2',4'-dienoyl)-*sn*-glycero-3-phosphocholine, was added as a probe for the vesicles.

3.2.2. Absorption and excitation spectral properties

A dispersion of the DMPC vesicles embedding **1** showed an absorption spectrum very similar to that of the methanolic monomer (not shown). The sharp absorption peak of the vesicle dispersion suggests that there is no interaction of the neighboring **1** complexes in the bilayer membrane. The shape of the fluorescence spectrum is well identified with that of the methanolic monomer solution except for its slight red shift. The intensity is, however, twice as large as that in methanol (Fig. 3). These results indicate that **1** is homogeneously dispersed in the bilayer membrane and surrounded by a hydrophobic molecular environment. Concomitantly, the fluorescence lifetime for **1** in the vesicle was found to be 2.5 ± 0.1 ns, which was also in fair agreement with that of the monomer in methanol (5.3 ± 0.9 ns) [9d].

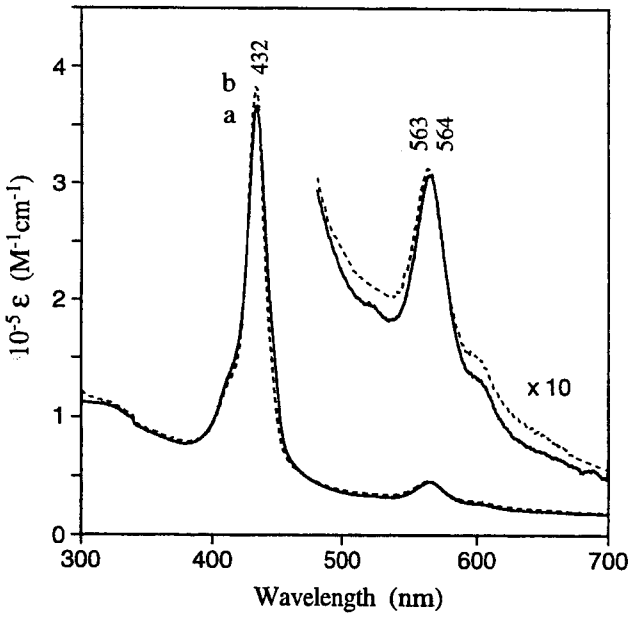

Fig. 4. (a) UV–Vis absorption spectrum of DMPC vesicles embedding **1** and **2** (molar ratio: 500/1/1) and (b) the superposition of those of DMPC vesicles embedding individual chromophores subtracted by that of vacant DMPC vesicles as a blank.

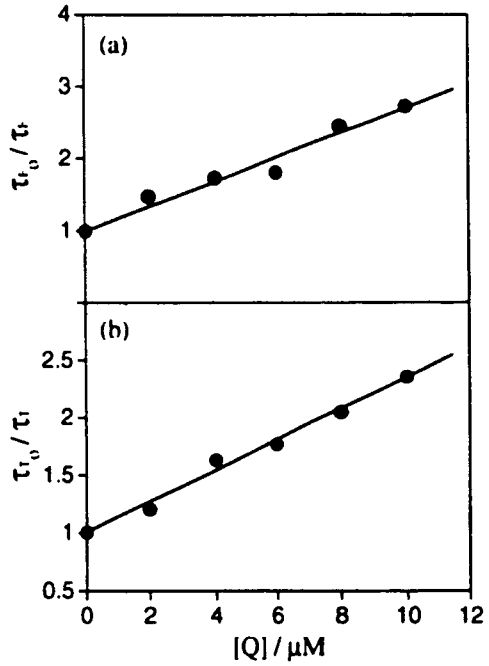

Fig. 5. Stern–Volmer plots of (a) fluorescence-lifetime quenching and (b) triplet-state quenching of **1** by **2** in the DMPC membrane.

3.2.3. Singlet quenching

The UV–Vis absorption spectrum of the vesicles embedding both **1** and **2** is almost identical with the superposition of those of the vesicles incorporating individual chromophores from which is subtracted that of the vacant DMPC vesicles as a blank (Fig. 4). This result suggests that there is no interaction between the two chromophores in the DMPC membrane. However, the quantum yield of the fluorescence of this hybrid vesicle significantly decreased; a little increase of **2** led to effective quenching of the fluorescence. The decrease in the fluorescence intensity would be ascribed to the electron transfer from the excited singlet state (S_1) of **1** to **2**. The Stern–Volmer plots for the fluorescence lifetime are shown in Fig. 5(a) in which a linear correlation was obtained in the range of the corresponding **2** concentration. From the slope, the apparent Stern–Volmer constant, K_{sv}, was calculated to be 1.7×10^5 M^{-1}. Under the assumption that the rate constant for the sum of all competing processes corresponds to the reciprocal singlet lifetime, the quenching rate constant was calculated to be 6.7×10^{13} M^{-1} s^{-1}. This quantitative evaluation led to an unreasonably high value. Therefore, the real concentration of **2** in the DMPC bilayer membrane should be considered for the interpretation of the Stern–Volmer plots. The rate constant corrected by the inner volume of the membrane was estimated to be 1.2×10^{11} M^{-1} s^{-1} or less[3], because the space in which the porphyrin moieties exist in the vesicles is limited around the center of the membrane. Although the rate constant is high, the quenching in the present system would not be static because the iron complex in the corresponding range did not cause a spectroscopic shift in the absorption band of **1**. This quenching cannot be interpreted in terms of dynamic and static quenching as in homogeneous organic solutions. The rate constant, which is much larger than the order of the diffusion-controlled value, shows that the electron transfer via the excited singlet state occurs by tunneling of the excited electron to the acceptor

[3] The volume was estimated from the diameter of the vesicle, the thickness of the bilayer membrane and the areas occupied by a DMPC and a lipidporphyrin molecule in each compact film (0.6 and 2.8 nm^2 per molecule, respectively) (see Ref. [9d]).

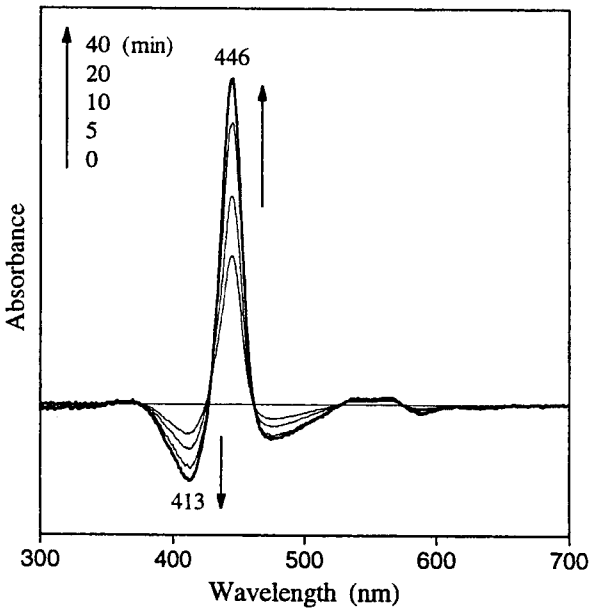

Fig. 6. Difference absorption spectra of DMPC vesicles embedding **1** and **2** (molar ratio: 500/1/5) in water containing triethanolamine (10 vol%) on photoirradiation (> 500 nm) under argon.

molecule when the nearest neighboring **2** exists in the quenching sphere of **1**. The fixed location and orientation of the porphyrin moieties in the gel-state membrane probably allow the proportionate quenching of the fluorescence lifetime of **1** up to the high concentration of **2**.

3.2.4. Triplet quenching

The transient spectra of the DMPC vesicle embedding **1** after nano-second laser excitation (λ_{ex}: 532 nm) displayed a triplet–triplet (T–T) absorption (λ_{max}: 470 nm). The dark decay obeyed first order kinetics (τ_T = 3.9 ms) which was 11-fold longer than that for the methanolic monomer (τ_T = 350 μs). In the case of the DMPC vesicles embedding **1** and **2**, the triplet decay showed predominantly first-order kinetics. The intensity of the T–T absorption of **1** became significantly smaller with the increasing concentration of **2**. This is due to the electron transfer from the S_1 state of **1** to **2**, which occurs in competition with the intersystem crossing. Part of the S_1 state of **1** is quenched, while the others, which are quite separated from **2**, can undergo intersystem crossing and thus the excited triplet state was observed. Stern–Volmer plots of the relative triplet lifetime (τ_{To}/τ_T) versus the quencher concentration again showed a linear relationship in the concentration range 0–10 μM for **2** (Fig. 5(b)). From the slope, the corrected quenching rate constant was 6.2×10^4 M^{-1} s^{-1}. For the interpretation of this low value compared to that in homogeneous solvents (generally, 10^8–10^{10} M^{-1} s^{-1}) [12], we have to consider the viscosity of the DMPC bilayer membrane in which the diffusion constant under the gel-to-liquid crystal phase transition temperature becomes 10^4-times smaller [13]. In our heterogeneous system, the triplet quenching constant can be interpreted as being controlled by the diffusion reaction in the DMPC membrane.

Upon photoirradiation of the DMPC vesicle embedding the two chromophores in the presence of triethanolamine (TEA) as an electron donor, sacrificial photoreduction of **2** was observed. The obtained absorption difference spectra are shown in Fig. 6. After the irradiation for 40 min, the final spectrum was characterized by three peaks at 446, 542 and 567 nm and two valleys at 413 and 477 nm. They represent the conversion of the ferric porphyrin to the five *N*-coordinated ferrous porphyrin, which will act as an effective dioxygen transporter.

4. Conclusions

The self-assembled micelles made of **1** and **2** showed negligible fluorescence and T–T absorption, which are due to the formation of the photodeactive complex between the two chromophores in the ground state. On the other hand, DMPC vesicles embedding the two chromophores at moderate ratios represented photoinduced electron transfer. Because of the low mobility and high dispersibility of the lipidporphyrins anchored into the gel state of DMPC membrane, the Stern–Volmer plots for the fluorescence lifetime showed a straight line up to high concentrations of the quencher; the quenching rate constant was estimated to be 1.2×10^{11} M^{-1} s^{-1}. The electron transfer presumably occurs by a tunneling mechanism when the nearest neighboring **2** exists in the quenching sphere of **1**. A Stern–Volmer analysis of the triplet quenching again exhibited a linear relationship. The estimated quenching constant was 6.2×10^4 M^{-1} s^{-1}, which was rate-limiting by the diffusion reaction in the DMPC membrane. The electron transfer allows sacrificial electron transport from **1** to **2** in the presence of TEA. This hybrid vesicle embedding Zn(II)- and Fe(III)-lipidporphyrins is expected to act as a light-initiated O_2-carrying system in aqueous medium.

Acknowledgements

This work was partially supported by the Core Research for Evolutional Science and Technology, JST and a Grant-in-Aid for Scientific Research (No. 11650935) from the Ministry of Education, Science, Culture and Sports, Japan.

References

[1] I. Fujita, T.L. Netzel, C.K. Chang, C.-B. Wang, Proc. Natl. Acad. Sci. USA 79 (1982) 413.

[2] R.L. Brookfield, H. Ellul, A. Harriman, J. Chem. Soc., Faraday Trans. 81 (1985) 1837.

[3] N. Mataga, H. Yao, T. Okada, Y. Kanda, A. Harriman, Chem. Phys. 131 (1989) 473.

[4] T. Komatsu, E. Tsuchida, C. Böttcher, D. Donner, C. Messerschmidt, U. Siggel, W. Stocker, J.P. Rabe, J.-H. Fuhrhop, J. Am. Chem. Soc. 119 (1997) 11660.

[5] D. Heiler, G. McLendon, P. Rogalskj, J. Am. Chem. Soc. 109 (1987) 604.

[6] A. Osuka, K. Maruyama, N. Mataga, T. Asahi, I. Yamazaki, N. Tamai, J. Am. Chem. Soc. 112 (1990) 4958.

[7] J. Lahiri, G.D. Fate, S.B. Ungashe, J.T. Groves, J. Am. Chem. Soc. 118 (1996) 2347.

[8] (a) E. Tsuchida, Top. Curr. Chem. 132 (1986) 64. (b) M. Yuasa, H. Nishide, E. Tsuchida, J. Chem. Soc., Dalton Trans. (1987) 2493.

[9] (a) T. Komatsu, K. Nakao, H. Nishide, E. Tsuchida, Chem. Commun. (1993) 728. (b) E. Tsuchida, T. Komatsu, K. Arai, K. Yamada, H. Nishide, C. Böttcher, J.-H. Fuhrhop, Langmuir 11 (1995) 1877. (c) E. Tsuchida, T. Komatsu, K. Arai, K. Yamada, H. Nishide, C. Böttcher, J.-H. Fuhrhop, Chem. Commun. (1995) 1063. (d) T. Komatsu, T. Yanagimoto, Y. Furubayashi, J. Wu, E. Tsuchida, Langmuir 15 (1999) 4427.

[10] T. Komatsu, K. Yamada, E. Tsuchida, U. Siggel, C. Böttcher, J.-H. Fuhrhop, Langmuir 12 (1996) 6242.

[11] P.W.M. Van Dijck, B. De Kruijff, L.L.M. Van Deenen, J. De Gier, R.A. Demel, Biochim. Biophys. Acta 455 (1976) 576.

[12] (a) M.-C. Richoux, A. Harriman, J. Chem. Soc., Faraday Trans. 1, 78 (1982) 1873. (b) A. Harriman, G. Porter, P. Walters, J. Photochem. 19 (1982) 183.

[13] E.S. Wu, K. Jacobson, D. Papahadjopoulos, Biochemistry 16 (1977) 3936.

Bioconjugate Chem. **2001**, *12*, 648–652

TECHNICAL NOTES

Photoreduction of Autooxidized Albumin–Heme Hybrid in Saline Solution: Revival of Its O_2-Binding Ability

Akito Nakagawa, Teruyuki Komatsu, and Eishun Tsuchida*

Department of Polymer Chemistry, Advanced Research Institute for Science and Engineering, Waseda University, Tokyo 169-8555, Japan. Received September 5, 2000; Revised Manuscript Received January 20, 2001

Recombinant human serum albumin (rHSA) incorporating 2-[8-{*N*-(2-methylimidazolyl)}octanoyloxymethyl]-5,10,15,20-tetrakis(α,α,α,α-*o*-pivalamido)phenylporphinatoiron(II)s (Fe(II)Ps) [rHSA–Fe(II)P] is a synthetic hemoprotein which can bind and release O_2 reversibly under physiological conditions (saline solution [NaCl]: 150 mM, pH 7.3) as do hemoglobin and myoglobin. However, the central ferrous ions of Fe(II)Ps are slowly oxidized to O_2-inactive ferric forms. Based on the UV–vis. absorption spectroscopy, the majority of the autooxidized Fe(III)Ps in albumin are determined to be six-coordinate high-spin complexes with a proximal imidazole and a chloride anion, which show ligand-to-metal charge transfer (LMCT) absorption at 330 nm. Interestingly, photoirradiation of this LMCT band under an argon atmosphere led to reduction of the central ferric iron of Fe(III)P, allowing the revival of the O_2-binding ability. The ratio of the photoreduction reached a maximum of 83%, which is probably due to the partial dissociation of the axial imidazole. The same photoirradiation under a CO atmosphere provides the corresponding carbonyl rHSA–Fe(II)P. Laser flash photolysis experiments revealed that the reduction was completed within 100 ns. The quantum yields (Φ) of these photoreductions were approximately 0.01.

INTRODUCTION

The ferrous complexes of protoporphyrin IX in hemoglobin (Hb) are slowly oxidized even in the bloodstream, converting to the O_2-inactive ferric forms. If one can reduce these iron(III) complexes by light irradiation, this becomes the easiest way to revive their O_2-binding abilities. From this point of view, reduction of the porphyrinatoiron(III)s has been of great interest for several decades. The ferric complexes of porphyrins normally coordinate with counteranions and show a ligand-to-metal charge transfer (LMCT) transition in the near UV region. It has been shown that, in organic solvents, photoirradiation of this LMCT absorption led to reduction of the central metal involving a radical dissociation (Bartocci et al., 1980; Brault et al., 1980; Hoshino et al., 1992,1998; Inamura et al., 1985; Ward et al., 1982). Henderikson et al., for example, revealed the clean photoreduction of tetraphenylporphinatoiron(III) halide ([Fe(III)TPP]$^+X^-$) by 355-nm irradiation in benzene (Henderikson et al., 1987). In aqueous media, however, the produced radicals easily react with the formed porphyrinatoiron(II), so that the ferrous complex is not accumulated. Only when hyaluronic acid coexists in phosphate-buffered saline solution, the self-organized fibers of amphiphilic Fe(III)TPP derivative could be reduced by the LMCT irradiation (Komatsu et al., 2000b).

On the other hand, recombinant human serum albumin (rHSA) incorporating *eight* 2-[8-{*N*-(2-methylimidazolyl)}octanoyloxymethyl]-5,10,15,20-tetrakis(α,α,α,α-*o*-pivalamido)phenylporphinatoiron(II) (Fe(II)P) [rHSA–Fe(II)P] is a synthetic hemoprotein which can bind and release O_2 under physiological conditions (in aqueous media, pH 7.3, 37 °C) as do Hb and myoglobin (Mb) (Komatsu et al., 1999; 2000a; Tsuchida et al., 1997; 1999). The 5 wt % solution of this albumin–heme hybrid satisfies the physiological requirements for a red blood cell substitute. In fact, administration of this solution into hemorrhagic shock rats showed an increase in the renal cortical O_2-tensions and skeletal tissue O_2-tensions (Tsuchida et al., 2000). Nevertheless, the remaining problem with this rHSA–Fe(II)P is also the relatively short lifetime as an O_2-carrying vehicle. Autoxidation of the central ferrous ion of Fe(II)P takes place slowly through a proton-driven process (Momentau et al., 1994). We report herein for the first time the unique coordination structure of Fe(III)P in albumin and the photoreduction of rHSA-Fe(III)P by LMCT excitation, which allows revival of the O_2-binding ability. Laser flash

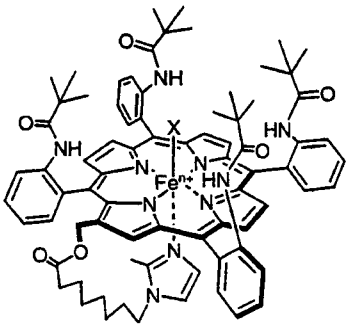

n: 2, X: none Fe(II)P

n: 3, X: Cl^- Fe(III)P

* To whom the correspondence should be addressed. CREST investigator, JST. Phone: +81 3-5286-3120; Fax: +81 3–3205–4740. E-mail: eishun@mn.waseda.ac.jp.

10.1021/bc000106j CCC: $20.00
Published on Web 06/14/2001

photolysis experiments also revealed that the reduction was completed within 100 ns.

EXPERIMENTAL PROCEDURES

Materials and Preparation. The synthetic heme, 2-[8-{*N*-(2-methylimidazolyl)}octanoyloxymethyl]-5,10,15,20-tetrakis(*o*-pivalamido)phenylporphinatoiron(II) (Fe(II)P) and the rHSA–Fe(II)P solution [rHSA/Fe(II)P = 1/8 (mol/mol), in phosphate-buffered saline (pH 7.4)] was prepared according to our previously reported procedures (Komatsu et al., 2000; Tsuchida et al., 1995). The recombinant human serum albumin (rHSA; 25 wt %) was obtained from the WelFide Corporation (Sumi et al., 1993). FeP concentrations of 20 μM were normally used for the UV–vis. absorption spectral measurements (Shimadzu V-570 spectrometer) within the range of 300–700 nm. Upon addition of the rHSA–Fe(II)P solution to O_2, the absorption spectrum showed the typical O_2-adduct of Fe(II)P (λ_{max}: 426, 552 nm). After incubation of this dioxygenated rHSA–Fe(II)P at 40 °C for 24 h, all the Fe(II)P sites in rHSA are oxidized, giving rHSA-Fe(III)P with absorption maxima at 330, 423, and 565 nm.

Photoreduction of Fe(III)P Incorporated into rHSA. The photoirradiation of this oxidized rHSA-Fe(III)P solution was performed with a 250-W ultrahigh-pressure Hg arc-lamp (Ushio UCH-250) under an argon or a CO atmosphere in a dark room (25 °C). The Hg lamp was held in a special lamp housing (Koken Kogyo LHX-150), which was connected to a PSX-75 power supply. The light filtered by a U-370 colored filter was irradiated into the rHSA-Fe(III)P solution in a 10-mm cuvette with a constant distance of 7.5 cm. The UV–vis. absorption spectra of the solutions were measured at several intervals. The reduction rates were calculated from the Soret band absorption (A_t) divided by that of the 100% reduced form for the deoxy state (A_{deoxy} at 443 nm) or carbonyl state ($A_{carboxy}$ at 427 nm). The quantum yield (Φ) was determined by the well-established procedure with an oxalight Fe(II) complex (Michaelson et al.).

Transient Absorption Spectroscopy. The transient absorption spectra after the laser flash photolysis were measured using an ICCD detector (ANDOR DH520-18F-WR) with an imaging monochromator (ORIEL MS-257). The excitation laser pulse was generated from the THG (355 nm; pulse width, 5 ns) of a Nd:YAG laser (Spectron SL803G-10). The pulse xenon flash lamp (10 W, 10 Hz, 100 ns pulse width) was used as the monitor light source. The path length of the cuvette was 10 mm, and all measurements were carried out using a two-channel simultaneous detection system (Tokyo Instruments, Ltd.) at 25 °C.

Resonance Raman Spectroscopy. Resonance Raman spectroscopy measurements were performed using a laser Raman spectrometer equipped with a CCD multichannel detector (JASCO NRS-2000). Excitation was carried out with the 457.9 nm line of an NEC GLG2162 Ar^+ ion laser in a backscattering geometry at 25 °C. The FeP concentrations of 1 mM in special liquid cells were normally used for the measurements.

RESULTS AND DISCUSSION

Coordination Structure of Autooxidized Fe(III)P in Albumin. Although the rHSA–Fe(II)P hybrid can bind molecular O_2 reversibly under physiological conditions, the central ferrous ions of the Fe(II)Ps are slowly oxidized to O_2-inactive ferric forms by a proton-driven process (Momentau et al., 1994). This oxidation, *namely autoxidation*, generally obeyed the first-order kinetics with a half-life of ca. 8 h at 25 °C (Tsuchida et al., 1997). The UV–vis absorption spectrum of the final compound showed maxima at 330, 423, and 565 nm. We have reported that the amphiphilic Fe(III)TPP derivative formed a five-coordinated high-spin complex with a chloride anion (Cl^-) in phosphate-buffered saline solution (Fleischer et al., 1971; Komatsu et al., 2000b). However, this is not true for rHSA-Fe(III)P. On the basis of the absorption pattern, we determined that the dominant species of Fe(III)P in rHSA is an octahedral six-coordinate high-spin ferric complex with a Cl^- and an intramolecularly coordinated imidazole nitrogen (Figure 1, 3) (Shantha et al., 1998; Walker et al., 1976). In general, this type of six-coordination with sterically hindered imidazole, such as 1,2-dimethylimidazole (1,2-Me_2Im), is formed when a large excess of imidazole is present in the solution, because of the extremely low equilibrium constant of 1,2-DMIm to $[Fe(III)TPP]^+Cl^-$; 3.4 M^{-1} (Walker et al., 1976). However, in albumin, each Fe(III)P molecule is incorporated into the small space of the hydrophobic domain, so that the six-coordination to the ferric complex is presumably formed. We assigned the small absorption band at 330 nm to a ligand-to-metal charge transfer (LMCT) transition between the central ferric ion and the Cl^- (Shantha et al., 1998). In the case of the five-coordinate high-spin $[Fe(III)TPP]^+Cl^-$, the LMCT absorption maxima shift to the lower energy with the decreasing electronegativity of the halides ($I^- < Br^- < Cl^-$), while the Soret and Q-bands, which are $\pi-\pi^*$ transitions, are not affected (Hendrikson et al., 1987; Komatsu et al., 2000). However, the λ_{max} of the LMCT absorption of the six-coordinated Fe(III)P in rHSA was constant versus the electron negativity of the counteranions ($[X^-]$: 150 mM) (Table 1).

We then employed resonance Raman spectroscopy to detect the vibration stretching mode of the porphyrin ring

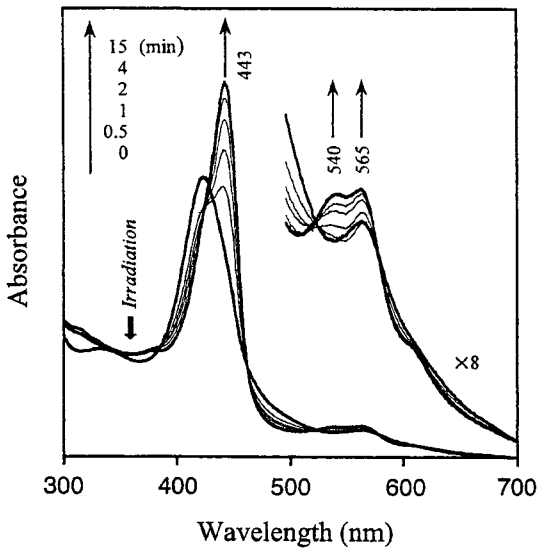

Figure 1. UV-vis absorption spectral changes in photoreduction of rHSA-Fe(III)P in phosphate-buffered saline (150 mM NaCl, pH 7.3) solution under argon atmosphere at 25 °C.

Table 1. Absorption Maxima of γHSA-Fe(III)P Solution with Sodium Halide (150 mM) at 25 °C

	electron negativity	LMCT (nm)	Soret (nm)	Q (nm)
F^-	4.0	330	423	566
Cl^-	3.0	330	423	565
Br^-	2.8	332	422	569
I^-	2.5	333	422	569

(ν_2) which is expected in the 1541–1554 cm^{-1} for the six-coordinated high-spin [Fe(III)TPP]$^+$Cl$^-$(1,2-Me_2Im) analogue (Parathati et al., 1987). The obvious absorption appeared in this region as double peaks at 1566 and 1547 cm^{-1} (not shown). The latter is likely to be the ν_2 band of the six-coordinate Fe(III)P in albumin.

Photoreduction of Autooxidized Fe(III)Ps in Albumin. The 365-nm irradiation of the saline solution of rHSA-Fe(III)P under argon atmosphere led to reduction of the central ferric ion; the visible absorption spectrum changed to the typical five-*N*-coordinate high-spin Fe(II)P complex (λ_{max}: 443, 542, and 565 nm) within 15 min (Figure 1). The isosbestic points (431, 461, 524, and 580 nm) throughout the measurement revealed that no side reactions occurred.

The following two results indicate that the photoreduction of rHSA-Fe(III)P occurs through the intramolecular electron transfer initiated by LMCT excitation. (i) In the absence of NaCl (in deionized water), the reduction proceeded by only 20%, suggesting that a Cl^- is essential for this reaction. (ii) The Soret band irradiation also reduced the ferric center, but by less than 40%. Irradiation of the LMCT band causes only the efficient reduction of the autooxidized rHSA-Fe(III)P. Shantha and co-workers revealed that the coordination of 2-methylimidazole to [Fe(III)TPP]$^+$Cl$^-$ results in a clean photoreduction of the central ferric ion by 407-nm irradiation (Shantha et al., 1998). They also inferred that a photoreactive state with a λ_{max} at 315–335 nm is responsible for this reduction.

For accumulation of the reduced Fe(II)P, a radical scavenger should be present in the solution to avoid the back electron transfer. Actually, irreversible photoreduction of the molecular fibers of the amphiphilic Fe(III)-TPP derivative occurred only in a phosphate-buffered saline solution containing a small amount of hyaluronic acid (Komatsu et al., 2000). We can therefore assume that the albumin host itself, for instance, the amino acid residues located nearby Fe(III)P, immediately traps the chloride radicals after the charge separation, then the reaction becomes irreversible. The most probable candidates are tyrosine and tryptophan. It is also remarkable that the photoreduction rate was not affected by the kinds of halide ions (I^-, Br^-, Cl^-, F^-).

Upon exposure of the aqueous solution of the photoreduced rHSA–Fe(II)P to O_2, the UV–vis absorption spectrum changed to that of the dioxygenated complex (λ_{max}: 426, 552 nm). The O_2 coordination reversibly depended on the O_2-partial pressure. An interesting observation is that the photoreduction rates reached a maximum of 83% (Figure 2). This is probably due to the base elimination in the ferric state; the imidazolyl group once dissociated from the central iron cannot coordinate again to the iron(III) center. This is consistent with our previously reported results on the reduction of the autooxidized rHSA-Fe(III)P by ascorbic acid with red blood cells (Tsuchida et al., 2000).

Photoirradiation into the LMCT band of the rHSA-Fe(III)P under CO atmosphere provides carbonyl rHSA–Fe(II)P (λ_{max}: 427, 540 nm) (Figure 3). CO coordinates with Fe(II)P immediately after the photoreduction of the central ferric ion, affording the stable carbonyl complexes. The reduction rate was estimated to be 93% under CO atmosphere. The real concentration of the carbonyl Fe(II)P in rHSA should not be as high, around 83%, because the Soret band absorption includes that of the five-coordinated Fe(II)P(CO) complex without axial imidazole bonding, which has a large molecular coefficient.

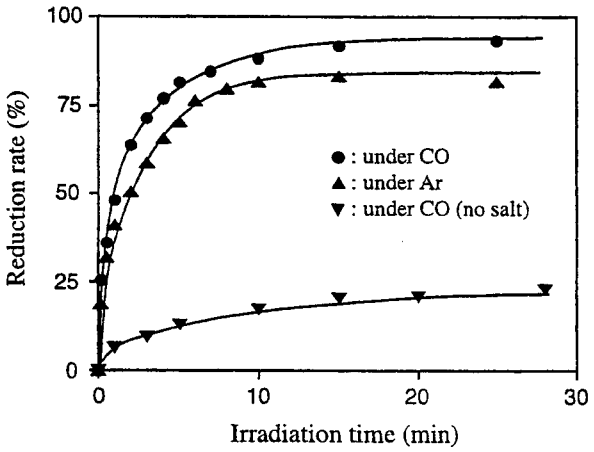

Figure 2. UV-vis absorption spectral changes in photoreduction of rHSA-Fe(III)P in phosphate-buffered saline (150 mM NaCl, pH 7.3) solution under CO atmosphere at 25 °C.

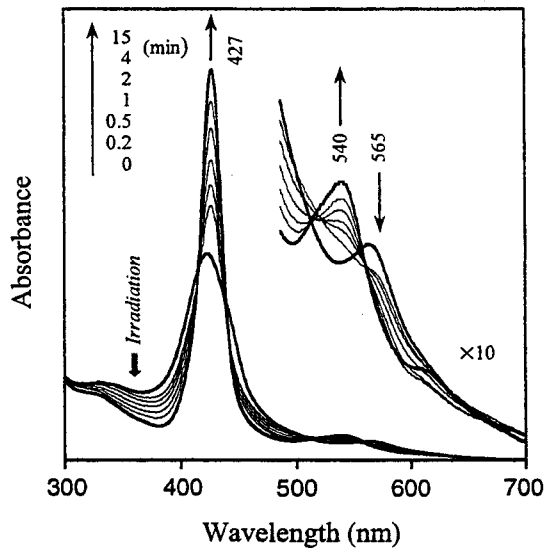

Figure 3. Relationship between the reduction rate and the irradiation time of rHSA-Fe(III)P in in phosphate-buffered saline (150 mM NaCl, pH 7.3) solution at 25 °C.

Laser flash photolysis at 355 nm (THG of Nd:YAG) of the deaerated aqueous rHSA-Fe(III)P solution showed that the photoreduction was finished within the duration of the laser pulse; the transient absorption spectral pattern measured at 100 ns after the pulse was in good agreement with the difference spectrum of the rHSA–Fe(II)P solution minus the autooxidized rHSA-Fe(III)P solution (Figure 4). The primary reaction step appears to be the homolytic cleavage of the axial Cl^-, and Fe(II)P with intramolecularly coordinated axial imidazole is immediately formed. The produced chloride radical should have reacted with the active hydrogen in the amino acid residues of rHSA.

The quantum yields (Φ) of this photoreduction system were determined to be 0.01 under a CO atmosphere and 0.008 in argon. Because the LMCT excitation state (LMCT*) is located above the S_1 and S_2 states, the photoexcited species has two pathways for decaying (Figure 5). The first is quenching to the S_2 state with a rate constant of k_d, and the second one yields Fe(II)P via intramolecular electron transfer. Of course, the former decay is major, and the charge recombination to Fe(III)-P$^+$Cl$^-$ with a rate constant of k_b is also a facile reaction which returns to the ground state. However, if the

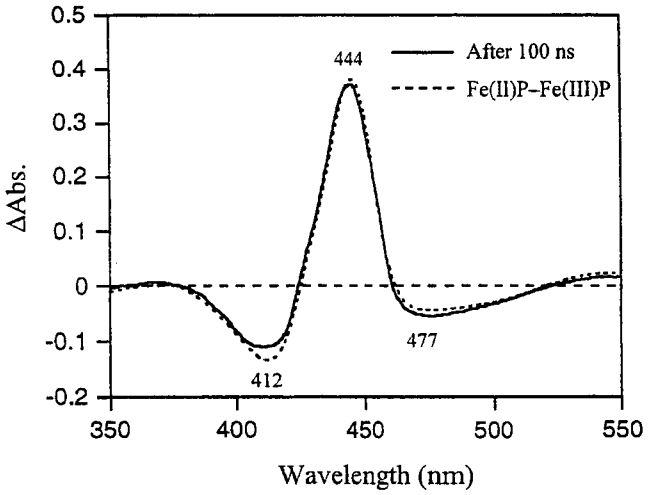

Figure 4. Transient absorption spectrum of rHSA-Fe(III)P in phosphate-buffered saline (150 mM NaCl, pH 7.3) solution at 100 ns after the laser flash photolysis (355 nm) at 25 °C. The spectral pattern is in good agreement with the difference spectrum of rHSA–Fe(II)P minus rHSA-Fe(III)P.

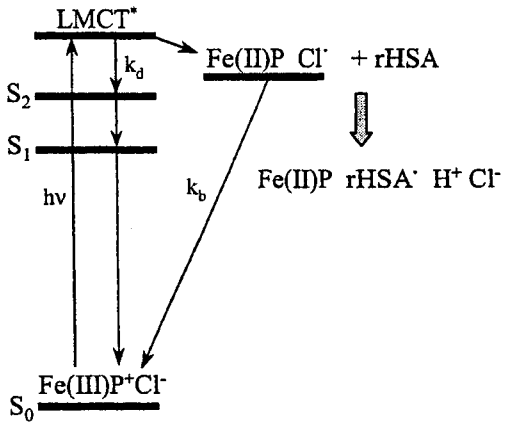

Figure 5. Transient states and interconversion pathways for photoreduction of rHSA-Fe(III)P.

albumin cage traps the chloride radical, the photoinduced electron transfer to the ferric ion becomes irreversible. That is to say, the low quantum yield of this photoreduction is due to the high probabilities of (i) the deactivation of LMCT* to S_2, and (ii) back electron transfer between the ferrous ion and the chloride radical.

CONCLUSIONS

The autooxidized Fe(III)P in the albumin hybrid formed a unique six-coordinate high-spin ferric complex, which shows the LMCT absorption at 330 nm. Photoirradiation of this band under an argon atmosphere led to a clean reduction of Fe(III)P to revive its O_2-binding ability. The partial Fe(III)P which eliminates the axial base could not be reduced, because of the imidazole rebinding is probably interfered by the steric hindrance of the amino acid residues in the albumin interior. The relatively low quantum yield of this photoreduction may increase in the serum solution, because the biological system contains some scavengers for radicals. Picosecond laser flash photolysis experiments to reveal the detailed mechanism of this photoreduction are now in progress.

ACKNOWLEDGMENT

This work was partially supported by the Core Research for Evolutional Science and Technology, JST, Health Science Research Grants (Artificial Blood Project) of the Ministry of Health and Welfare, Japan, and a Grant-in-Aid for Scientific Research (No. 11650935) form the Ministry of Education, Science, Culture and Sports, Japan.

LITERATURE CITED

(1) Bartocci, C., Scandola, F., Ferri, A., and Carassiti, V. (1980) Photoreduction of Hemin in Alcohol-Containing Mixed Solvents. *J. Am. Chem. Soc. 102,* 7067–7072.

(2) Brault, D., Bizet, C., Morliere, P., Rougee, M., Land, E. J., Santus, R., and Swallow, A. J. (1980) One-Electron Reduction of Ferrideuterioporphyrin IX and Reaction of the Oxidized and Reduced Forms with Chlorinated Methyl Radicals. *J. Am. Chem. Soc. 102,* 1015–1019.

(3) Fleischer, E. B., Palmer, J. M., Srivastava, T. S., and Chatterjee, A. (1971) Thermodynamic and Kinetic Properties of an Iron-Porphyrin System. *J. Am. Chem. Soc. 93,* 3162–3167.

(4) Hendrickson, D. V., Kinnaird, M. G., and Suslick, K. S. (1987) Photochemistry of (5,10,15,20-Tetraphenylporphyrinato)iron(III) Halide Complexes, Fe(TPP)(X). *J. Am. Chem. Soc. 109,* 1243–1244.

(5) Hoshino, M., Ueda, K., Takahashi, M., Yamaji, M., and Hama, Y. (1992) Photoreduction of Iron(III) Tetraphenylporphyrin in Ethanol studied by Laser Flash Photolysis: Effects of Concentration on Quantum Yields. *J. Chem. Soc., Faraday Trans. 88,* 405–408.

(6) Hoshino, M. and Baba, T. (1998) Laser Photolysis of Iron(III) Tetraphenylporphyrin in Methanol. Kinetic Study on the Formation of the Superoxide Anion Radical from the Dioxygen Adduct of Iron(II) Tetraphenylporphyrin. *J. Am. Chem. Soc. 120,* 6820–6821.

(7) Imamura, T., Jin, T., Suzuki, T., and Fujimoto, M. (1985) Photoreduction of Manganese(III), Iron(III), Cobalt(III), and Molybdenum(V) Tetraphenyporphyrins in 2-Methyltetrahydrofuran. *Chem. Lett. 1985,* 847–850.

(8) Komatsu, T., Hamamatsu, K., Wu, J., and Tsuchida, E. (1999) Physicochemical Properties and O_2–Coordination Structure of Human Serum Albumin Incorporating Tetrakis(*o*-pivalamido)phenylporphyrinatoiron(II) Derivatives. *Bioconjugate Chem. 10,* 82–86.

(9) Komatsu, T., Matsukawa, Y., and Tsuchida, E. (2000a) Kinetics of O_2- and CO–Binding to Human Serum Albumin-Hybrid. *Bioconjugate Chem. 11,* 772–776.

(10) Komatsu, T., Yanagimoto, T., Nakagawa A., and Tsuchida, E. (2000b) Photoreduction of Self-Assembled Lipidporphinatoiron(III) Chloride with Hyaluronic Acid under Semi-Physiological Conditions. *Chem. Lett..* 84–85.

(11) Michaelson, R. C., and Loucks, L. F. (1975) *J. Chem. Educ. 52,* 652–653.

(12) Momentau, M., and Reed, C. A. (1994) Synthetic Hemes. *Chem. Rev. 110,* 7690–7697.

(13) Parthasarathi, N., Hansen, C., Yamaguchi S., and Spiro T. G. (1987) Metalloporphyrin Core Size Resonance Raman Marker Bands Revisited: Implications for the Interpretation of Hemoglobin Photoproduct Raman Frequencies. (1987) *J. Am. Chem. Soc. 109,* 3865–3871.

(14) Shantha, P. K., Thanga, H. H., and Verma. A. L. (1998) Photoreduction of Fe(TPP)Cl in CH_2Cl_2 and DMSO in the Presence of and in Neat 1,2-Dimethylimidazole without Alcohol; Evidence for a Photoreactive State from Resonance Raman and Optical Absorption Studies. *J. Raman Spectrosc. 29,* 997–1001.

(15) Sumi, A., Ohtani, W., Kobayashi, K., Ohmura, T., Yokoyama, K., Nishida, M., and Suyama, T. (1993) Purification and Physicochemical Properties of Recombinant Human Serum Albumin. *Biotechnology of Blood Proteins* (C. Rivat, J.-F. Stoltz, Ed.) Vol. *227,* pp 293–298, John Libbey Eurotext (Montrouge).

(16) Tsuchida, E., Komatsu, T., Kumamoto, S., Ando, K., and Nishide, H. (1995) Synthesis and O_2–Binding Properties of Tetraphenylporphyrinatoiron(II) Derivatives Bearing a Proximal Imidazole Covalently Bound at the β-pyrrolic Position. *J. Chem. Soc., Perkin Trans. 2* 747–753.

(17) Tsuchida, E., Ando, K., Maejima, H., Kawai, N., Komatsu, T., Tekeoka, S., and Nishide, H. (1997) Properties of and Oxygen Binding by Albumin- Tetraphenylporphinatoiron(II) Derivative Complexes. *Bioconjugate Chem. 8,* 534−538.
(18) Tsuchida, E., Komatsu, T., Matsukawa, Y., Hamamatsu, K., Wu, J. (1999) Human Serum Albumin Incorporating Tetrakis(*o*-pivalamido)phenylporphinatoiron(II) Derivative as a Totally Synthetic O_2−Carrying Hemoprotein. *Bioconjugate Chem. 10,* 797−802.
(19) Tsuchida, E., Komatsu, T., Hamamatsu, K., Matsukawa, Y., Tajima, A., Yoshizu, A., Izumi, Y., and Kobayashi, K. (2000) Exchange Transfusion with Albumin-Heme as an Artificial O_2-Infusion into Anesthetized Rats: Physiological Responses, O_2-Delivery, and Reduction of the Oxidized Hemin Sites by Red Blood Cells. *Bioconjugate Chem. 11,* 46−50.
(20) Walker, F. A., Lo, M.-W., and Ree, M. T. (1976) Electronic Effects in Transition Metal Porphyrins. The Reaction of Imidazoles and Pyridines with a Series of Para-Substituteed Tetraphenylporphyrin Complexes of Chloroion(III). *J. Am. Chem. Soc. 98,* 5552−5560.
(21) Ward, B., and Chang, C. K. (1982) A Convenient Photochemical Method for Reduction of Ferric Hemes. *Photochem. Photobiol. 35,* 757−759.

BC000106J

Photoreduction of a Self-Assembled (Lipidporphyrinato)iron(III) Complex in Saline by LMCT Excitation: Co-Aggregated Hyaluronic Acid Allows an Irreversible Electron Transfer

Tetsuya Yanagimoto, Akito Nakagawa, Teruyuki Komatsu, and Eishun Tsuchida*,#

Department of Polymer Chemistry, Advanced Research Institute for Science and Engineering, Waseda University, Tokyo 169-8555

(Received June 15, 2001)

An amphiphilic (tetraphenylporphyrinato)iron(III) derivative with four alkylphosphocholine groups and a proximal imidazole [(lipidporphyrinato)iron(III); **1a**] was self-assembled in phosphate-buffered saline (pH 7.3, [NaCl] = 0.15 M) to form spherical micelles with a diameter of 10 nm. The obtained solution showed a distinct absorption band at 362 nm, which was assigned to the ligand-to-metal [Cl^- to iron(III)] charge transfer (LMCT) transition. Light irradiation into this CT band under an Ar atmosphere did not induce any changes in the UV-vis absorption spectrum. On the other hand, the addition of glucose (150 mM) to the solution led to complete photoreduction of the central iron(III) ion, giving a five-N-coordinated high-spin iron(II) complex. It has also been found that a small excess amount of hyaluronic acid ([units] = 100 μM) showed the same effect. The photoreduction was only seen by LMCT irradiation in the presence of the saccharide. It probably occurred via intramolecular electron transfer from Cl^- to iron(III), and the produced chlorine radical was scavenged by the saccharide, which prevented a back electron transfer reaction (the quantum yields; ca. 0.007). Interestingly, hyaluronic acid changed the morphology of the **1a** assembly from the micelle to a thin fiber. This co-aggregated structure with hyaluronic acid would be responsible for the effective photoreduction of **1a**. The viscosity of the fiber solution significantly decreased during the photoreduction, which suggests that radical trapping induces depolymerization of the hyaluronic acid. Laser flash photolysis experiments showed that the reduction and the imidazole association to the iron(II) center are completed within 50 ns after a laser pulse. The photoreduced (lipidporphyrinato)iron(II) fibers can reversibly bind and release O_2 similar to the same fibers which were prepared by chemical reduction using ascorbic acid.

The photochemistry of Fe(III) porphyrins, especially photoreduction of the central iron(III) ion, has been extensively investigated over the past two decades, because of considerable interest in the photomanipulation of the native hemoproteins' activities.[1–10] A counter anion generally coordinates the Fe(III) porphyrin and shows a ligand-to-metal charge transfer (LMCT) transition in the UV region, which is often responsible for photoinduced electron transfer from a ligand to a metal.[1–9] In contrast to the fact that many of the previous studies concerning the photoreduction of metalloporphyrins have required external sensitizers,[11–16] photoexcitation of the LMCT excitation provides a clean reduction through intramolecular electron transfer. For instance, the alcoholate complexes of the Fe(III) porphyrins in aqueous or nonaqueous alkaline alcohols undergo photocleavage of the Fe^{III}–O bond to give Fe(II) porphyrins and alkoxy radicals.[1–5] In a benzene solution, the chloro(tetraphenylporphyrinato)iron(III) [$Fe^{III}Cl$(tpp)] can be reduced to the iron(II) complex upon LMCT irradiation.[6,7] The mechanism of this photoreduction was postulated to be photolysis of the Fe^{III}–Cl^- bond. This basic photochemistry for the Fe(III) porphyrins has been expected to be adapted to control of functions of natural hemoproteins and the model hemes under physiological conditions. However, such a development has never been realized, because the produced radicals easily recombine with the Fe(II) porphyrin in water. Gilbert et al. only reported the irreversible photoreduction of the carboxy(porphyrinato)iron(III) complexes in aqueous solution containing a large excess amount of carboxylic acid or amino acid.[8,9]

We have recently found that the (tetraphenylporphyrinato)iron(II) derivative with four alkylphosphocholine groups and an axially coordinated imidazole [(lipidporphyrinato)iron(II); **1b**, Chart 1] formed tubular fibers in water, and can reversibly bind and release O_2 like hemoglobin and myoglobin.[17] The only drawback of this fiber as an O_2 transporter is its relatively short lifetime of the O_2-adduct complex. The O_2-biniding capability is slowly inactivated accompanying autooxidation of the central iron(II) ion by a proton-driven process.[18] If we can reduce the autooxidized iron(III) center by light irradiation, this method would become the simplest way to revive their O_2-binding abilities and to maintain their activity for a longer time. This paper describes the photoreduction of the self-assembled (lipidporphyrinato)iron(III) complex (**1a**, Chart 1) in phosphate-buffered saline by LMCT excitation. The co-aggregated saccharide prevents back electron transfer and allows the photoreduction to be irreversible. The resulting **1b** fiber permitted a reversible O_2 binding.

CREST investigator, JST.

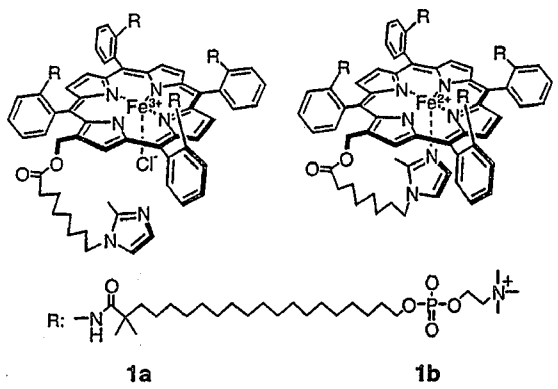

Chart 1.

Experimental

Materials and General Methods. 2-[8-(2-Methylimidazole-1-yl)octanoyloxymethyl]-5,10,15,20-tetrakis{$\alpha,\alpha,\alpha,\alpha$-*o*-[2,2-dimethyl-20-({[2-trimethylammonio]ethoxy}phosphonatoxy)-icosanamide]phenyl}porphyrinatoiron(III) (**1a**) was prepared according to our previously reported procedures.[17] The hyaluronic acid sodium salt (from human umbilical cord) and amylose were purchased from Sigma Chem. Co. Glucose and other chemicals were obtained from the Kanto Chem. Co. and used without further purification. The water was deionized using an ADVANTEC GS-200 system.

Preparation of Aqueous (Lipidporphyrinato)iron(III) Solution. A methanol solution of **1a** (< 5 μL) was injected into phosphate buffered-saline (PBS; 1 mM, pH 7.3, [NaCl] = 150 mM, 2.5 mL) and the obtained homogeneous solution was incubated for 4 h at room temperature. The remaining methanol ([CH_3OH] < 0.2 vol%) was completely removed by dialysis with a cellulose tube in PBS for 1 h (2 times) and for another 15 h at 4 °C. The final concentration of **1a** was normally adjusted to 10 μM based on its molar extinction coefficient (ε_{424}: 5.8 × 10^4 M^{-1} cm^{-1}), and saccharides were directly added to this solution. The samples were held in a cuvette (optical path length 10 mm) and degassed by Ar bubbling for at least 30 min. Spectrophotometric measurements were performed using a JASCO UV-570 spectrophotometer.

Transmission Electron Microscopy (TEM). Negatively stained specimens for TEM were prepared according to our previously reported method.[19,20] The obtained grids were observed using a JEOL JEM-100CX electron microscope at an accelerating voltage of 100 kV.

Photoreduction of (Lipidporphyrinato)iron(III) Fibers. Continuous light irradiations were performed with a 250 W ultra-high-pressure Hg arc-lamp or a 150 W xenon arc-lamp under an Ar atmosphere in a dark room (25 °C). The light was filtered with cut-off filters (HOYA B-390, L-42, U-360, Y-50) to isolate the desired wavelength region. The filtered light was irradiated into a solution of **1a** contained in a 10-mm cuvette at a distance of 75 mm from the center of the light source. The UV-vis absorption spectra of the solution were measured at regular intervals. The quantum yield (Φ) was determined using the ferrioxalate actinometric procedure.[21]

Transient Absorption Spectroscopy. The transient absorption spectra after nano-second laser flash photolysis were measured using an ANDOR DH520-18F-WR ICCD detector with an ORIEL MS-257 imaging monochromator. The excitation laser pulse was generated from the THG (355 nm; pulse width, 5 ns) of a Spectron SL803G-10 Nd:YAG laser. A pulse xenon flash lamp (10 W, 10 Hz, 100 ns pulse width) was used as the monitor's light source. The path length of the cuvette was 10 mm, and all measurements were carried out using a two-channel simultaneous detection system (Tokyo Instruments, Ltd.) at 25 °C. The femto-second transient absorption spectra were measured by a Ti:sapphier laser system.[22] An excitation light pulse was obtained by amplifying a femtosecond Ti:sapphier laser (Mira 900 Basic, Coherent) pulse with a Q-switched YAG-pumped conventional regenerative amplifier (TR70-10, Continuum). The fundamental output from the regenerative amplifier (780 nm, 3–4 mJ/pulse, fwhm 170 fs,10 Hz) was frequency-doubled (390 nm) and used as an excitation light source. The residual of the fundamental output was focused into a quartz cuvette containing H_2O to generate a white-light continuum as the probe light.

Electron Spin Resonance (ESR) Spectroscopy. (a) (Lipidporphyrinato)iron(III) solution. The deaerated PBS solution of **1a** (0.2 mM) or **1a**/hyaluronic acid in a quartz sample tube was immersed in a Dewar flask filled with liquid nitrogen; they were applied to a JEOL JES-TE200 spectrometer equipped with a 100 kHz field modulator.

(b) (Lipidporphyrinato)iron(II) solution after photoirradiation. A deaerated PBS solution of **1a**/hyaluronic acid was irradiated with high-pressure Hg arc-light for 5 min. It was immediately transferred to a flattened quartz cell (width: 1 mm) under an argon atmosphere, and observed under the ambient condition.

Viscosity Measurements. The viscosity of a PBS solution of **1a**/hyaluronic acid was measured with a capillary viscometer (Oscillatory Capillary Rheometer and Density Meter, OCR-D, Anton Paar) at 25 °C with a shear rate range of 1–332 s^{-1} (capillary diameter and length of 0.9948 and 100.2 mm, respectively).

Results and Discussion

The phosphate buffered-saline solution (PBS; 1 mM, pH 7.3, [NaCl] = 150 mM) of the iron(III) **1a** complex was homogeneous and stable for more than 6 months without any precipitate. Transmission electron microscopy (TEM) of the obtained colloid showed spherical micelles with a diameter of 10 nm (the molecular length of **1a** is 4.6 nm) (Fig. 1a). This is in contrast to the corresponding iron(II) **1b** complex, which produces unique tubular fibers in water.[17] Most probably, the imidazolylalkyl arm of **1a** dissociates from the central iron(III)

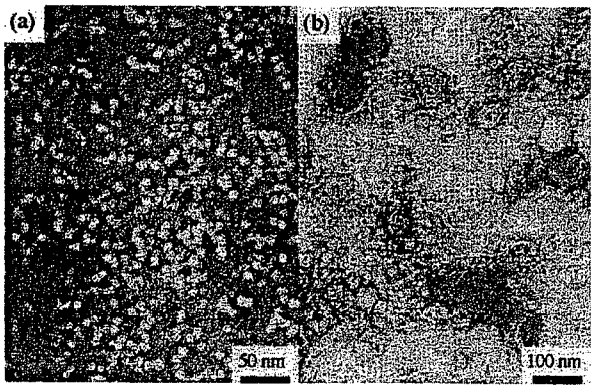

Fig. 1. Transmission electron micrographs of negatively stained samples of (a) iron(III) **1a** micelles and (b) iron(II) **1b** fibers with hyaluronic acid.

and acts as an amphiphilic chain at the porphyrin periphery. That is, the iron(III) **1a** is more hydrophilic than the iron(II) **1b**, which may prevent long fiber formation.

In the UV-vis absorption spectrum of the **1a** solution, a distinct band has appeared at 362 nm in the blue region of the Soret band (424 nm). Suslick et al. reported that $Fe^{III}Cl$(tpp) showed a similar absorption band in the UV region, which was a ligand-to-metal charge-transfer (LMCT) transition between the central iron(III) and a chloride anion (Cl^-).[6,7] On the basis of the following three experimental results, we also assigned this peak (ε: 2.5×10^4 M^{-1} cm^{-1}) as a LMCT band of Fe^{III}–Cl^-. (i) The absorption maximum significantly shifted to the lower energy region with a decrease in the electronegativity of the coordinated halide anions ($I^- < Br^- < Cl^-$), while the Soret and Q bands, which are attributed to the π-π^* transitions, were not affected (Fig. 2). (ii) The absorption spectral pattern was dependent on the pH, due to a ligand exchange of the central iron(III) (Fig. 3). The spectrum of the five-coordinated iron(III) complex with a Cl^- at pH 4 (λ_{max}: 362, 424, 510, 577 nm) changed with an increase in the pH, and finally reached that of the five-coordinated complex with an OH^- at pH 10 (λ_{max}: 335, 422, 577 nm).[23,24] These spectral changes were reversibly observed (pK_a: 7.7). Under physiological pH (7.3), more than half of **1a** was the iron(III) high-spin complex with a Cl^-. The probable six-coordinated Fe(III) complex with both an axially coordinated imidazole and a Cl^- was excluded, because the binding constant of 1,2-dimethylimidazole to the Fe(III) porphyrin was extremely low.[25,26] (iii) ESR spectroscopy also supported the five-coordinated structure of the micellar aggregated **1a**. The spectrum of the **1a** solution (0.2 mM) at 77 K exhibited the typical shape of the high-spin $Fe^{III}Cl$(tpp), and the obtained g values ($g_\perp = 5.3062$ and $g_{//} = 1.9945$) were all in good agreement with those in a previous report.[27]

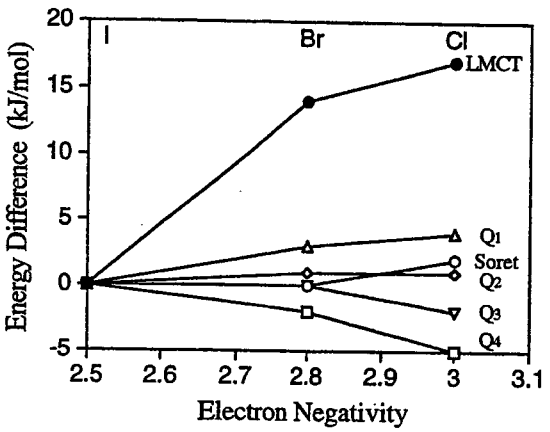

Fig. 2. Spectral changes of Fe^{III}-X^- (X: Cl, Br, I) as a function of electron negativity of the counter anion X^- (energy differences were calculated versus Fe^{III}-I^-).

The photoirradiation of this **1a** micelle solution by the 365 nm-line of a high-pressure Hg arc-lamp under an Ar atmosphere did not induce any changes in the UV-vis absorption spectrum. On the other hand, the addition of glucose (150 mM) to the solution led to complete photoreduction of the central iron(III) ion. This absorption change was completed within 45 min, and the final spectrum suggested the formation of a five-N-coordinated iron(II) high-spin complex (λ_{max}: 443, 536, 566 nm) (Fig. 4). The well-defined isosbestic points (431, 462, 533, 589, 603, 625 nm) throughout the measurement reveal that no side reactions occurred. The reduction yield clearly depended on the amount of dissolved glucose, and a relatively high concentration (> 150 mM) was necessary for 100% reduction. Furthermore, it has been found that hyaluronic acid was much more effective compared to glucose. Only a small coexistence (21 μgL^{-1}, [unit] = 100 μM) of hyaluronic acid achieved complete photoreduction, which also gave the spectrum of the five-N-coordinated iron(II) high-spin complex (λ_{max}: 443, 538, 565 nm) similar to that in Fig. 4.[28] The addition of glucose or hyaluronic acid in the dark led only negligibly small changes in the absorption and ESR spectra, which exhibited the typical shape of the high-spin iron(III) complex,

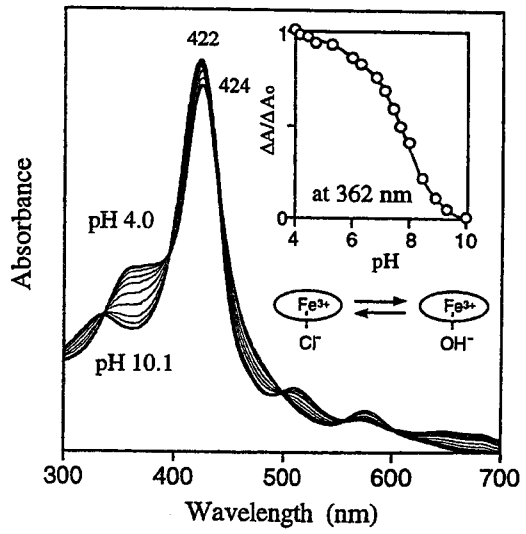

Fig. 3. Absorption spectral changes of the PBS solution of **1a** complex at various pH values (4.0, 5.0, 6.0, 7.0, 7.5, 8.0, 8.5, 9.0 and 10.1).

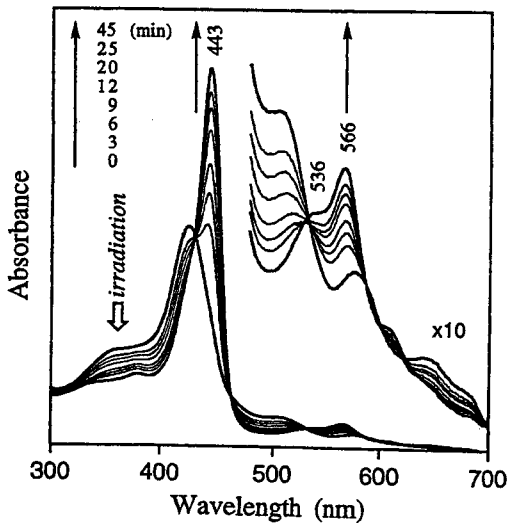

Fig. 4. UV-vis absorption spectral changes of the PBS solution of **1a** complex (10 μM) with glucose (150 mM) upon irradiation at 365 nm under an Ar atmosphere.

as seen in the homogeneous **1a** solution. These results suggest that the co-existence of saccharide neither affects the coordination structure of **1a** nor reduces the central iron(III) ion.

The photoactive region of the absorption spectrum of the **1a**/hyaluronic acid solution was then evaluated by light irradiation in the three wavelength regions: (a) < 400 nm, (b) 420–510 nm, and (c) > 500 nm. Irradiation of the CT band [region (a)] only led to an effective reduction of the iron(III) complex (Fig. 5). This wavelength dependence was quite similar to Hendrickson's result.[6] The obtained initial rates of the reduction for each case were 1.7×10^{-3}, 1.7×10^{-4} and 2.7×10^{-5} s^{-1}, respectively. Based on these findings, we can postulate that the irreversible photoreduction of **1a** is due to scavenging of the chlorine radicals ($Cl^{\bullet}$) produced by photocleavage of the Fe^{III}–Cl^{-} bond. It is also known that hydroxyl (porphyrinato)iron(III) can be photoreduced upon irradiation with light, $\lambda > 300$ nm.[29] Therefore, the other species, hydroxyl(lipidporphyrinato)iron(III), is also photoactive in the same manner as well. If the formed radical is trapped by hyaluronic acid, the disproportionation involving the oxygen atom of the glycoside group should be caused by the abstraction of hydrogen from the polysaccharide backbone.[30] Indeed, mucopolysaccharides are easily to be attacked by free radicals on the hydrogen at the carbon-5 adjacent to the carboxyl group.[31] Consequently, the mechanism of this irreversible photoreduction can be proposed as shown in Fig. 6. The LMCT excitated state (LMCT*) is located above the S_1 and S_2 states in energy, and the photoexcited species has two pathways for decay. The first is relaxation to the S_2 state, and the second affords Fe(II) porphyrin via intramolecular electron transfer. A part of the formed $Cl^{\bullet}$ that escapes from the solvent cage reacts with the active hydrogen of the neighboring hyaluronic acid, and then the iron(II) **1b** complex could accumulate. However, the charge recombination to $Fe^{III}Cl$(Lp) is a facile reaction which returns to the ground state. The quantum yields (Φ) of this photoreduction for the **1a**/hyaluronic acid became 0.007, which is consistent with the former reported values of the photoreduction by LMCT excitation.[7] That is, the low quantum yield of this system is presumably due to the high probabilities of the deactivation of LMCT* to S_2, and back electron transfer from the iron(II) ion to the chlorine radical.

Interestingly, the TEM of the **1a**/hyaluronic acid solution showed the formation of unique thin fibers with a width of 5–10 nm (Fig. 1b). The co-existence of a small amount of hyaluronic acid obviously changed the morphology of the **1a** assembly from the micelle to the fiber, which is probably made of a polysaccharide coil combined the **1a** molecule. On the other hand, a larger excess amount of glucose should be necessary for complete photoreduction (vide supla), and no clear structure could be observed in the TEM of the **1a**/glucose solution. Gulcose is homogeneously dispersed in PBS in contrast to hyaluronic acid. Hence, the fibrous co-aggregate structure composed of **1a** and hyaluronic acid would be responsible for the radical trapping and the effective photoreduction.

Our attempt to detect the radicals by ESR spectroscopy unfortunately failed. No radicals were observed, probably due to their short lifetimes.[31] However, the ring opening and the cleavage of the glycosidic linkage should induce a decrease in viscosity.[29] Indeed, the viscosity of the PBS solution of **1a**/hyaluronic acid was simultaneously decreased as the photoreduction proceeded (Fig. 7).

The efficacy of other saccharides on the photoreduction of

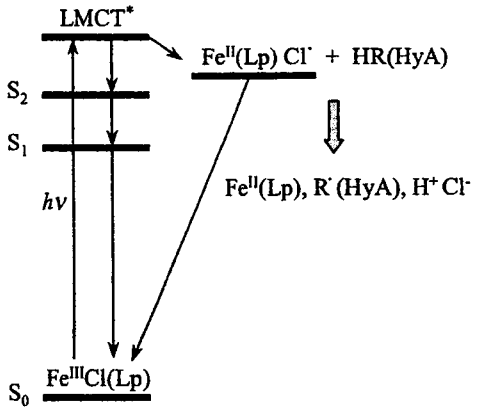

Fig. 6. Transient states and interconversion pathways for photoreduction of **1a**. Fe(Lp): (lipidporphyrinato)iron.

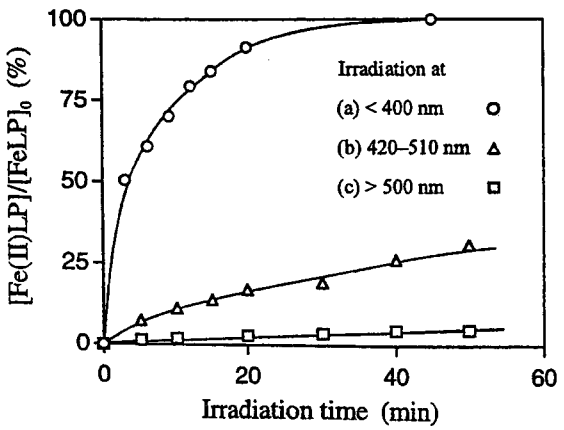

Fig. 5. Photoreduction of **1a** complex with hyaluronic acid ([unit] = 100 μM) in PBS solution by different wavelength light irradiation.

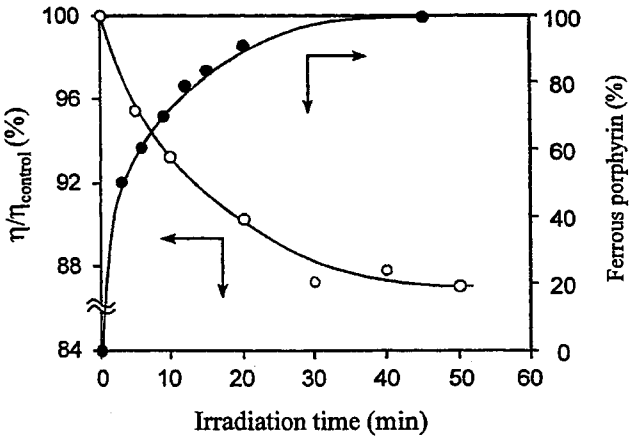

Fig. 7. The time dependence of viscosity and photoreduction ratio of the central iron(III) ion of the PBS solution of **1a**/hyaluronic acid.

the **1a** complex was compared (Fig. 8). The 100% reduction occurred only when hyaluronic acid or glucose coexisted. Amylose ([unit] = 100 μM), chondroitin 6-sulfate ([unit] = 100 μM), and glucronic acid (0.1 mM) did not contribute very much to the photoreduction of the central iron(III). These differences in the reduction behavior can be interpreted by the disparity in the rate of saccharide dehydrogenation, which competes with the recombination between the photolytically produced **1b** and the chlorine radical.

In order to analyze the photoreduction and imidazole binding to the reduced central iron(II), laser flash photolysis experiments were carried out. The deaerated **1a**/hyaluronic acid fiber solution showed that the reduction of the central iron(III) occurred within the duration time of the nano-second laser pulse. The transient absorption spectrum measured at 50 ns after the pulse was in good agreement with the difference spectrum of the five-N-coordinated iron(II) complex minus the iron(III) complex (λ_{max}: 443 nm, λ_{min}: 414 nm).[28] This result reveals that the axial base immediately associates with the photoreduced iron(II) ion, following the radical-scavenging by the saccharide. Femto-second laser flash photolysis was also performed (Fig. 9). We could not detect the LMCT* excitation of the **1a**/hyaluronic acid fiber, but bleaching of the ground state was seen in the Soret band region, and a broad band of the triplet state of the π-π^* transition appeared around 455 nm. Within 100 ps, the bleaching of the ground state in the Soret region was recovered and the transient absorption disappeared with a slight delay. The lifetime of the excited state was calculated to be approximately 11 ps. These spectral changes are consistent with those of $Fe^{III}Cl$(tpp), which shows a T–T lifetime of 50 ps and no fluorescence.[32] It can be concluded that fiber formation with hyaluronic acid does not influence the excited triplet lifetime of the **1a** complex, itself.

By bubbling O_2 gas through the photoreduced **1b** fiber solution, the UV-vis absorption spectrum changed to that of the O_2-adduct complex (λ_{max}: 425, 548 nm) in a fashion similar to the

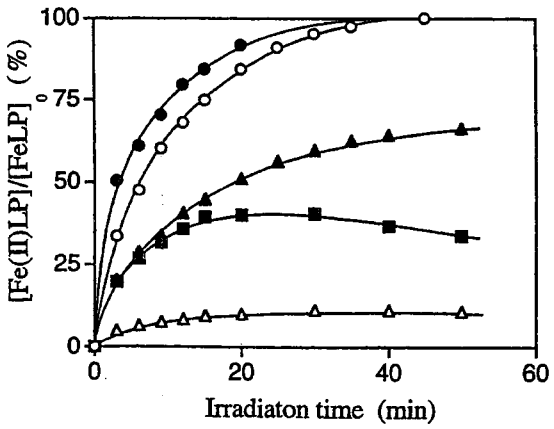

Fig. 8. Photoreduction of **1a** complex with several saccharaides in PBS solution by 365 nm-irradiation; ○: glucose 150 mM, ●: hyaluronic acid 21 mg/L ([unit] = 100 μM), ▲: amylose 25 mg/L ([unit] = 100 μM), ■: condroitin 6-sulfate 23 mg/L ([unit] = 100 μM), △: glucronic acid 0.1 mM.

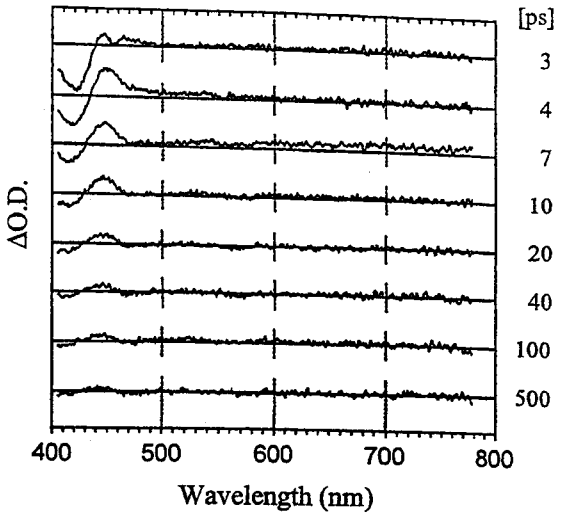

Fig. 9. Transient absorption spectra of the PBS solution of **1a**/hyaluronic acid. The sample was excited at 390 nm, and the shallow basin on the top of the 455 nm band at 3 ps is attributed to the Raman scattering of water.

1b fiber, which was prepared by a previously reported procedure using chemical reduction of the central iron(III) with ascorbic acid.[16] The O_2 coordination was reversible at 25 °C depending on the O_2-partial pressure, and the O_2-binding abilities were identical to those of the **1b** fibers prepared with ascorbic acid.

Conclusion

Photoirradiation into the LMCT band of the self-assembled **1a** complex with hyaluronic acid led to a reduction of the central iron(III), providing a five-N-coordinated iron(II) **1b** complex, which could reversibly bind and release O_2. Hyaluronic acid plays a vital role as a radical scavenger. The abstraction of hydrogen atoms from the saccharides by the produced chlorine radical, following the photoinduced homolysis of the Fe^{III}–Cl^- bond, is a key step for accumulating the iron(II) complex. This is supported by a decrease in the viscosity of the **1a**/hyaluronic acid fiber solution during photoreduction, which means the depolymerization of hyaluronic acid by radical scavenging. The laser flash photolysis experiments revealed that the photoreduction of the central iron(III) ion and the imidazole association were completed within 50 ns. Further investigation and the application of this photoreduction for synthetic hemoproteins are now underway.

We are grateful to Professors Hiroshi Masuhara and Tsuyoshi Asahi (Osaka University) for the femto-second laser flash photolysis experiments and their helpful discussions. Prof. Katsumi Tokumaru (Tsukuba University) is also gratefully acknowledged for his useful discussions and suggestions. This work was partially supported by the Core Research for Evolutional Science and Technology, JST and a Grant-in-Aid for Scientific Research (No. 11650935) from the Ministry of Education, Science, Sports and Culture.

References

1 C. Bartocci, F. Scandola, A. Ferri, and V. Carassiti, *J. Am. Chem. Soc.*, **102**, 7067 (1980).

2 C. Bartocci, A. Maldotti, G. Varani, P. Battioni, and V. Carassiti, *Inorg. Chem.*, **30**, 1255 (1991).

3 C. Bizet, P. Morlière, D. Brault, O. Delgado, M. Bazin, and R. Santus, *Photochem. Photobiol.*, **34**, 315 (1981).

4 M. Hoshino, K. Ueda, M. Takahashi, M. Yamaji, and Y. Hama, *J. Chem. Soc., Faraday Trans.*, **88**, 405 (1982).

5 M. Hoshino and T. Baba, *J. Am. Chem. Soc.*, **120**, 6820 (1998).

6 D. N. Hendrickson, M. G. Kinnard, and K. S. Suslick, *J. Am. Chem. Soc.*, **109**, 1243 (1987).

7 K. S. Suslick and R. A. Watson, *New J. Chem.*, **16**, 633 (1992).

8 B. C. Gilbert, J. R. Lindsay Smith, P. MacFaul, and P. Taylor, *J. Chem. Soc., Perkin Trans. 2*, **1993**, 2033.

9 B. C. Gilbert, J. R. Lindsay Smith, A. F. Parsons, and P. K. Setchell, *J. Chem. Soc., Perkin Trans. 2*, **1997**, 1065.

10 T. Imamura, T. Jin, T. Suzuki, and M. Fujimoto, *Chem. Lett.*, **1985**, 847.

11 B. Ward and C. K. Chang, *Photochem. Photobiol.*, **35**, 757 (1982).

12 I. Fujita, T. L. Netzel, C. K. Chang, and C.-B. Wang, *Proc. Natl. Acad. Sci. U.S.A.*, **79**, 413 (1982).

13 R. L. Brookfield, H. Ellul, and A. Harriman, *J. Chem. Soc., Faraday Trans.*, **81**, 1837 (1985).

14 A. Osuka, K. Maruyama, N. Mataga, T. Asahi, I. Yamazaki, and N. Tamai, *J. Am. Chem. Soc.*, **112**, 4958 (1990).

15 I. Hamachi, S. Tanaka, and S. Shinkai, *J. Am. Chem. Soc.*, **115**, 10458 (1993).

16 T. Yanagimoto, T. Komatsu, and E. Tsuchida, *Inorg. Chim. Acta.*, **305**, 26 (2000).

17 T. Komatsu, T. Yanagimoto, Y. Furubayashi, J. Wu, and E. Tsuchida, *Langmuir*, **15**, 4427 (1999).

18 M. Momenteau and C. A. Reed, *Chem. Rev.*, **191**, 95 (1994).

19 E. Tsuchida, T. Komatsu, K. Arai, K. Yamada, H. Nishide, C. Böttcher, and J.-H. Fuhrhop, *Langmuir*, **11**, 1877 (1995).

20 T. Komatsu, K. Yamada, E. Tsuchida, U. Siggel, C. Böttcher, and J.-H. Fuhrhop, *Langmuir*, **12**, 6242 (1996).

21 C. G. Hatchard and C. A. Parker, *Proc. R. Soc. London, Ser. A*, **235**, 518 (1956).

22 T. Asahi, A. Furube, and H. Masuhara, *Chem. Phys. Lett.*, **275**, 234 (1997).

23 R.-J. Cheng, L. Latos-Grazynski, and A. L. Balch, *Inorg. Chem.*, **21**, 2412 (1983).

24 E. B. Fleischer, J. M. Palmer, T. S. Srivastava, and A. Chatterjee, *J. Am. Chem. Soc.*, **93**, 3162 (1971).

25 F. A. Walker, M.-W. Lo, and M. T. Ree, *J. Am. Chem. Soc.*, **98**, 5552 (1976).

26 C. L. Coyle, P. A. Rafson, and E. H. Abbott, *Inorg. Chem.*, **12**, 2007 (1973).

27 T. Yonetani and H. Schleyer, *J. Biol. Chem.*, **212**, 3926 (1967).

28 T. Komatsu, T. Yanagimoto, A. Nakagawa, and E. Tsuchida, *Chem. Lett.*, **2000**, 84.

29 A. Tohara and M. Saito, *Chem. Lett.*, **1989**, 153.

30 J. E. Scott and M. J. Tigwell, *Carbohyd. Res.*, **28**, 53 (1973).

31 B. C. Gilbert, D. M. King, and C. B. Thomas, *Carbohyd. Res.*, **125**, 217 (1984).

32 M. P. Irrine, R. J. Harrison, M. A. Strahand, G. S. Beddard, *Ber. Bunsen-Ges. Phys. Chem.*, **89**, 226 (1985).